EXPERIMENTAL INVESTIGATION OF ULTIMATE LOADS CARRIED BY FLAT, UNSTIFFENED PANELS UNDER COMBINED SHEAR AND COMPRESSION

Thesis

by

Henry T. Nagamatsu

In Partial Fulfillment of the Requirements for the Degree of

Master of Science in Aeronautical Engineering

California Institute of Technology

Pasadena, California

1940

Table of Contents

Index of Figures

Index of Photographs

Table of Notation

Symbol	Definition	Unit
a	Length of panel	inches
b	Width of panel	inches
t	Thickness of panel	inches
P	Applied compression load	lbs.
S	Applied shear load	lbs.
σ_c	Compression stress	lbs./sq. in.
σ_{c_o}	Ultimate compression stress in pure compression	lbs./sq. in.
τ	Shear stress	lbs./sq. in.
τ_o	Ultimate shear stress in pure shear	lbs./sq. in.
δ_c	Total deflection parallel to compression axis	inches
ϵ	Unit deflection parallel to compression axis	in./in.
δ_s	Total deflection perpendicular to compression axis	inches
γ	Unit deflection perpendicular to compression axis	in./in.
E	Young's Modulus of Elasticity	lbs./sq. in.
ν	Poisson's Ratio	
G	Shear Modulus	lbs./sq. in.
G_e'	Apparent Shear Modulus	lbs./sq. in.

I. ACKNOWLEDGMENT

The author wishes to express his sincere appreciation to Dr. E. E. Sechler of the Guggenheim Aeronautical Laboratory, California Institute of Technology, for his valuable assistance and suggestions, and under whose direction this research project was performed.

He also wishes to thank the staff of the Guggenheim Aeronautical Laboratory for their constructive criticism and suggestions, and Mr. G. Tsubota for his helpful advice about the experimental technique.

II. SUMMARY

The behavior of flat, unstiffened panels was investigated for two length over width ratios and five thicknesses. In each case the panels were loaded until they failed. An empirical relation was developed for the variation of the ultimate combined shear and compression stress of the form

$$\left(\frac{\sigma_c}{\sigma_{c_o}}\right)^m + \left(\frac{\tau}{\tau_o}\right)^n = 1$$

The values of m and n were found to be: m = 1.65 and n = .9 for panels with length over width ratio equal to 2, and m = 1.4 and n = 1.3 for panels with length over width ratio equal to 1 1/3. The above equations agree very closely with the experimental results.

There was a variation in the apparent shear modulus under different combined loading conditions, but no definite result was obtained.

III. INTRODUCTION

For the modern types of airplanes which use stressed skin construction to carry the external loads in the most efficient manner, the designers are often confronted by the problem of panels loaded with combined shear and compression forces, such as panels in the wing, fuselage, rudder, etc. The method of determining the ultimate failure stress for panels under combined shear and compression forces is lacking.

With these problems in mind, the present research project was begun two years ago at the California Institute of Technology by Mr. Butterworth, and last year Mr. Tsubota redesigned the loading mechanism, so as to load a panel simultaneously by shear and compression.

Throughout the test, 17ST duralumin sheet was used for the test panels, since it was considered to be a representative material for structural elements in modern airplanes. All specimens were cut from the sheet with grain parallel to the lengthwise direction. This was done in order to have consistent test results, because duralumin sheet is not an isotropic material; the physical properties parallel to the grain are different from those perpendicular to the grain. Five nominal thicknesses, .010", .020", .032", .040" and .050",

considered to be used widely for stressed skin construction, were used for the panel thicknesses. Previously, Mr. Tsubota tested only three nominal thicknesses, .020", .032", and .040", but these were inadequate to obtain the relationship between the ultimate failure stress and thickness; hence, nominal thicknesses of .010" and .050" were included to obtain more adequate experimental data.

Two different panel dimensions were used for the specimens. Both were 12 inches in length, but the widths were 6 inches and 9 inches, and the ratios of length to width were 2 and 1 1/3. Inasmuch as a considerable difference was found in the strength properties of these two series of panels, further tests should be made with different lengths and widths to compare the results with those obtained for this research project.

There were seven combinations of loading used in the experimental investigation: shear over compression ratios of tan 15°, tan 30°, tan 45°, tan 60°, tan 75°, compression alone, and shear alone. The ratios of shear over compression were made as indicated, in order to get enough experimental data correctly spaced to plot the interaction curve, $\frac{\sigma_c}{\sigma_{c_o}}$ vs. $\frac{\tau}{\tau_o}$.

Enough data was taken for each specimen during the application of the loads to determine the vari-

ation, if any, of shear modulus, G, for various loading conditions. For simplicity, the edges of the panels were simply supported by steel tubes with slots, making a sliding contact support.

IV. EXPERIMENTAL PROCEDURE

(a) Description of the Testing Machine

The apparatus which was used in this research project was modified by Mr. Tsubota, so as to get both shear and compression forces acting simultaneously on the panel. A very detailed description is given in Reference 2; hence, only the basic parts will be discussed. The only modification which was made, in order to prevent the bottom edge of the panel to rotate, was to put another roller on the left hand side of the panel, indicated by s in the drawing (Fig. 1).

The testing machine was constructed in a manner to permit various combinations of forces on the panel. For only shear load, one end of the tension strap gage was connected to the frame, and the load applied to the specimen, by tightening the screw on the tension strap. In order to get various ratios of shear to compression load, one end of the loading mechanism was connected to the beam, and by means of a lever system the reaction of the shear force was transmitted as a compression load to the panel. There were five slots on the bottom I-beam, and by placing the knife edge in these slots, it was possible to obtain the following ratios of shear to compression: $\frac{\tau}{\sigma_c}$ tan 15°, tan 30°, tan 45°, tan 60°, and tan 75°. Pure compression

load was obtained by placing the end of the loading cable, which was connected to the angles, to the frame and the other end to the loading beam; then by tightening the loading screw, the load was transmitted by the lever system to the panel as pure compression.

Three steel balls were used to get approximately a point contact for the transmission of the force. Knife edges were used as pivot points for the application of the loads. Two Ames dial gages were used to measure the vertical deflection of the panel, and one for the horizontal deflection. The smallest division on the dial gages was one-hundredth of a millimeter.

The tension strap gage was calibrated in a standard tension testing machine, and a curve of deflection vs. load was plotted, as shown by Fig. 59. Since the shear failure load for a nine inch panel with a thickness of .040" was large, a heavier tension strap gage was made and calibrated.

Frictional forces in the testing machine was kept to a minimum by using roller bearings and rollers.

(b) Description of the Test

All panels were carefully cut out from 17ST duralumin sheet with the grain parallel to the lengthwise direction. The thickness of the panels was measured at three points on each side, and the average

value of the measured thicknesses was used to calculate the stress.

Before the specimen was placed into the testing machine, lead counter weights were placed on the loading beam to balance the loading system for each knife edge setting. After the system had been balanced, the panel was clamped between the angle sections. Slotted steel tubes were next attached to the panel to support the edges, and these tubes were clamped until sliding fit was made, in order to keep the load carried by the tubes, due to frictional forces, to a minimum. The resulting edge support can be assumed to be nearly simply supported.

There were four turnbuckles attached to the tubes by piano wire, which were used to prevent the tubes from spreading apart when the load was applied to the specimen. Care was taken when tightening the turnbuckles so that no edge moment was applied to the plate by the edge supporting tubes. At the corners of the specimen, between the tubes and the angle sections, additional supports were required in order to prevent a local failure from taking place.

After the plate was securely fastened to the apparatus, rollers at both sides of the panel were tightened to prevent the end of the panel from rotating, keeping the fixed and the movable ends

parallel throughout the test; but actually there was a slight rotation of the end.

The bottom I-beam with the knife edges was made horizontal by adjusting the jack. As the load was applied, the panel became shorter; hence, to keep the I-beam level, the jack had to be extended. Also, the loading cable attached to the angles was kept horizontal throughout the application of load by turning the screw x, attached to the pulley in Fig. 1.

The load was applied with an increment of about eight or ten readings, before the ultimate failure occurred. These readings were taken to determine whether there was a variation in shear modulus under various loading conditions; that is, various ratios of shear to compression. Near the maximum load the panel deflected without any increase in the load.

V. RESULTS

(a) Types of Failure

All panels that were tested failed by the formation of waves as shown by the photographs, Figs. 47-58. The panels of nominal thickness of .010" for both a/b ratios failed, by forming a number of secondary waves at the supporting edges as indicated by Fig. 47 and Fig. 53; thicker panels did not have many secondary waves at the edges.

Panels under compression failed at the center of the two edges. Before failure, one complete wave formed with a half wave length equal to half of the length for both a/b ratios. The wave became deeper and deeper until local failure took place at the center of the panel at both edges, illustrated by Figs. 52 and 58. When the panels of .010" were loaded by compression force, one complete wave formed at low stress; as the load was increased, secondary waves formed at the supports, the panels failing at many places along the edges, shown by Figs. 51 and 57 for both a/b ratios, similar to an Euler failure of a column.

The panels, when subjected to shear only, formed a diagonal wave, the angle of which was different for the two panel dimensions. For a/b = 2, the diagonal wave ran from one edge to the opposite edge at the

bottom of the panel; therefore, the angle with the horizontal for the wave was greater than 45 degrees. For panels with a/b = 1 1/3, the waves were nearly 45 degrees when subjected under shear and combined forces. The diagonal wave formed at low stress value, and it became deeper as the load was increased; secondary waves, induced by the main diagonal wave, formed at the edge supports. The panels failed locally at the supports, as shown by Figs. 48 and 54. The panels with thickness greater than .010" had only one secondary wave at the supports besides the main diagonal wave, but the panels of .010" thickness had many secondary waves at the supports, and when they failed, there were three or four local failures on both edges.

The wave formation for panels loaded with compression and shear was very similar to those subjected to shear alone.

(b) Variation of Ultimate Failure Stress with Thickness, a/b ratios, and width, b

For a/b = 2, b = 6 inches, the curve of τ vs. t, thickness, for various ratios of $\frac{\tau}{\sigma_c}$ is a straight line. The curves for shear alone and for $\frac{\tau}{\sigma_c} = \tan 75^\circ$ are very close together for thicknesses of .010 and .020 inches. The increment between curves do not follow any logical sequence. The slope of the curves changes for different

loading conditions, being greatest for shear alone and smallest for $\frac{\tau}{\sigma_c}$ = tan 15°. The experimental scatter as shown by Fig. 17 is not very great, for the loading condition $\frac{\tau}{\sigma_c}$ = tan 15° the scatter is very small.

The curves of τ vs. t for a/b = 1 1/3 are nearly a straight line similar for the panels with a/b = 2. As the ratio of $\frac{\tau}{\sigma_c}$ becomes larger, the curves of τ vs. t deviate from a straight line. The slopes of the curves become greater as the amount of compression acting on the panel compared to the shear force becomes smaller. The increments between curves become smaller as the ratio $\frac{\tau}{\sigma_c}$ increases. For the loading condition in which compression is the highest, the scatter of experimental points is very small, and the ultimate shear stress is very low.

For a/b = 2 and b = 6 inches, the curves of τ vs. t for various loading conditions are again a straight line. The slopes of these curves decrease with the $\frac{\tau}{\sigma_c}$ ratics, and the increments between curves are nearly constant, except for the case of pure compression, Fig. 18.

The curves of ultimate compression stress, σ_c, vs. t for a/b = 1 1/3, b = 9 inches are straight lines. The slopes of these curves for various ratios of $\frac{\tau}{\sigma_c}$ decrease with the increasing $\frac{\tau}{\sigma_c}$ ratios. For a/b = 2 the increments between the different loading conditions

of compression to shear were nearly constant, but for this case the increment increases with the increase in the $\frac{\tau}{\sigma_c}$ ratios.

(c) **Variation of the Ultimate Combined Stresses**

(1) Variation of Ultimate Combined Stress with Thickness, σ_c vs. τ.

The ultimate failure stresses were plotted as σ_c vs. τ for various thicknesses and for two a/b ratios.

For the smaller panels with a/b = 2, and b = 6 inches, the family of curves for the thickness are shown by Fig. 15 and are quite similar. By applying a small compression, there is a slight tendency for the thinner panels to increase the failure shear stress. This effect is very marked for a panel with nominal thickness of .010 inches. For thickness of .050 inches the effect is not very pronounced. When only compression force is acting on the panel, the ultimate failure compression stress is greatly reduced by the application of slight shear force.

The curves of ultimate compression stresses vs. ultimate shear stresses for a/b = 1 1/3 are different from those for a/b = 2. The curve for panels with t = .010 inches is different from the rest of the curves; it is similar to the curves for panels with a/b = 2. For the other thickness there is no tendency

for the ultimate shear stress to increase with the application of small compression force. The effect of shear load on the ultimate compression stress is not as great as for the panels with a/b = 2. The curves of σ_c vs. τ approach a circular shape with the increase in thickness of the specimen. Experimental scatter is small for both of the panels.

(2) Variation of Ultimate Combined Stresses

To indicate the variation of the ultimate combined stresses, the ratio of ultimate failure compression stress to ultimate compression stress without any shear load was plotted against the ratio of ultimate shear stress to ultimate shear stress without any compression force, $\frac{\sigma_c}{\sigma_{c_o}}$ vs. $\frac{\tau}{\tau_o}$.

When the values of $\frac{\sigma_c}{\sigma_{c_o}}$ and $\frac{\tau}{\tau_o}$ were obtained for panels with a/b = 2, for the five thicknesses, the resulting curves were practically coincident. The resulting curve has a vertical tangent with respect to the $\frac{\tau}{\tau_o}$ axis, and the curvature is greatest for low $\frac{\sigma_c}{\sigma_{c_o}}$ values. It has a shape similar to a cubic parabola. The scatter of experimental curves about the mean curve is not very great, especially for specimens with nominal thickness of .040 inches as shown by Fig. 7.

For panels with a/b = 1 1/3 and b = 9 inches,

the curves of $\frac{\sigma_c}{\sigma_{c_o}}$ vs. $\frac{\tau}{\tau_o}$ for the various thicknesses did not fall on one common curve as for the panels with a/b = 2. The curve for a nominal thickness of .010 inches deviated from the others and is similar to the results for a panel with a/b = 2. Other curves are more or less symmetrical about a 45° line. These curves do not have nearly constant slope for low τ as for the panel with a/b = 2 as shown by Fig. 9. The experimental values are plotted with the mean curve in Figs. 4-14.

(d) Stress Strain Diagrams

Shear stress vs. shear strain curves are shown in Figs. 21-26. Shear stress, τ, was calculated from the following equation:

$$\tau = \frac{S}{A}$$

S = shear load

A = bt = width times thickness

Unit shear strain, γ, was defined as

$$\gamma = \frac{\delta_s}{\ell}$$

where δ_s = deflection in the shear load direction

ℓ = length of the panel = a

For thin panels the load did not drop off sharply as for the thicker panels. Near the maximum stress the curve was poorly defined, because it was difficult

to obtain data, since the specimens deflected without any increase in the applied load. For low shear and compression stresses the curves are nearly a straight line. The stress at which the panels buckled was low; therefore, these curves show how the panels behave after they have entered the buckled state.

Compression stress vs. compression strain are shown by Figs. 27-32. The compression strain was calculated from the following equation:

$$\sigma_c = \frac{P}{A}$$

where P = compression load

A = bt = width times thickness

The compression strain was obtained by dividing the deflection in the direction of the compression load, P, by the length of the panel.

$$\varepsilon = \frac{\delta}{\ell}$$

δ_c = deflection in the direction of P

ℓ = a = length of the panel

ε = compression strain, in./in.

These stress strain curves are similar to the shear stress strain curves, with a gradual drop off of compression load beyond the maximum load for the thin panel.

(e) Variation of Apparent Shear Modulus

The apparent shear modulus, G'_c, was obtained from

the shear stress strain curves by measuring the slope of the curve at shear stress equal to zero. In order to get the slope with a reasonable degree of accuracy, the stress strain curves were plotted to a large scale from which the slope was determined.

For all thicknesses the apparent shear modulus reaches a maximum value when there is a slight compression on the panel. The rate of increase in apparent shear modulus with compression is greater than the rate of decrease in G_e' after the maximum value has been reached. The apparent shear modulus is greater for thicker panels, but the value of modulus G_e' is much lower than the shear modulus obtained from the following equation:

$$G = \frac{E}{2(1+\nu)}$$

where: E = modulus of elasticity = 10.3×10^6 lbs./sq. in.

ν = Poisson's ratio = 0.3

$$G = \frac{10.3 \times 10^6}{2(1+.3)} = 3.96 \text{ lbs./sq. in.}$$

For both panel dimensions, the variation of G_e' vs. $\frac{G}{\tau}$ is shown by Figs. 45-46.

Due to the fact that there are many possible sources of errors, the scatter of experimental points is great in the above two figures.

V. DISCUSSION OF RESULTS

(a) Ultimate Combined Stress

The curve faired through the experimental values for the $\frac{\sigma_c}{\sigma_{c_o}}$ vs. $\frac{\tau}{\tau_o}$ has the form of

$$\left(\frac{\sigma_c}{\sigma_{c_o}}\right)^m + \left(\frac{\tau}{\tau_o}\right)^n = 1 \qquad (1)$$

When the variation of thickness was eliminated by using the faired values to obtain $\frac{\sigma_c}{\sigma_{c_o}}$ and $\frac{\tau}{\tau_o}$ from the curve of σ_c vs. t and τ vs. t, Fig. 41 and 42, the curves for various thicknesses were coincident for the panels with a/b = 2. Such success was not obtained for the panels with a/b = 1 1/3; the .010 inch panel being very different from the other thicknesses, as shown by Fig. 9.

Other investigators have used Eq. 1 with different values for m and n. Wagner found that m = 1 and n = 2 for buckling of flat strip under combined shear and compression (Ref. 4). Bridget used the formula with m = 1 and n = 3 for the critical stress in an unstiffened circular cylinder under combined shear and compression. Two investigators at the Guggenheim Aeronautical Laboratory, California Institute of Technology, have also used the above formula and obtained different values for n. Butterworth found that m = 1 and n = 4 for panels with a/b = 2 and 3

and for thickness of .020 and .032. His experimental results agree very closely for n = 4. Tsubota, with a different method of applying the combined shear and compression on the panel, found that it was safe to use m = 1 and n = 1 for design purposes.

The values of m and n obtained from the present experimental investigation were: for panels with a/b = 2, m = 1.4 and n = 1.3, and for panels with a/b = 1 1/3, m = 1.65 and n = .9; hence, using m = 1 and n = 4 in Eq. 1 is unsafe and also using the values of m = 1 and n = 1 is conservative, especially when the compression load on the panel is small. Further tests should be made to determine whether varying the length and keeping a/b = 2 has any effect on the values of m and n in Eq. 1. To obtain an empirical equation for the ultimate combined stresses which can be used for design purposes, further investigations should be made for a/b = 3, and 1, so as to extend the results obtained by this investigation.

(b) Ultimate Stress

On Figs. 15-16 the curves of σ_c vs. τ for various thicknesses were plotted. For panels with a/b = 2 and for thinner thicknesses, the ultimate shear stress is slightly increased by applying a small compression load; therefore, after the above mentioned a/b ratios

have been investigated, it would be advantageous to investigate panels with slight tension, to see what effect it has on the ultimate shear stress.

The tendency to increase the ultimate shear stress by small compression load is not present for panels with a/b = 1 1/3. This may be due to the fact that the magnitude of ultimate shear stress for shear alone is nearly equal to the ultimate compression stress without any shear.

(c) Apparent Shear Modulus

The present investigation has shown that there is variation in the effective shear modulus with various combined loading conditions. An analysis was made to determine why the apparent shear modulus was low even in the unbuckled stage. This analysis was carried out for the case when the panel was loaded only with a shear force, and is given in the Appendix.

It was found that the horizontal deflection, i.e., the deflection in the direction of the applied shear force, was caused mainly by the bending deflection and the deflection due to shear was only about 17% of the total deflection in the unbuckled state.

Further deflection was caused by the rotation of the ends of the panel. Great care was taken to keep

the ends parallel throughout the application of the load, but actually there was a slight rotation of the loaded end. If the rotation of the end was taken into consideration, the calculated values for the apparent shear modulus were close to the experimental values obtained from the slope of the shear stress-strain curve. These results are indicated in the analysis given in the Appendix.

Another reason why the experimental values for G' were low for thin panels was due to the fact that the thin panels buckled at very low stresses.

Further theoretical investigations should be made to find the explanation for the increase in the apparent shear modulus with slight compression force on the panel. The data obtained for this research project can be used to check the analysis.

(d) Conclusion

The results obtained by this investigation are not conclusive enough to formulate any general empirical formula for the combined ultimate stresses which can be used by the designers. The present research project should be continued until such a general formula is obtained, which can be used with confidence in desighing airplane structures.

VII. REFERENCES

1. Sechler, E. E.: "Stress Distribution in Stiffened Panels under Compression." Journ. Aero. Sciences, June 1937, pp. 320-323.

2. Tsubota, G. Y.: "Experimental Investigation of Ultimate Loads Carried by Flat, Unstiffened Panels under Combined Shear and Compression." Thesis for M.S. in Aeronautical Engineering, California Institute of Technology, 1939.

3. Butterworth, W. T.: "Experimental Investigation of Ultimate Loads Carried by Flat, Unstiffened Panels under Combined Shear and Compression." Thesis for M.S. in Aeronautical Engineering, California Institute of Technology, 1938.

4. Wagner, H.: "Structures of Thin Sheet Metal." TM 490, N.A.C.A.

5. Wagner, H.: "Flat Sheet Metal Girder with Very Thin Metal Web." TM 604, N.A.C.A.

6. Lahde, R. and Wagner, H.: "Experimental Studies of the Effective Width of Buckled Sheets." TM 814, N.A.C.A.

7. Schapitz, E.: "Contribution to the Theory of Incomplete Tension Bay." TM 831, N.A.C.A.

8. Timoshenko, S.: "Theory of Elastic Stability." McGraw-Hill, 1936.

9. Timoshenko, S.: "Theory of Elasticity." McGraw-Hill, 1934.

10. Kuhn, P.: "Stress Analysis of Beams with Shear Deformation of the Flanges." TR 608, N.A.C.A.

11. Seydel, E.: "The Critical Shear Load of Rectangular Plates." TM 705, N.A.C.A.

VIII. GRAPHICAL RESULTS

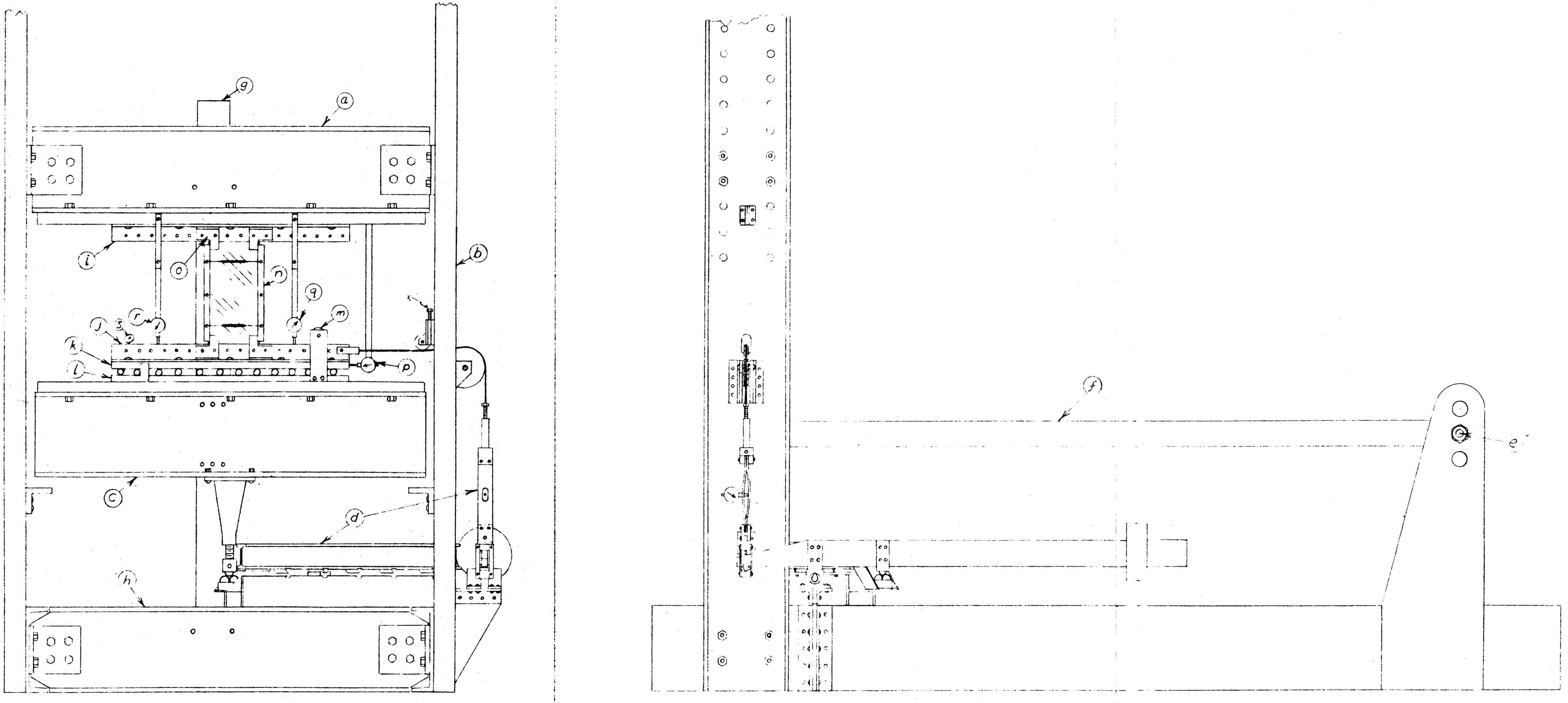

FIGURE 1

VARIATION OF ULTIMATE COMBINED STRESS

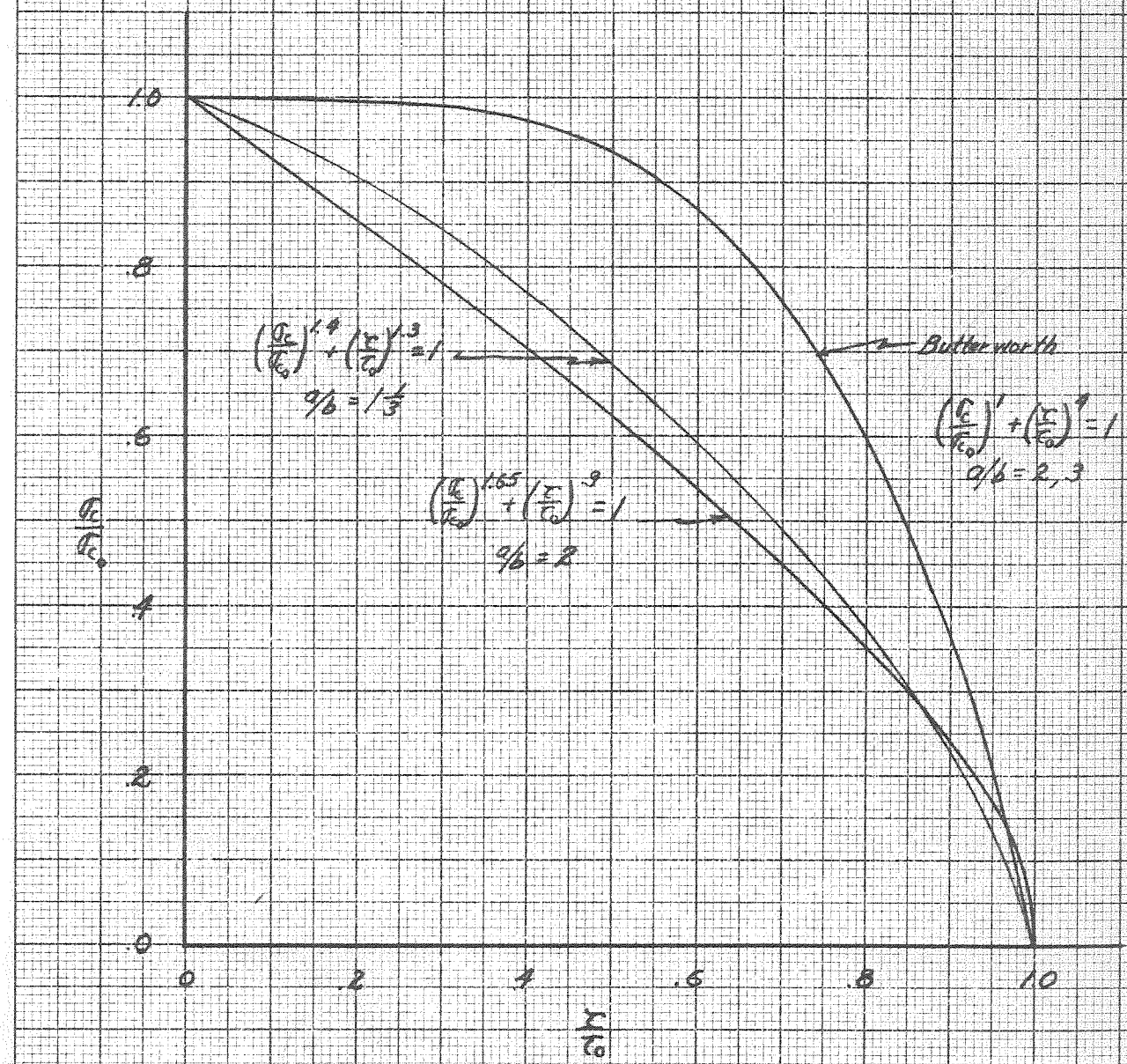

FIG. 2

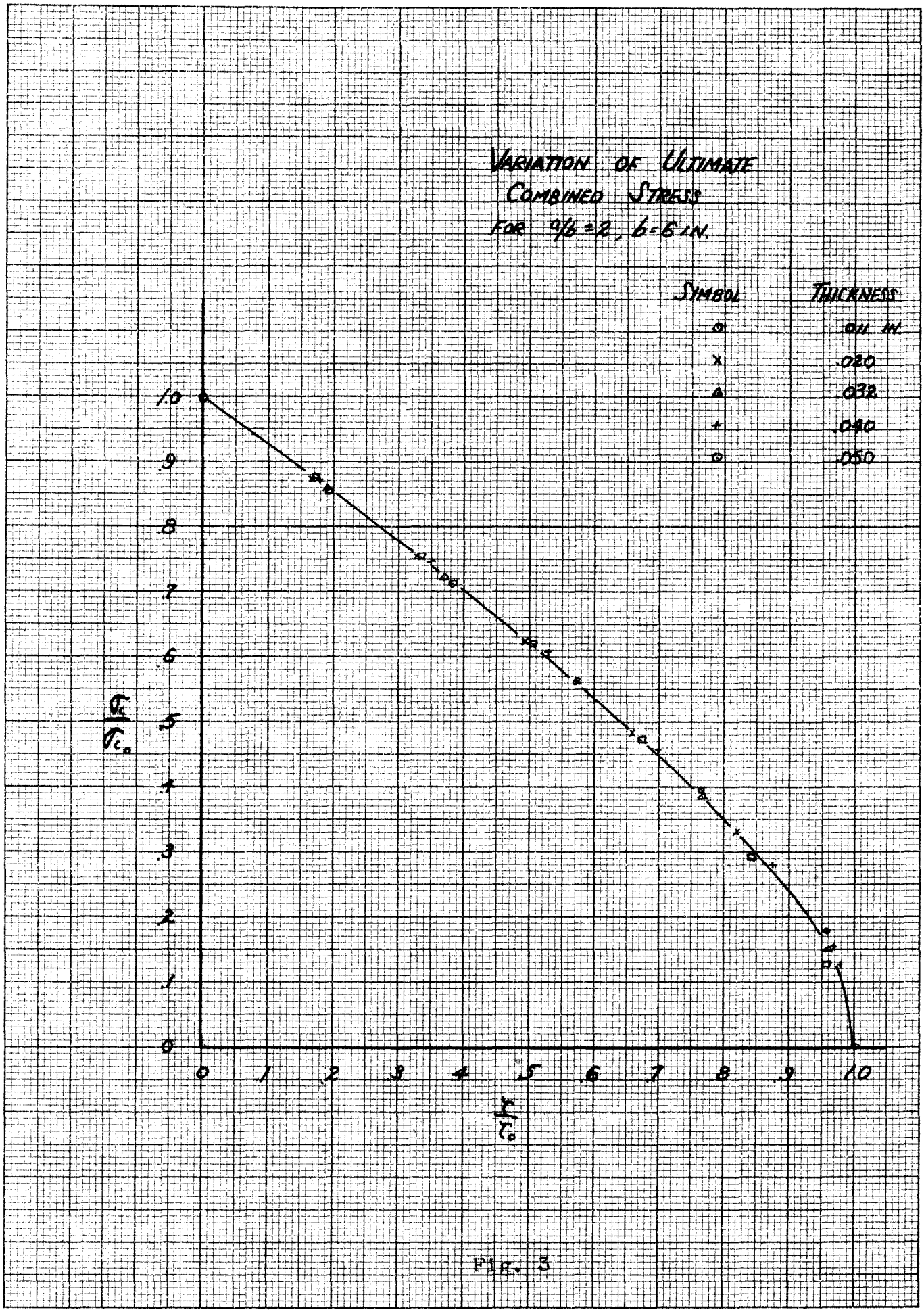
VARIATION OF ULTIMATE
COMBINED STRESS
FOR a/b = 2, b = 6 IN.
SYMBOL
THICKNESS
ON IN.
.020
.032
.040
.050
1.0
.9
.8
.7
.6
.5
.4
.3
.2
.1
0
σc / σc0
0
.1
.2
.3
.4
.5
.6
.7
.8
.9
1.0
τ / τ0

Fig. 3

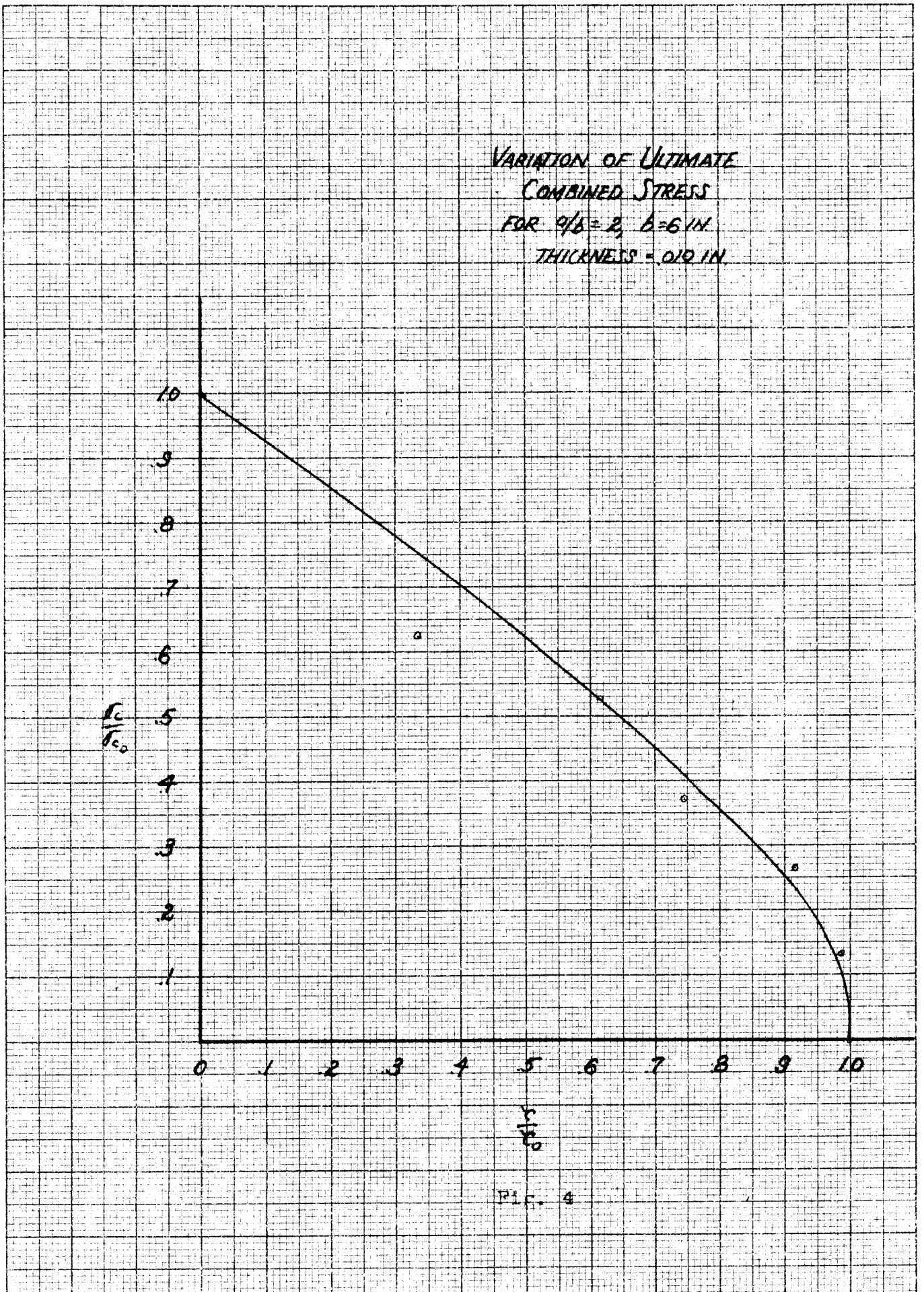
VARIATION OF ULTIMATE COMBINED STRESS
FOR a/b = 2, b = 6 IN.
THICKNESS = .010 IN.
1.0
.9
.8
.7
.6
.5
.4
.3
.2
.1
0
.1
.2
.3
.4
.5
.6
.7
.8
.9
1.0
$\frac{f_c}{f_{c_0}}$
$\frac{f_r}{f_{r_0}}$

Fig. 4

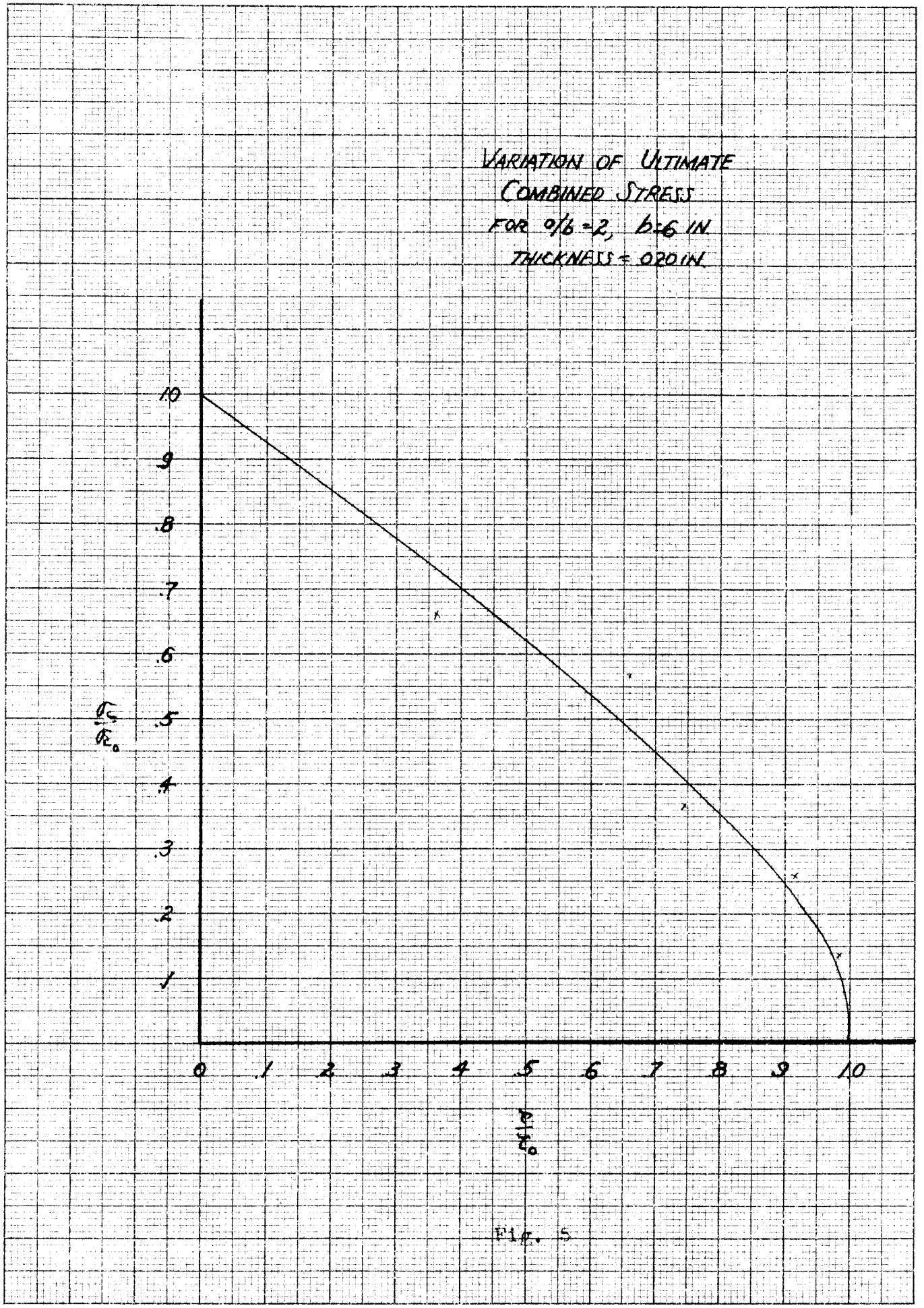
VARIATION OF ULTIMATE
COMBINED STRESS
FOR a/b = 2, b = 6 IN.
THICKNESS = .020 IN.
10
9
.8
.7
.6
.5
.4
.3
.2
.1
0
1
2
3
4
5
6
7
8
9
10

Fig. 5

VARIATION OF ULTIMATE COMBINED STRESS FOR $\alpha/b = 2$, $b = 6$ IN. THICKNESS = .032 IN.

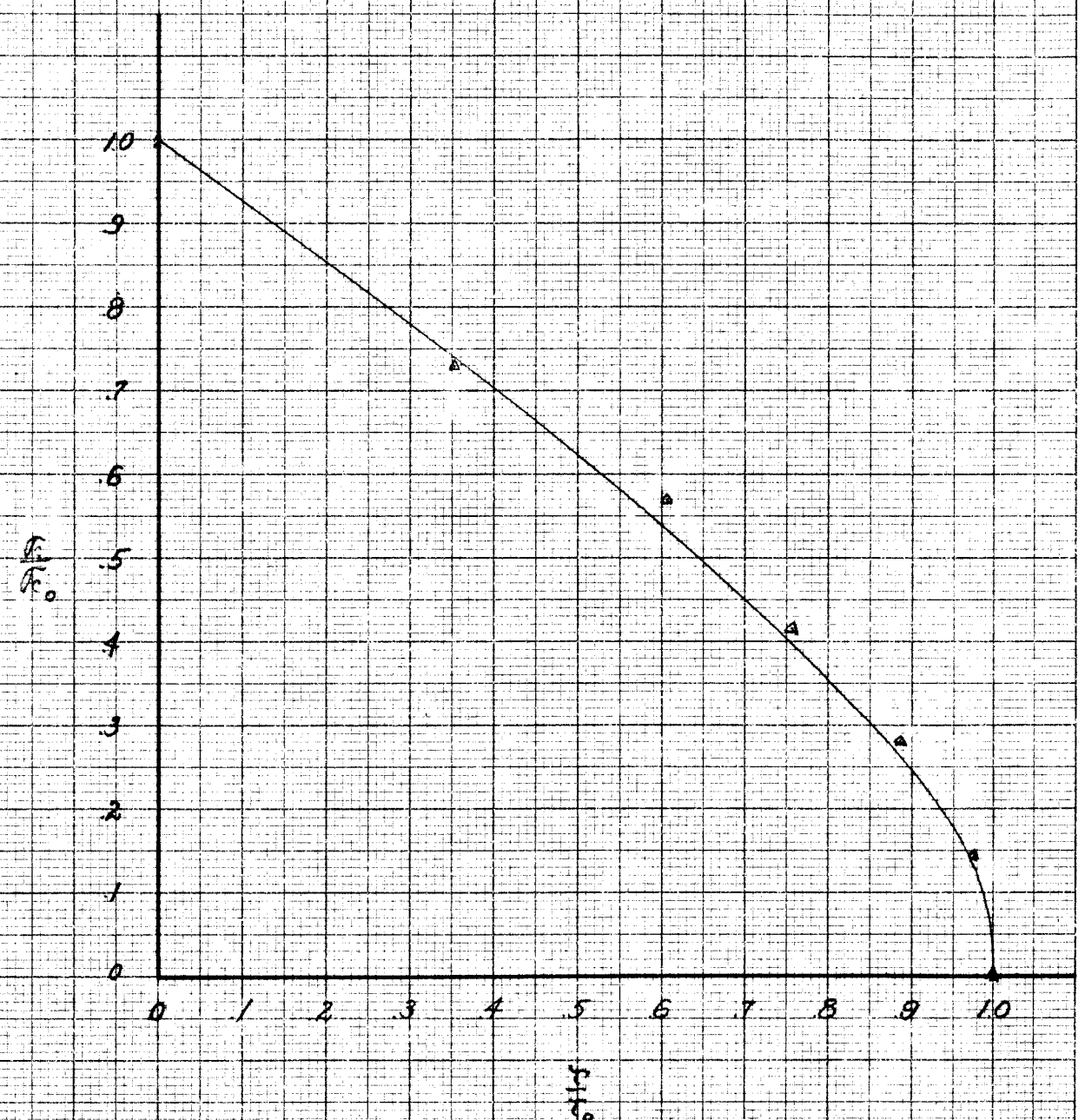

Fig. 6

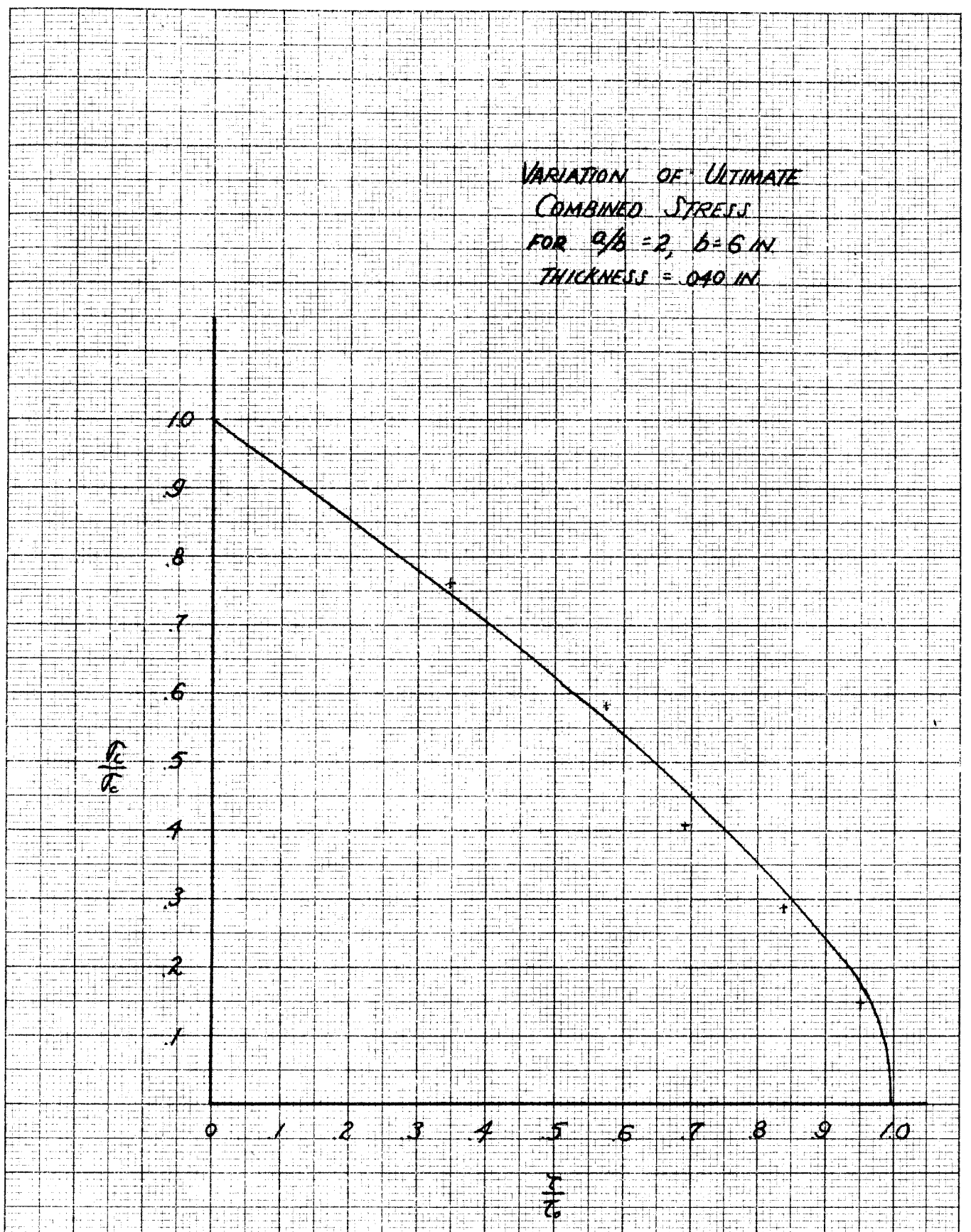
VARIATION OF ULTIMATE
COMBINED STRESS
FOR a/b = 2, b = 6 IN.
THICKNESS = .040 IN.
1.0
.9
.8
.7
.6
.5
.4
.3
.2
.1
$\frac{f_c}{f_c}$
0
.1
.2
.3
.4
.5
.6
.7
.8
.9
1.0
$\frac{f}{f_c}$

Fig. 7

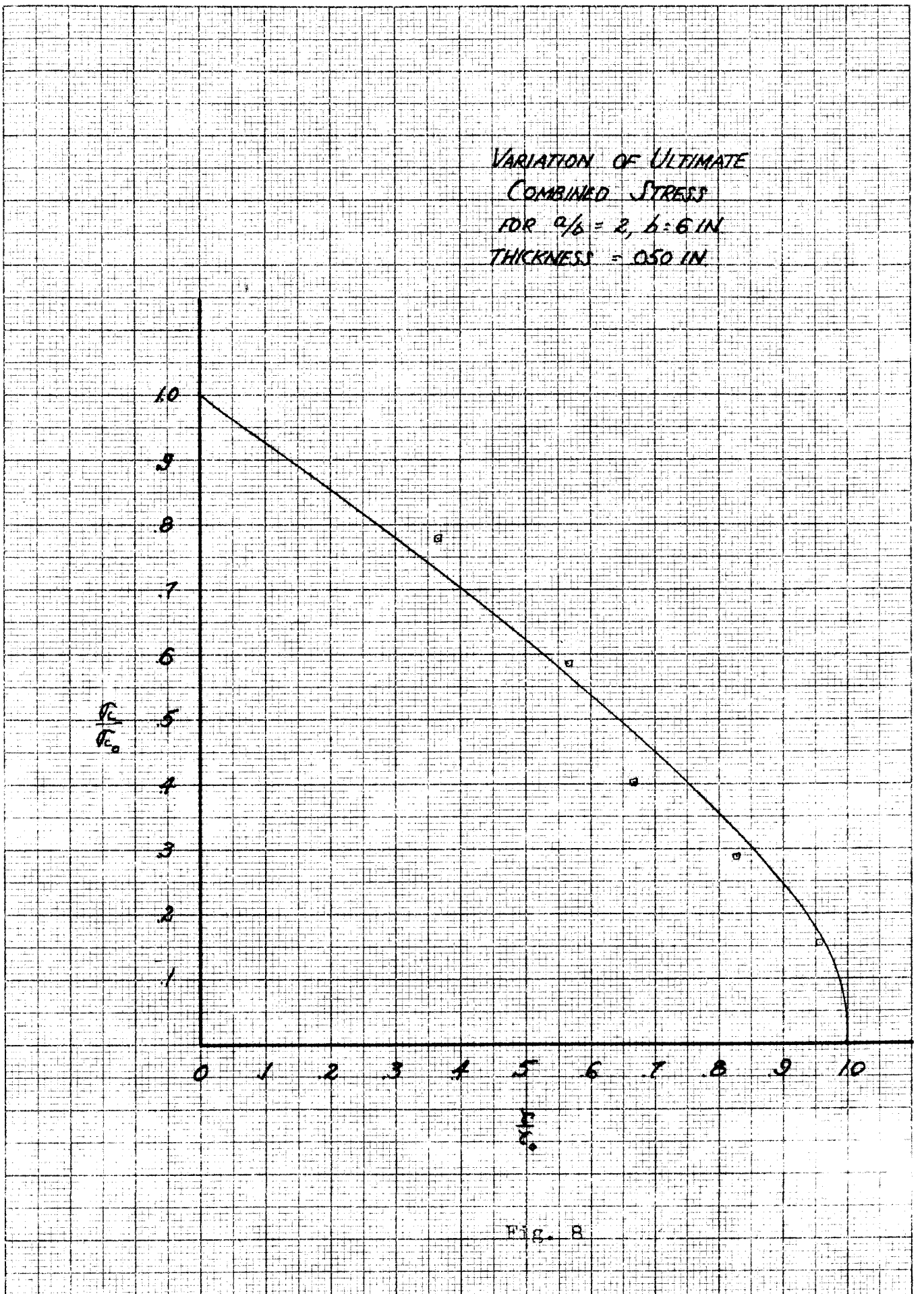
VARIATION OF ULTIMATE
COMBINED STRESS
FOR a/b = 2, b = 6 IN
THICKNESS = .050 IN
1.0
.9
.8
.7
.6
.5
.4
.3
.2
.1
0
.1
.2
.3
.4
.5
.6
.7
.8
.9
1.0

Fig. 8

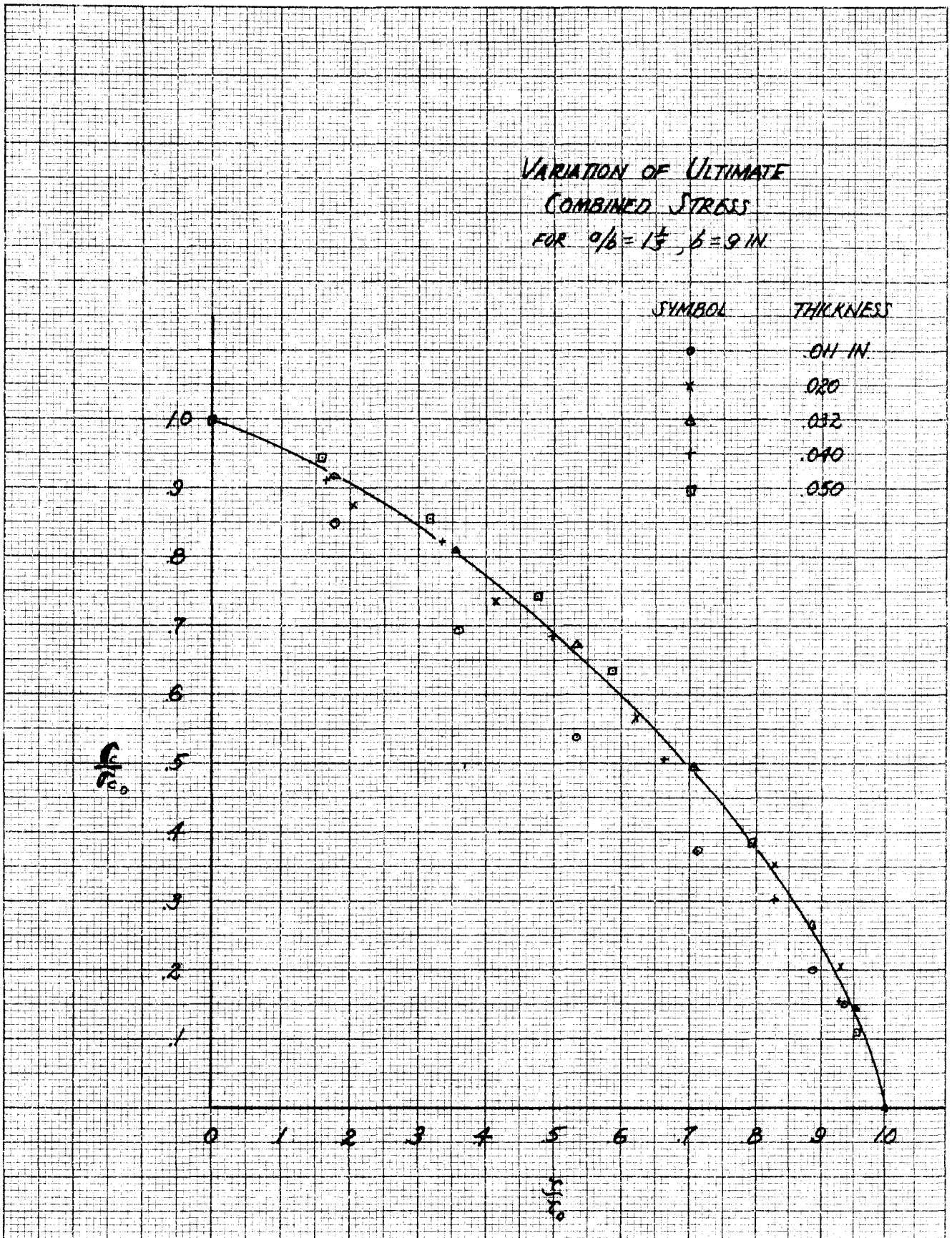
VARIATION OF ULTIMATE COMBINED STRESS FOR a/b = 1 1/3, b = 9 IN.
SYMBOL
THICKNESS
.011 IN.
.020
.032
.040
.050
1.0
.9
.8
.7
.6
.5
.4
.3
.2
.1
fc/fc0
0
1
2
3
4
5
6
7
8
9
10
fx/fx0

Fig. 9

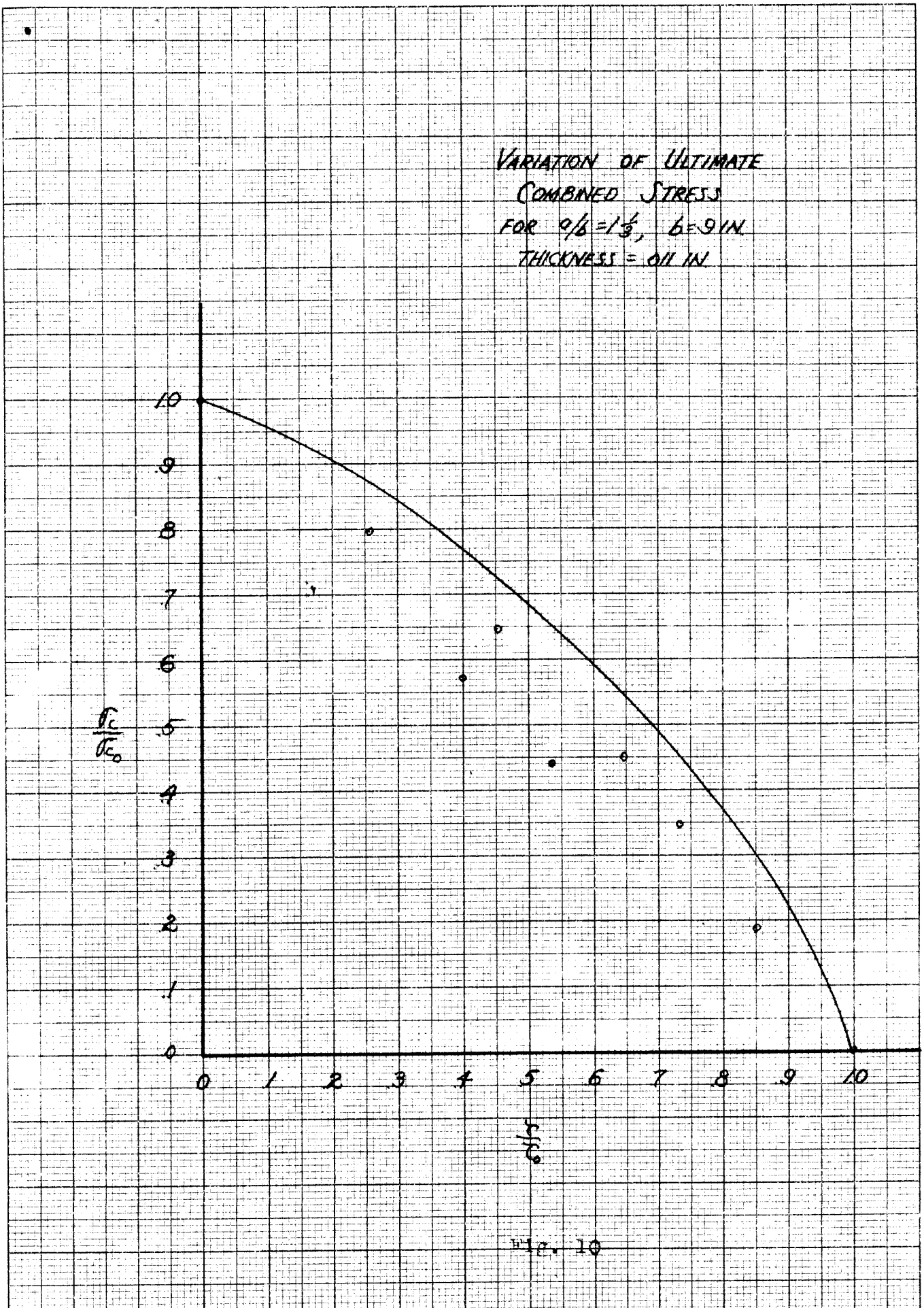
VARIATION OF ULTIMATE
COMBINED STRESS
FOR $a/b = 1\frac{1}{3}$, $b = 9$ IN.
THICKNESS = .011 IN.
$\frac{\sigma_c}{\sigma_{c_0}}$
$\frac{\tau_c}{\tau_{c_0}}$
0
1
2
3
4
5
6
7
8
9
10

Fig. 10

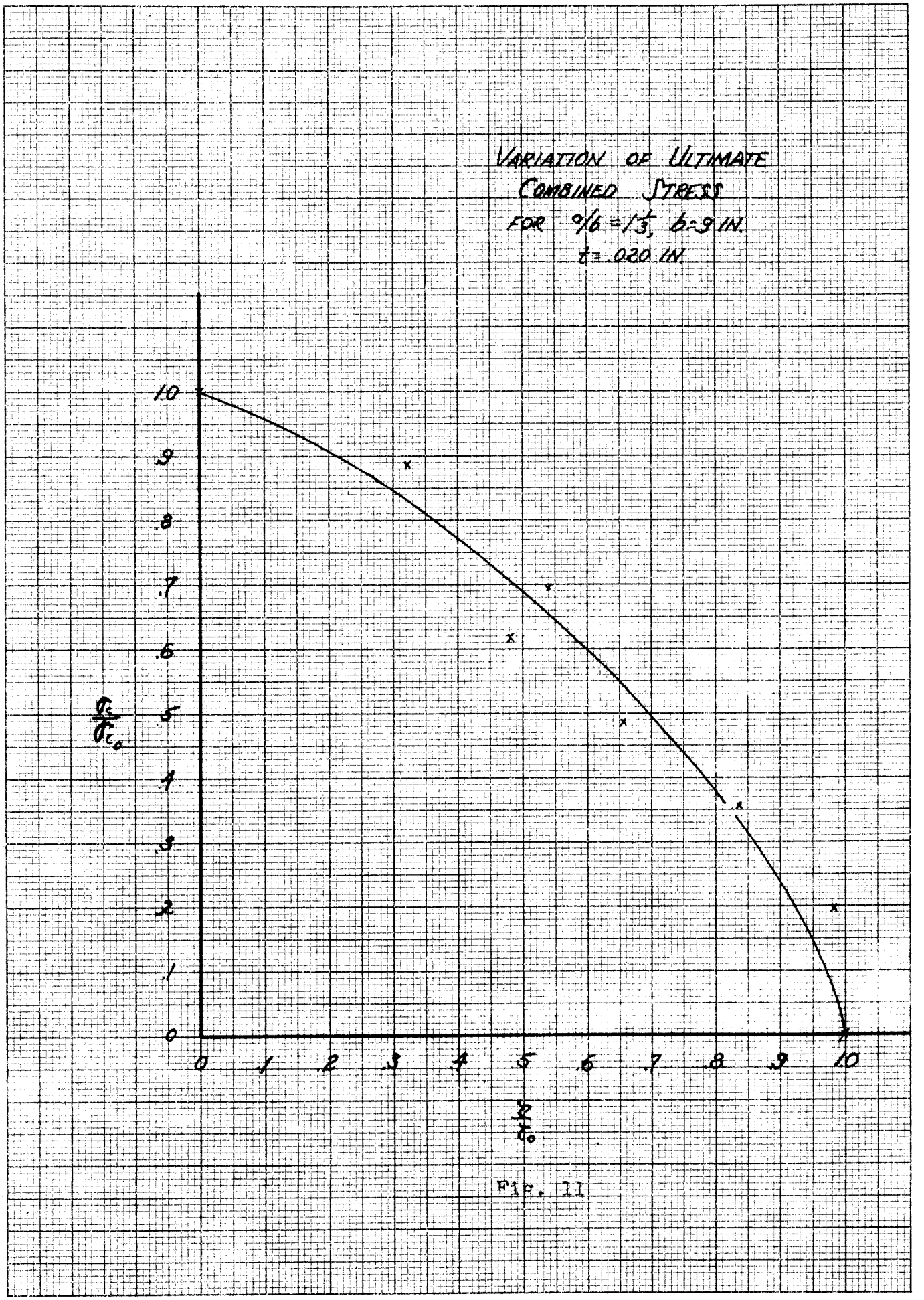
VARIATION OF ULTIMATE COMBINED STRESS
FOR σ/δ = 1/3, b = 9 IN.
t = .020 IN.
1.0
.9
.8
.7
.6
.5
.4
.3
.2
.1
0
0
.1
.2
.3
.4
.5
.6
.7
.8
.9
1.0

Fig. 11

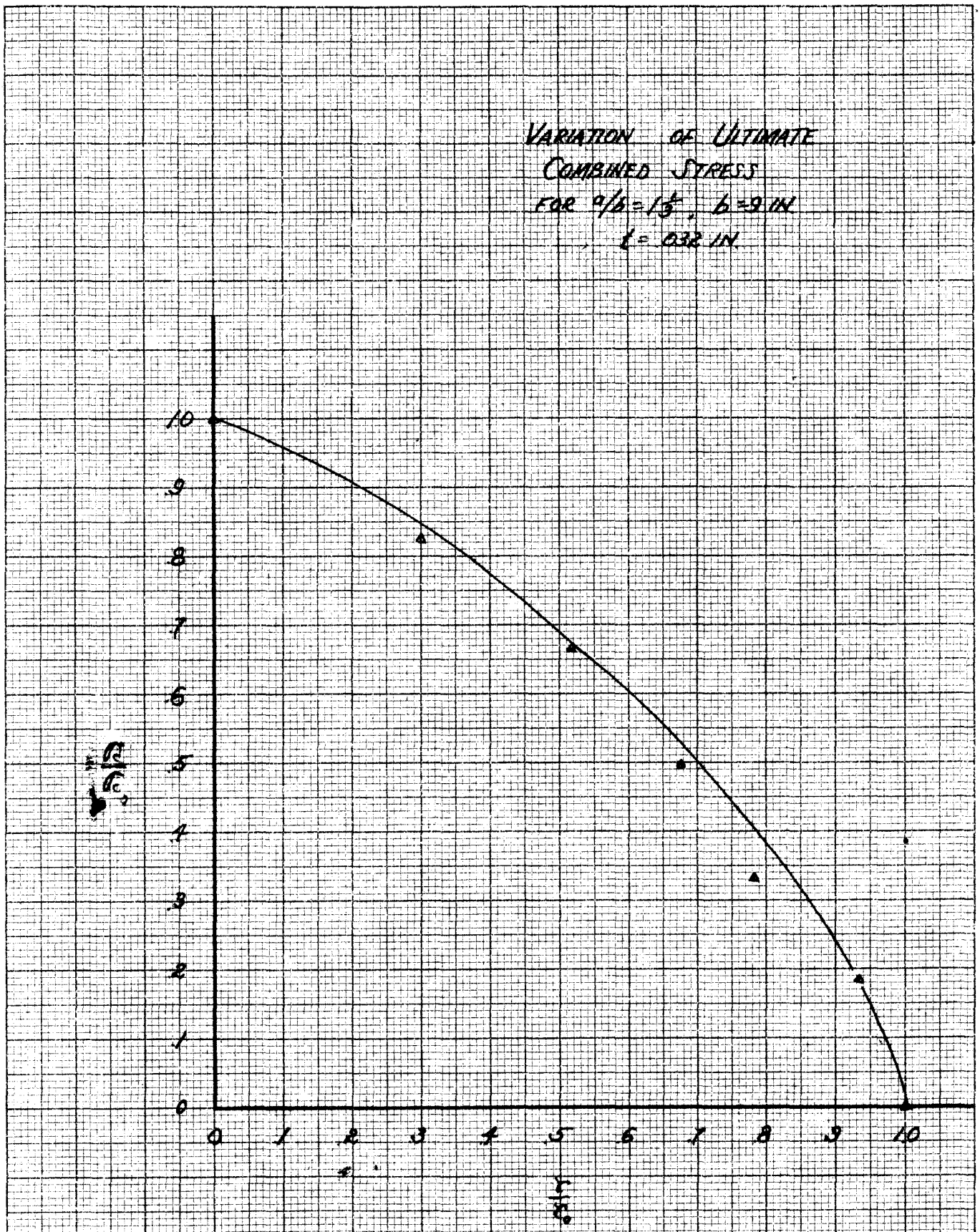
VARIATION OF ULTIMATE
COMBINED STRESS
FOR $\ell/b = 15$, $b = 9$ IN
$t = .032$ IN.
$\frac{\sigma_2}{\sigma_{c_2}}$
$\frac{\sigma_1}{\sigma_{c_1}}$
0
1
2
3
4
5
6
7
8
9
10

FIG. 12

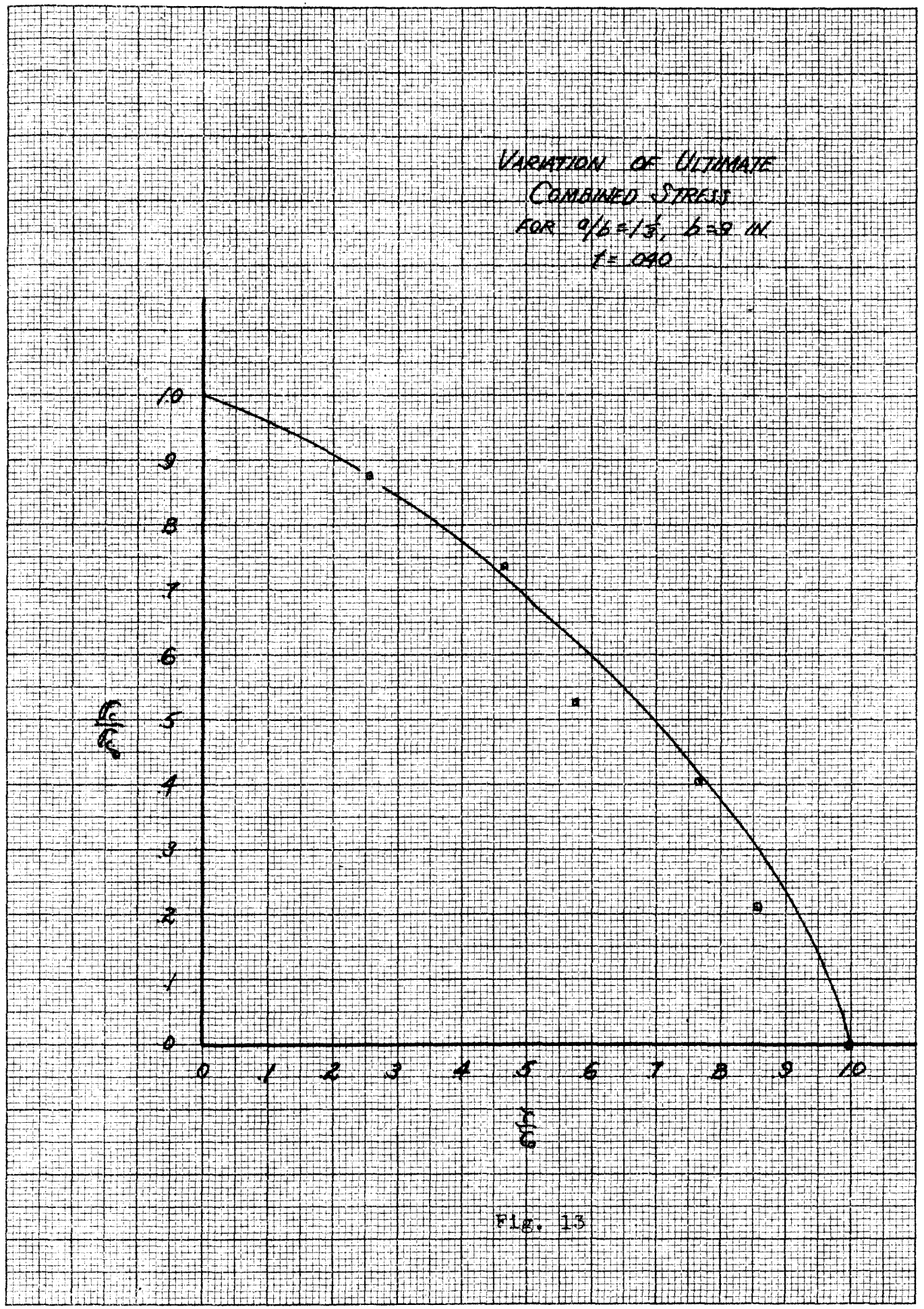
VARIATION OF ULTIMATE COMBINED STRESS
FOR g/b = 1/3, b = 9 IN.
t = .040
10
9
8
7
6
5
4
3
2
1
0
0
1
2
3
4
5
6
7
8
9
10

Fig. 13

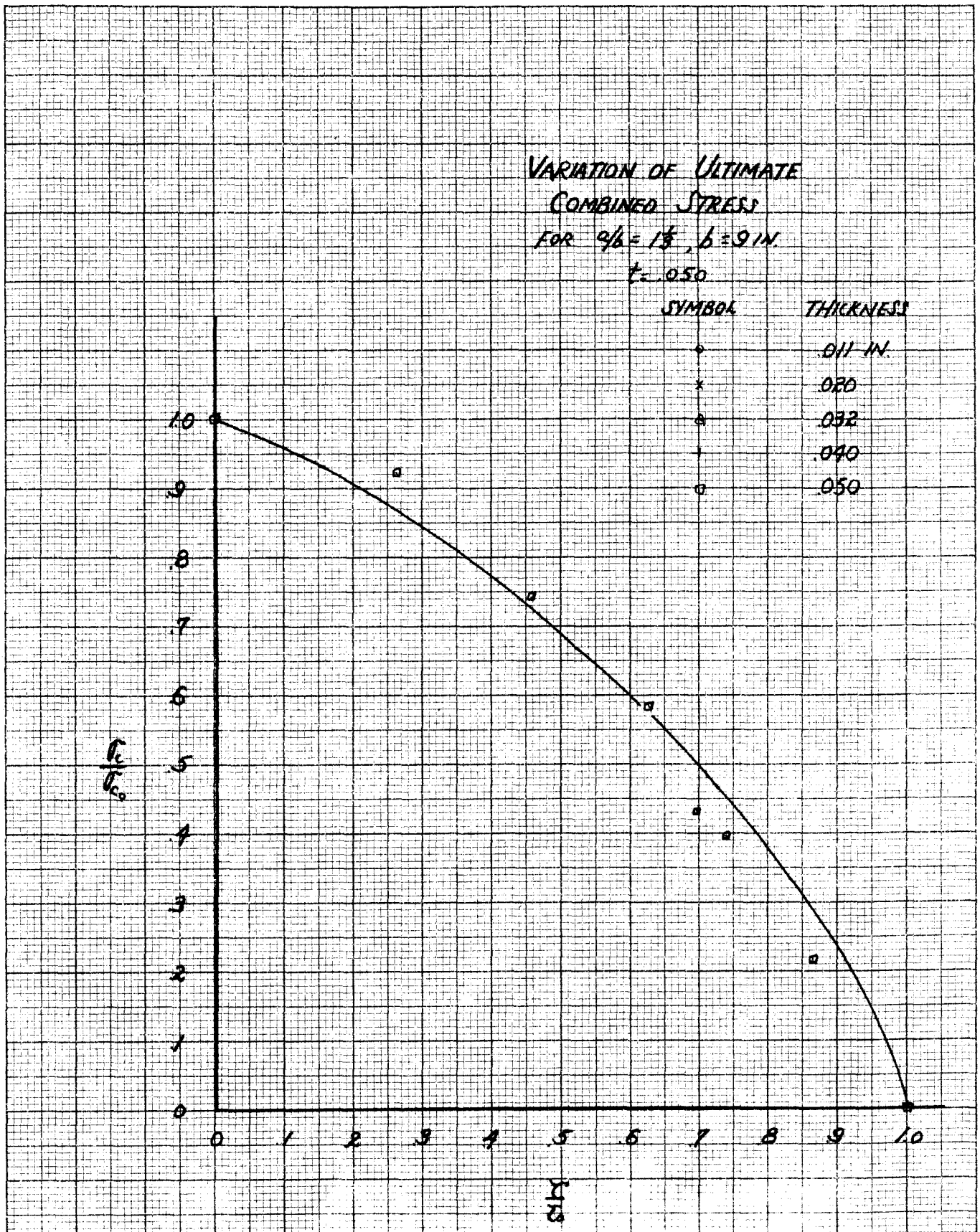
VARIATION OF ULTIMATE
COMBINED STRESS
FOR a/b = 1⅓ , b = 9 IN.
t = .050
SYMBOL
THICKNESS
.011 IN.
.020
.032
.040
.050
1.0
.9
.8
.7
.6
.5
.4
.3
.2
.1
0
$\frac{f_c}{f_{c_0}}$
0
.1
.2
.3
.4
.5
.6
.7
.8
.9
1.0
$\frac{f_c}{f_{c_0}}$

Fig. 14

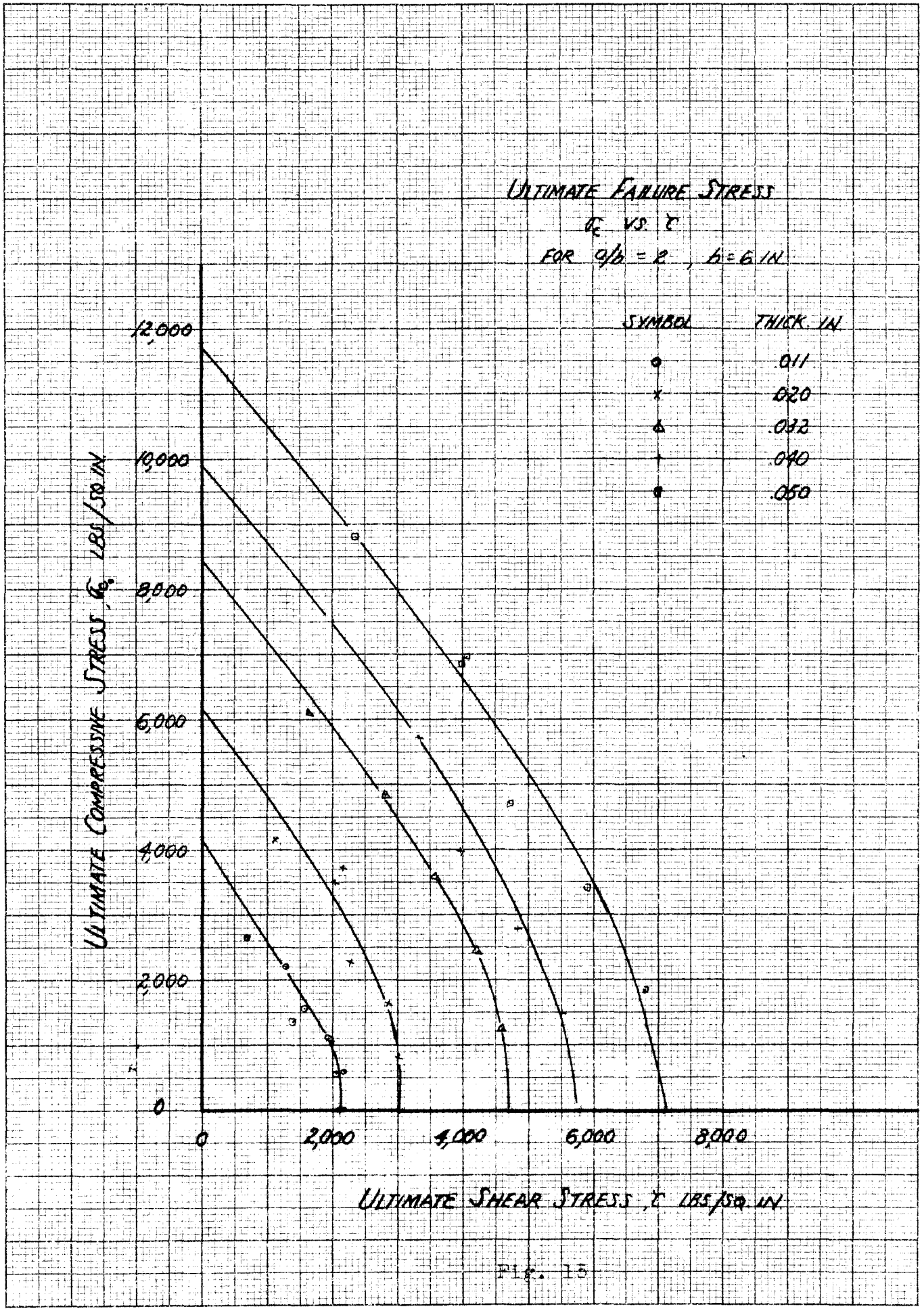
ULTIMATE FAILURE STRESS
σ_c VS. τ
FOR a/b = 2 , b = 6 IN.
SYMBOL
THICK IN
.011
.020
.032
.040
.050
12,000
10,000
8,000
6,000
4,000
2,000
0
ULTIMATE COMPRESSIVE STRESS, σ_c LBS/SQ IN
0
2,000
4,000
6,000
8,000
ULTIMATE SHEAR STRESS, τ LBS/SQ IN

Fig. 15

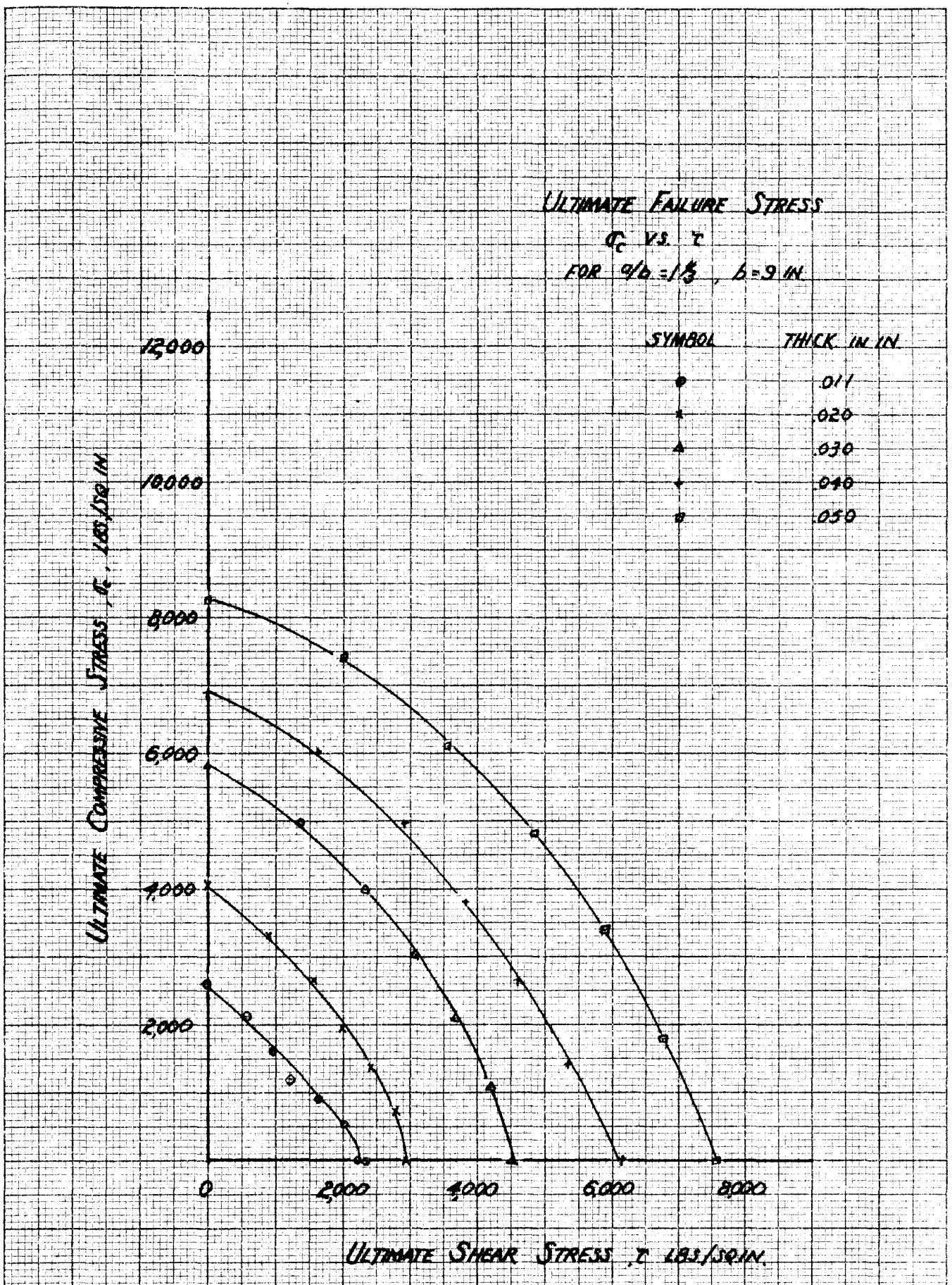
ULTIMATE FAILURE STRESS
σ_c VS. τ
FOR a/b = 1/3, b = 9 IN.
SYMBOL
THICK IN IN
.011
.020
.030
.040
.050
12,000
10,000
8,000
6,000
4,000
2,000
0
2,000
4,000
6,000
8,000
ULTIMATE COMPRESSIVE STRESS, σ_c, LBS/SQ IN.
ULTIMATE SHEAR STRESS, τ LBS/SQ IN.

Fig. 16

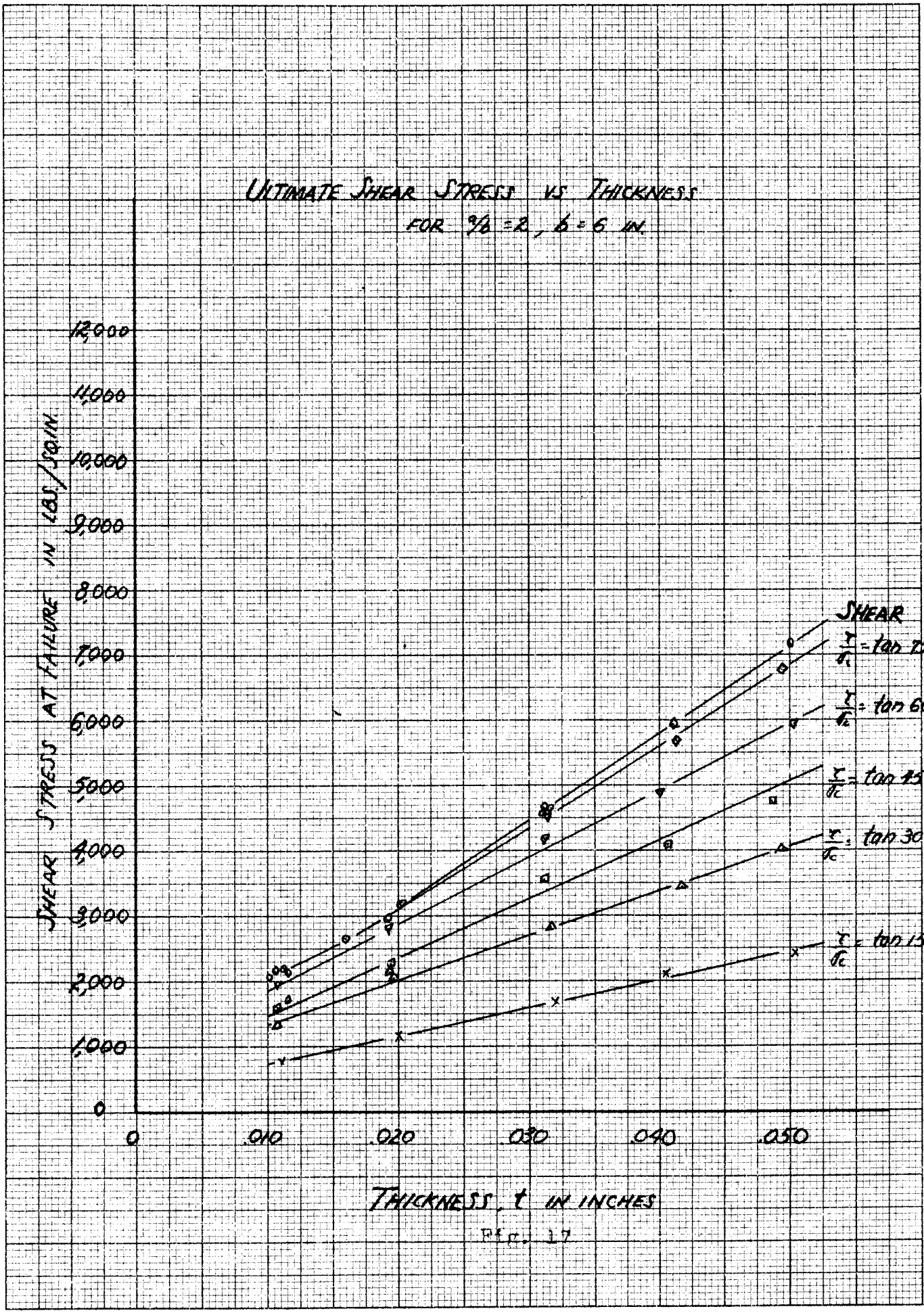
ULTIMATE SHEAR STRESS VS THICKNESS
FOR a/b = 2, b = 6 IN.
SHEAR STRESS AT FAILURE IN LBS/SQ.IN.
12,000
11,000
10,000
9,000
8,000
7,000
6,000
5,000
4,000
3,000
2,000
1,000
0
0
.010
.020
.030
.040
.050
THICKNESS, t IN INCHES
SHEAR
τ/σc = tan 75°
τ/σc = tan 60°
τ/σc = tan 45°
τ/σc = tan 30°
τ/σc = tan 15°

Fig. 17

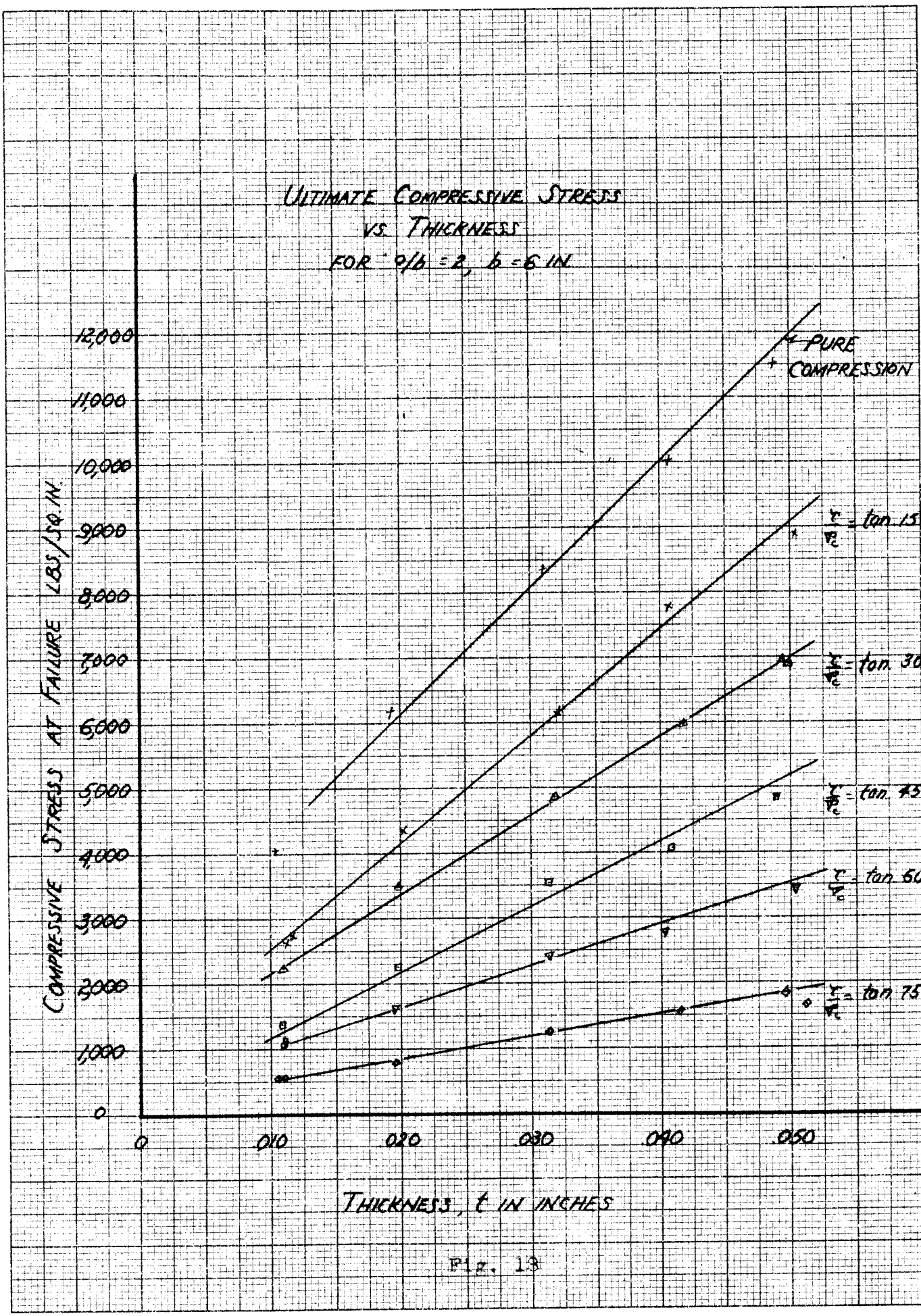
ULTIMATE COMPRESSIVE STRESS
VS. THICKNESS
FOR a/b = 2, b = 6 IN.
PURE COMPRESSION
τ/σc = tan 15°
τ/σc = tan 30°
τ/σc = tan 45°
τ/σc = tan 60°
τ/σc = tan 75°
COMPRESSIVE STRESS AT FAILURE LBS./SQ. IN.
12,000
11,000
10,000
9000
8000
7000
6000
5000
4000
3000
2000
1000
0
0
.010
.020
.030
.040
.050
THICKNESS, t IN INCHES

Fig. 13

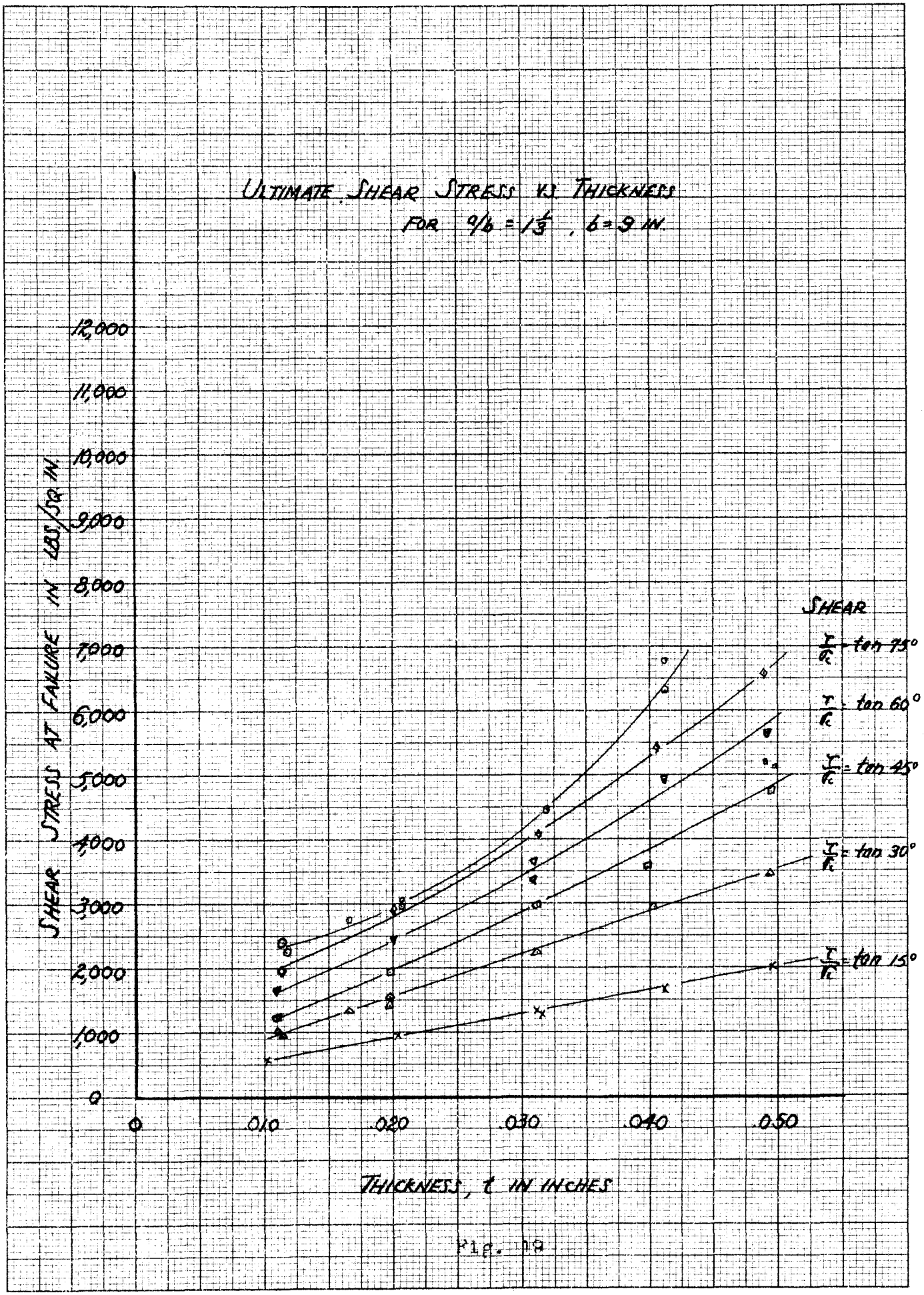
ULTIMATE SHEAR STRESS VS. THICKNESS
FOR a/b = 1/3 , b = 9 IN.
SHEAR STRESS AT FAILURE IN LBS/SQ IN
12,000
11,000
10,000
9,000
8,000
7,000
6,000
5,000
4,000
3,000
2,000
1,000
0
0
.010
.020
.030
.040
.050
THICKNESS, t IN INCHES
SHEAR
τ/f_c = tan 75°
τ/f_c = tan 60°
τ/f_c = tan 45°
τ/f_c = tan 30°
τ/f_c = tan 15°

Fig. 19

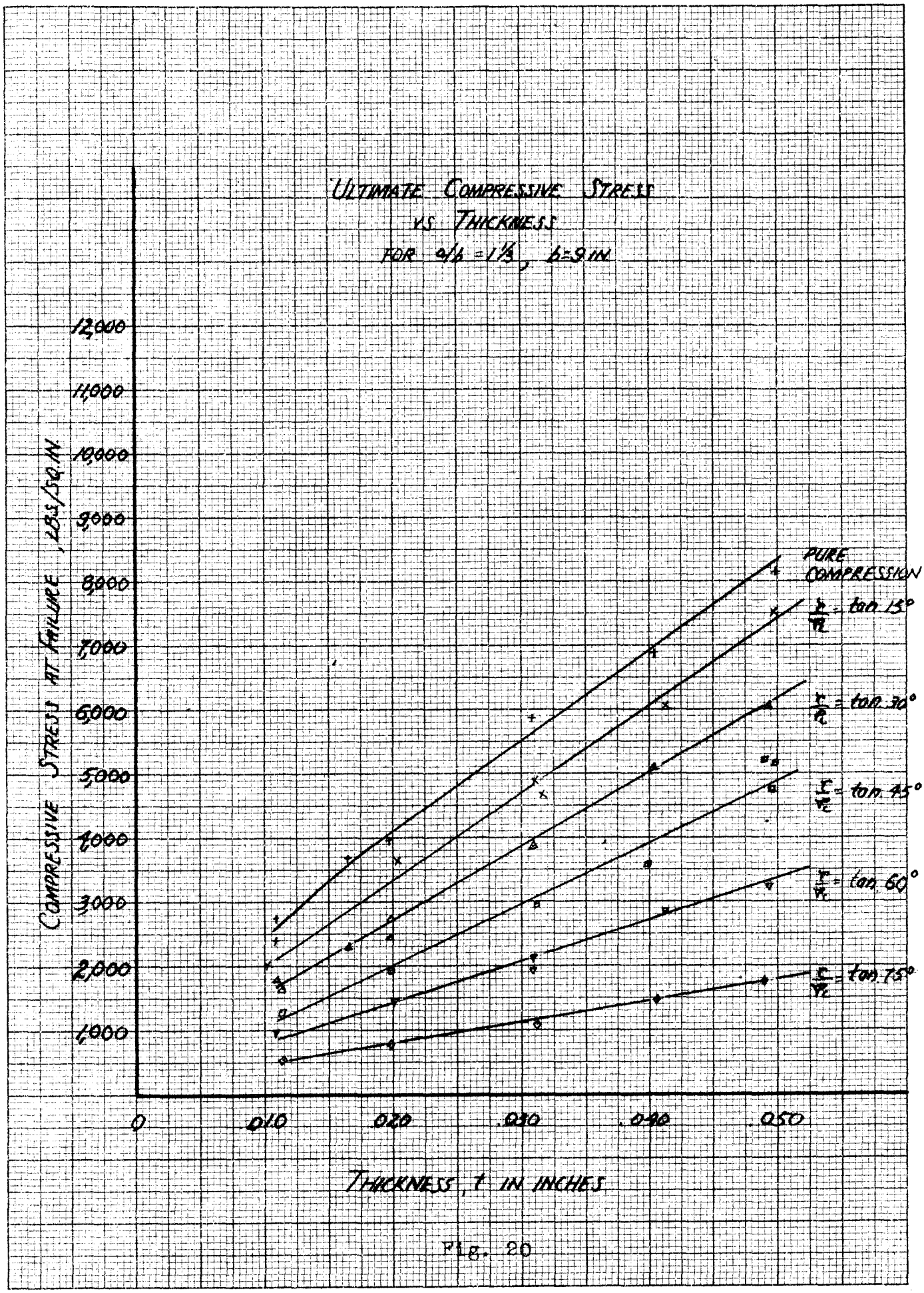
ULTIMATE COMPRESSIVE STRESS
VS THICKNESS
FOR a/b = 1/3, b=9 IN.
COMPRESSIVE STRESS AT FAILURE, LBS/SQ.IN.
12,000
11,000
10,000
9,000
8,000
7,000
6,000
5,000
4,000
3,000
2,000
1,000
0
.010
.020
.030
.040
.050
THICKNESS, t IN INCHES
PURE COMPRESSION
r/rc = tan 15°
r/rc = tan 30°
r/rc = tan 45°
r/rc = tan 60°
r/rc = tan 75°

Fig. 20

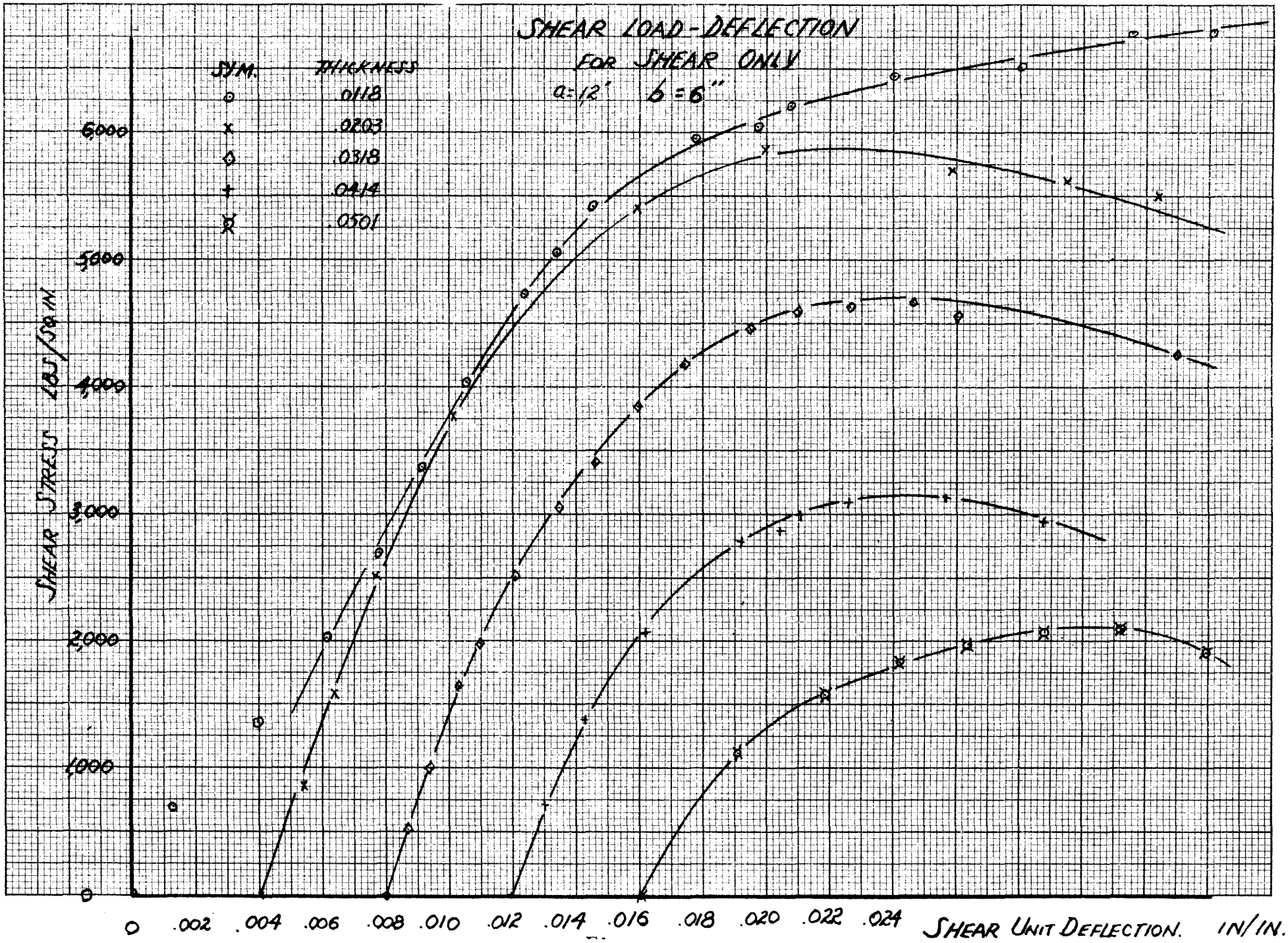
SHEAR LOAD-DEFLECTION
FOR SHEAR ONLY
a=12" b=6"
SYM. THICKNESS
.0118
.0203
.0318
.0414
.0501
SHEAR STRESS LBS/SQ IN
6000
5000
4000
3000
2000
1000
0
0 .002 .004 .006 .008 .010 .012 .014 .016 .018 .020 .022 .024
SHEAR UNIT DEFLECTION. IN/IN.

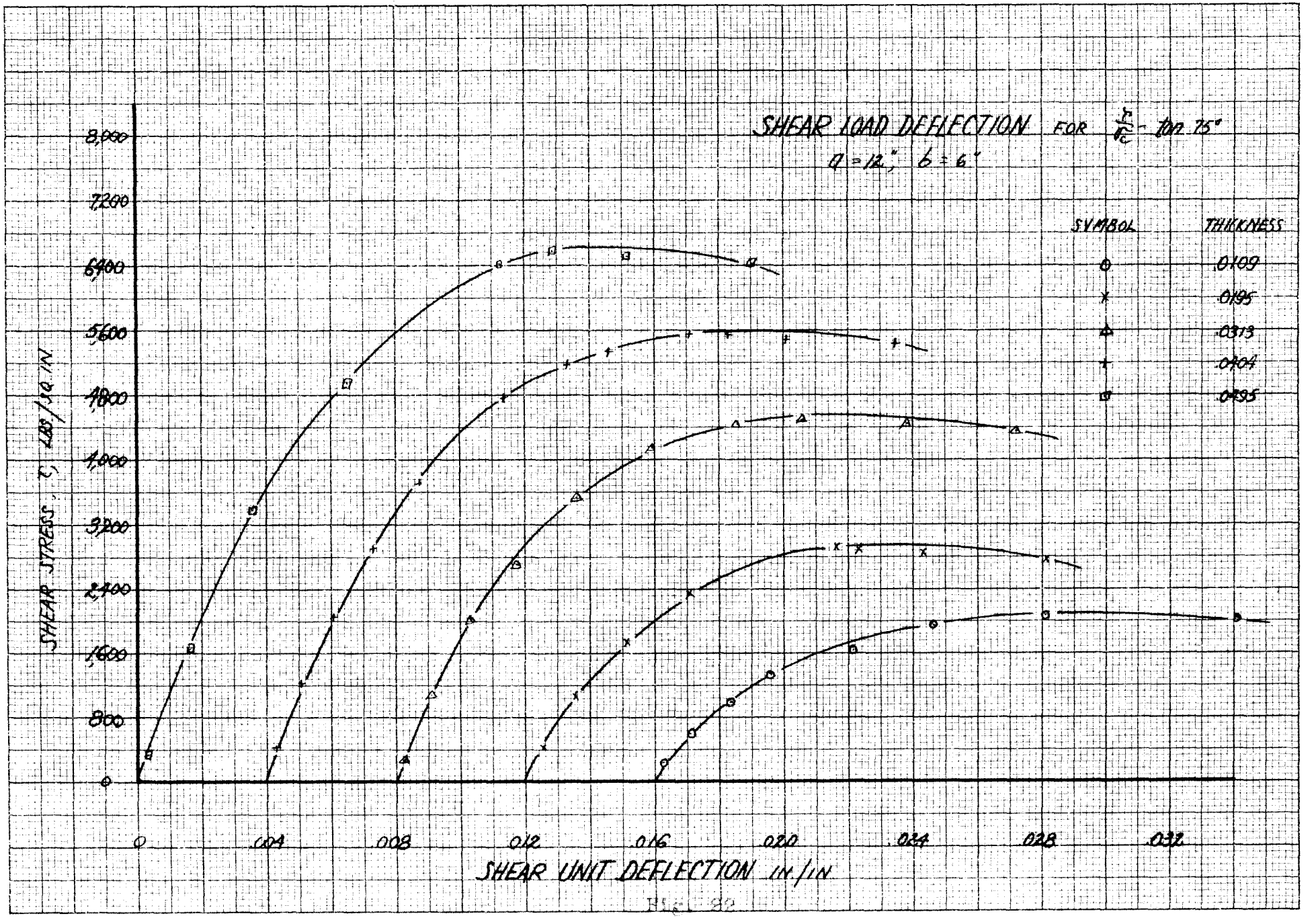
SHEAR LOAD DEFLECTION FOR $\frac{a}{\rho_c}$ = TAN 75°
a = 12", b = 6"
SYMBOL
THICKNESS
0 .0109
X .0195
Δ .0373
+ .0404
□ .0495
SHEAR STRESS, τ, LBS/SQ IN
8,000
7200
6400
5600
4800
4000
3200
2400
1600
800
0
0
.004
.008
.012
.016
.020
.024
.028
.032
SHEAR UNIT DEFLECTION IN/IN

Fig. 30

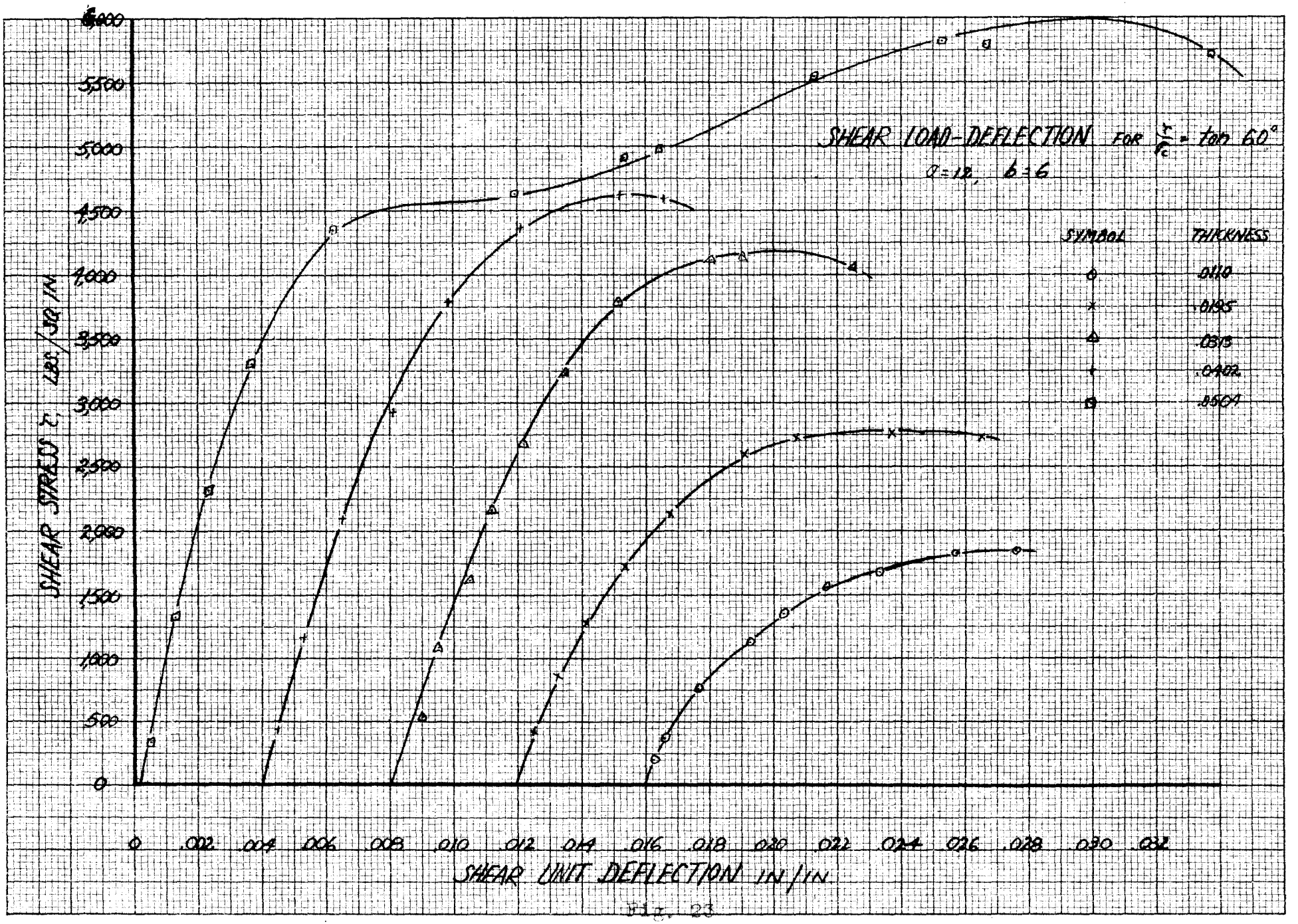
SHEAR LOAD-DEFLECTION FOR $\frac{\tau}{\sigma_c}$ = tan 60°
ℓ = 12, b = 6
SYMBOL
THICKNESS
0110
.0195
.0315
.0402
.0504
SHEAR STRESS τ, LBS/SQ IN
6000
5500
5000
4500
4000
3500
3000
2500
2000
1500
1000
500
0
0
.002
.004
.006
.008
.010
.012
.014
.016
.018
.020
.022
.024
.026
.028
.030
.032
SHEAR UNIT DEFLECTION IN/IN.

Fig. 23

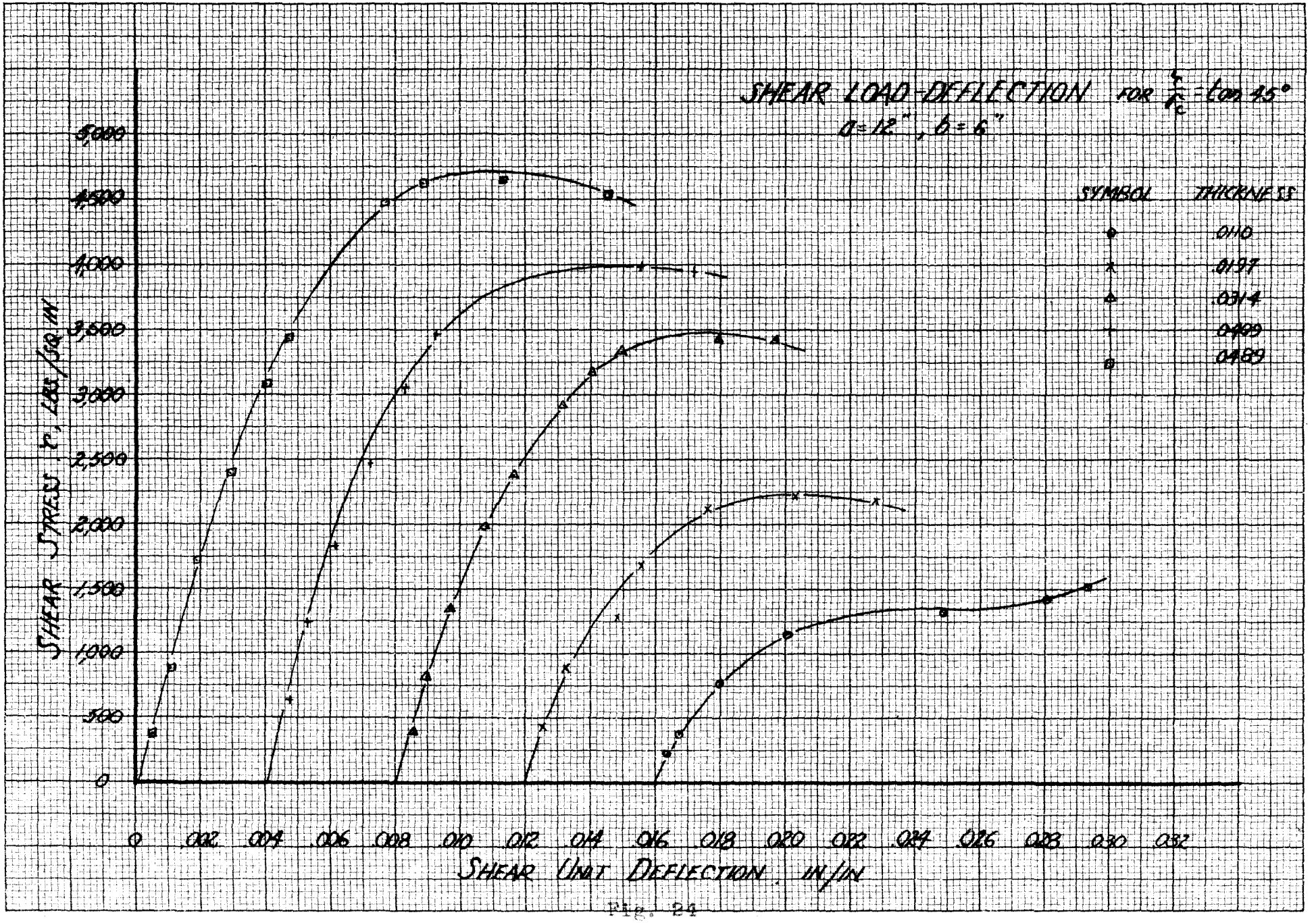
SHEAR LOAD-DEFLECTION FOR $\frac{t}{r_c}$ = tan 15°
a = 12", b = 6"
SYMBOL
THICKNESS
.0110
.0197
.0314
.0409
.0489
SHEAR STRESS τ, LBS/SQ IN
5,000
4,500
4,000
3,500
3,000
2,500
2,000
1,500
1,000
500
0
0
.002
.004
.006
.008
.010
.012
.014
.016
.018
.020
.022
.024
.026
.028
.030
.032
SHEAR UNIT DEFLECTION, IN/IN

Fig. 24

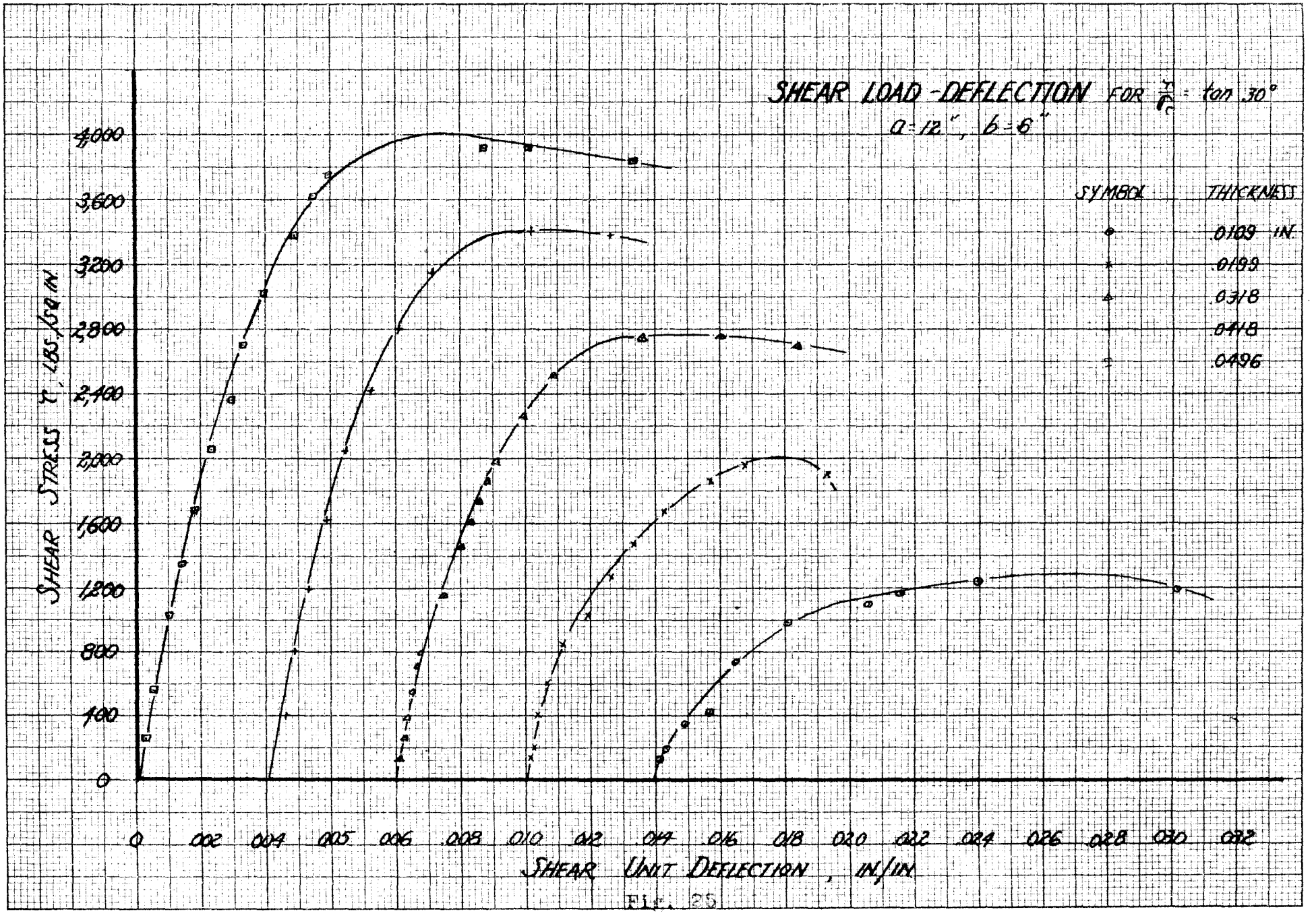
SHEAR LOAD - DEFLECTION FOR $\frac{\tau}{\sigma_c}$ = tan 30°
a = 12", b = 6"
SYMBOL
THICKNESS
.0109 IN.
.0199
.0318
.0418
.0496
SHEAR STRESS τ, LBS./SQ. IN.
4000
3600
3200
2800
2400
2000
1600
1200
800
400
0
0
.002
.004
.006
.008
.010
.012
.014
.016
.018
.020
.022
.024
.026
.028
.030
.032
SHEAR UNIT DEFLECTION, IN./IN.

Fig. 25

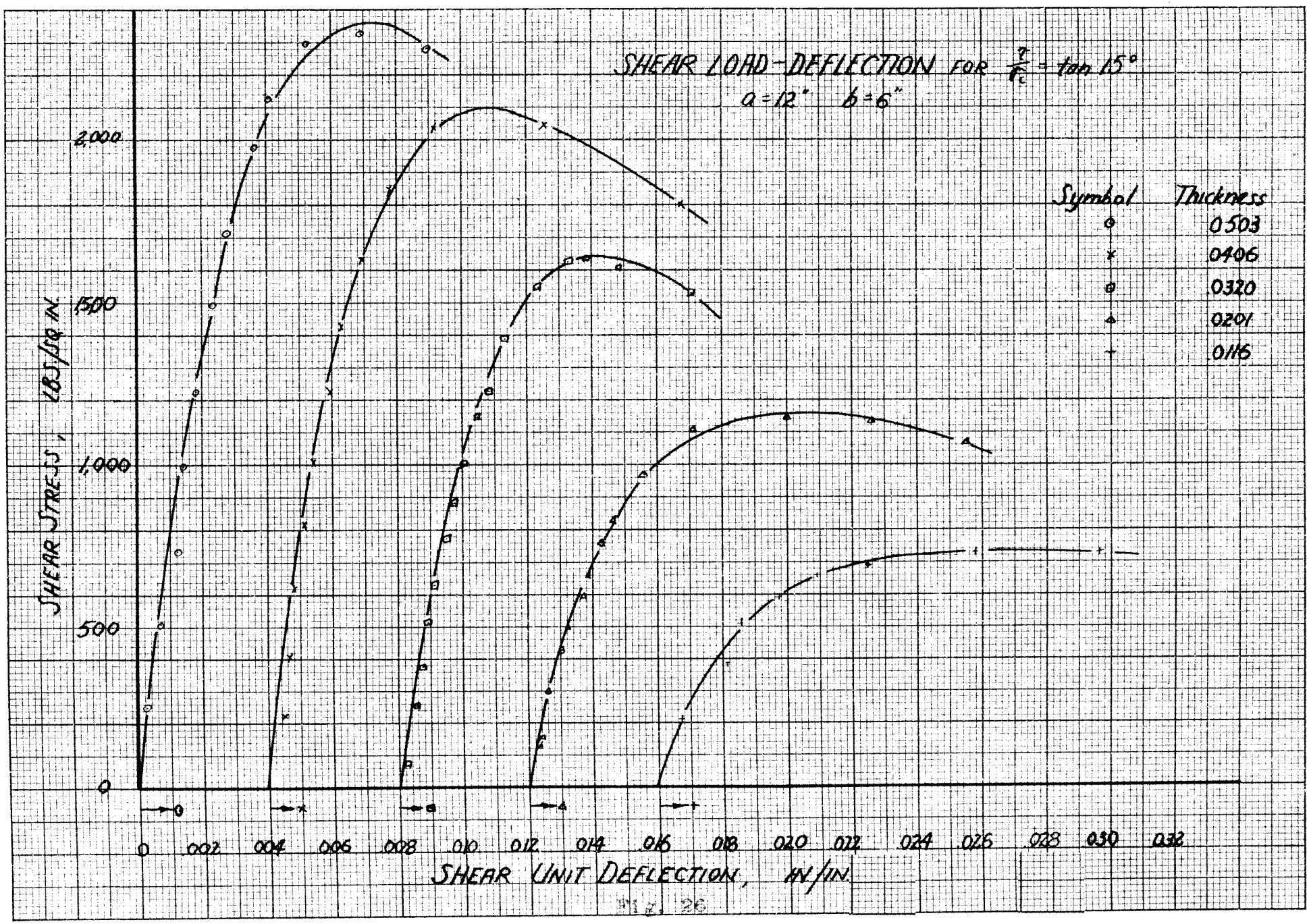
SHEAR LOAD-DEFLECTION FOR $\frac{?}{f_c}$ = tan 15°
a = 12" b = 6"
Symbol Thickness
0503
0406
0320
0201
0116
SHEAR STRESS, LBS/SQ IN
2,000
1,500
1,000
500
0
0 002 004 006 008 010 012 014 016 018 020 022 024 026 028 030 032
SHEAR UNIT DEFLECTION, IN/IN.

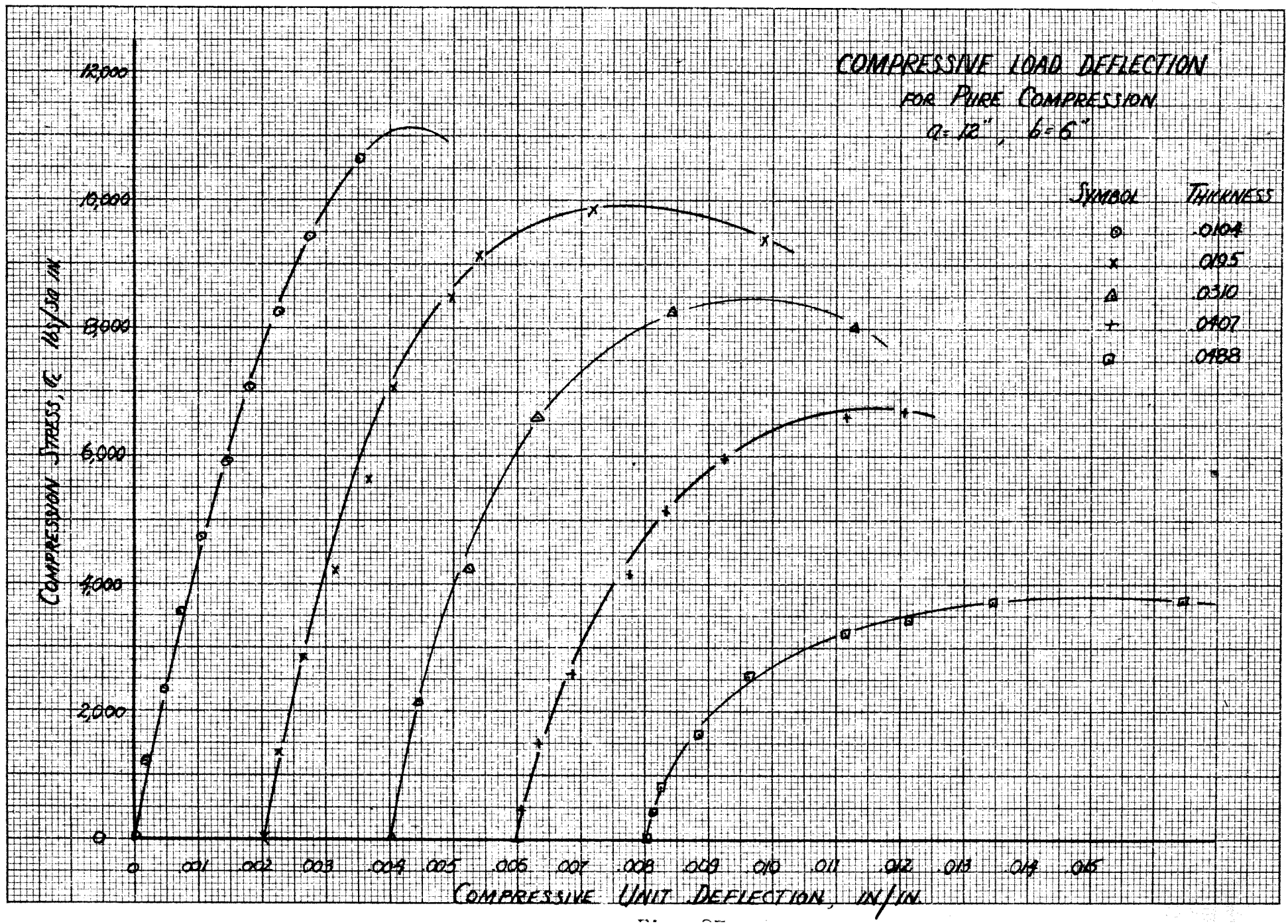
COMPRESSIVE LOAD DEFLECTION
FOR PURE COMPRESSION
a = 12", b = 6"
SYMBOL
THICKNESS
.0104
.0195
.0310
.0407
.0488
COMPRESSION STRESS, σc lbs/sq in
12,000
10,000
8,000
6,000
4,000
2,000
0
.001
.002
.003
.004
.005
.006
.007
.008
.009
.010
.011
.012
.013
.014
.015
COMPRESSIVE UNIT DEFLECTION, IN/IN

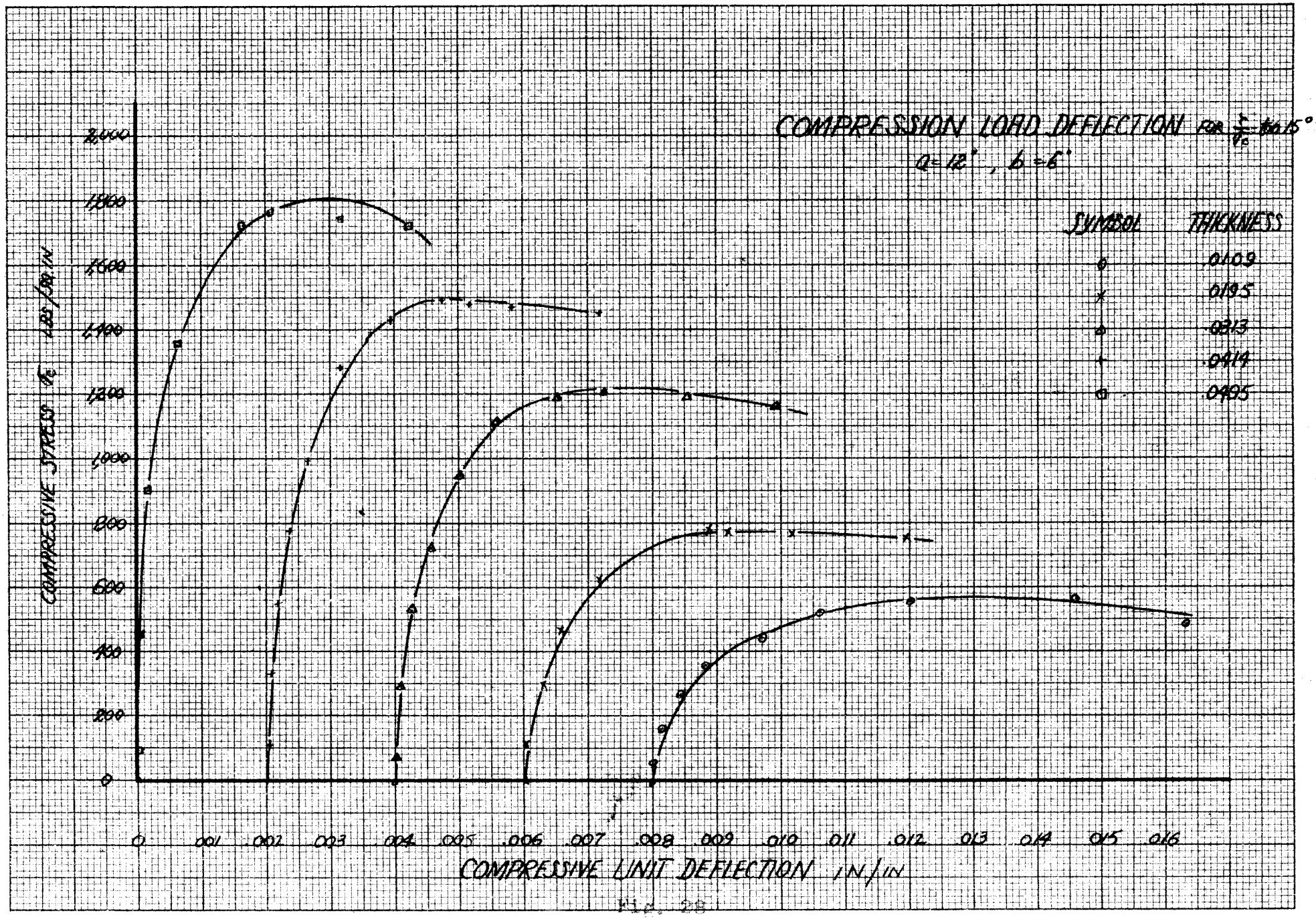
COMPRESSION LOAD DEFLECTION FOR $\frac{r}{t_0}$ = 166.6°
a = 12", b = 6"
SYMBOL THICKNESS
0 .0109
X .0195
Δ .0213
+ .0414
□ .0495
COMPRESSIVE STRESS $\frac{P}{A_0}$ LBS/SQ. IN.
2,000
1800
1600
1400
1200
1000
800
600
400
200
0
0 .001 .002 .003 .004 .005 .006 .007 .008 .009 .010 .011 .012 .013 .014 .015 .016
COMPRESSIVE UNIT DEFLECTION, IN/IN

Fig. 28

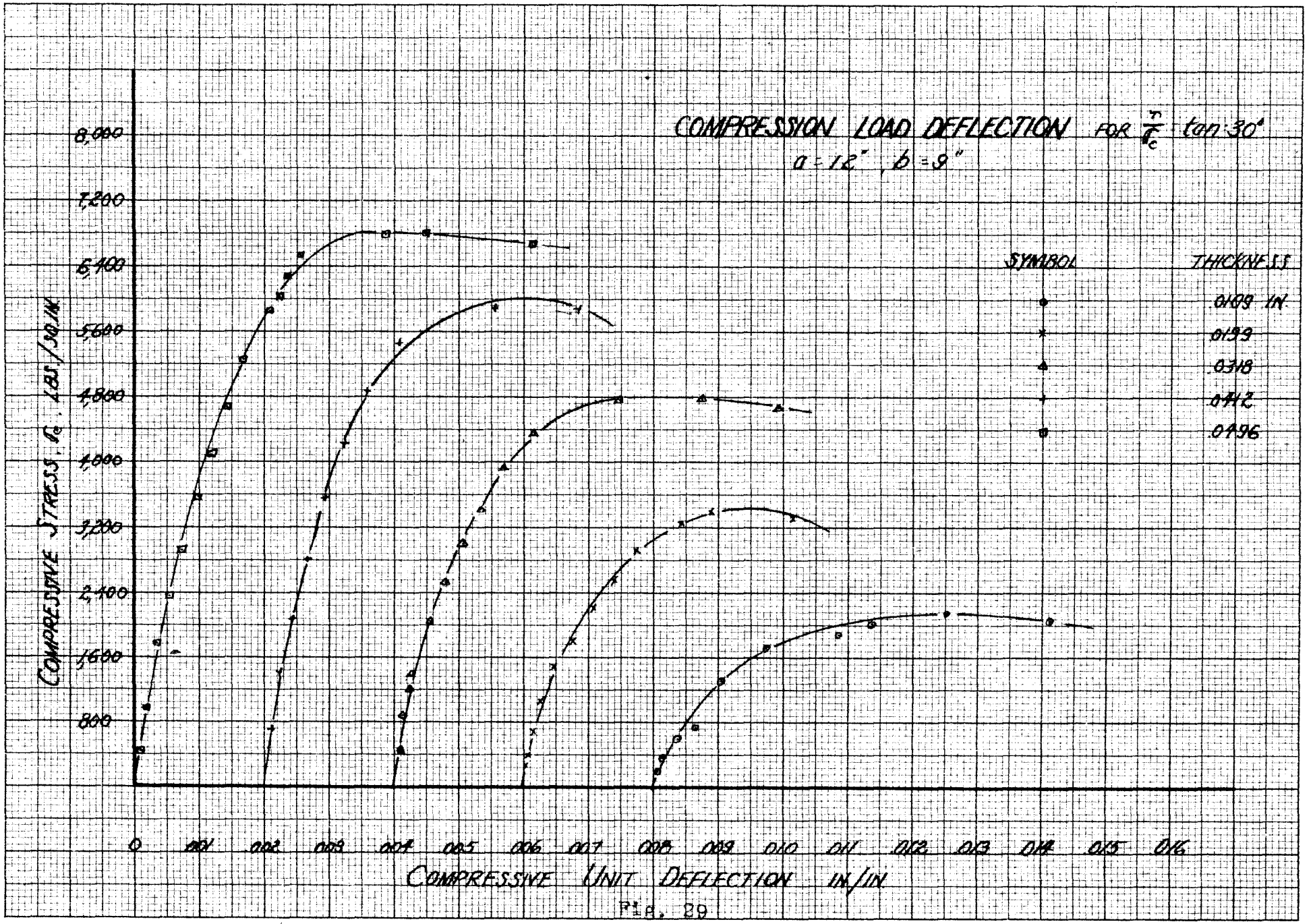
COMPRESSION LOAD DEFLECTION FOR $\frac{\sigma_r}{\sigma_c}$ tan 30°
a = 12", b = 8"
SYMBOL
THICKNESS
.0109 IN
.0193
.0318
.0412
.0496
COMPRESSIVE STRESS σ_c, LBS/SQ IN
8,000
7,200
6,400
5,600
4,800
4,000
3,200
2,400
1,600
800
0
.001
.002
.003
.004
.005
.006
.007
.008
.009
.010
.011
.012
.013
.014
.015
.016
COMPRESSIVE UNIT DEFLECTION IN/IN

Fig. 29

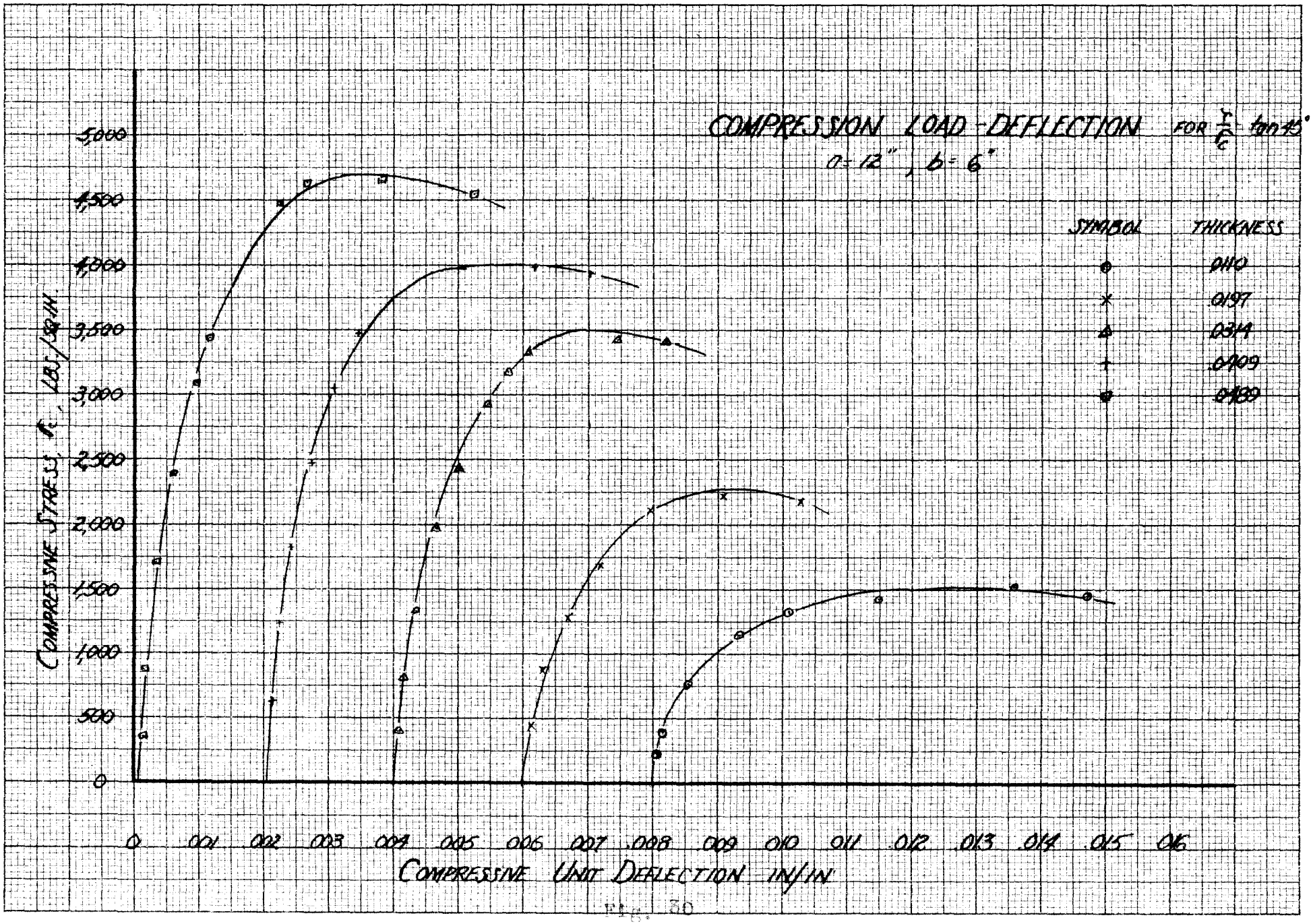
COMPRESSION LOAD-DEFLECTION FOR $\frac{t}{L}$ tan 45°
a = 12", b = 6"
SYMBOL
THICKNESS
.0110
.0197
.0314
.0709
.0980
COMPRESSIVE STRESS, f_c, LBS/SQ IN.
5,000
4,500
4,000
3,500
3,000
2,500
2,000
1,500
1,000
500
0
0
.001
.002
.003
.004
.005
.006
.007
.008
.009
.010
.011
.012
.013
.014
.015
.016
COMPRESSIVE UNIT DEFLECTION IN/IN

Fig. 30

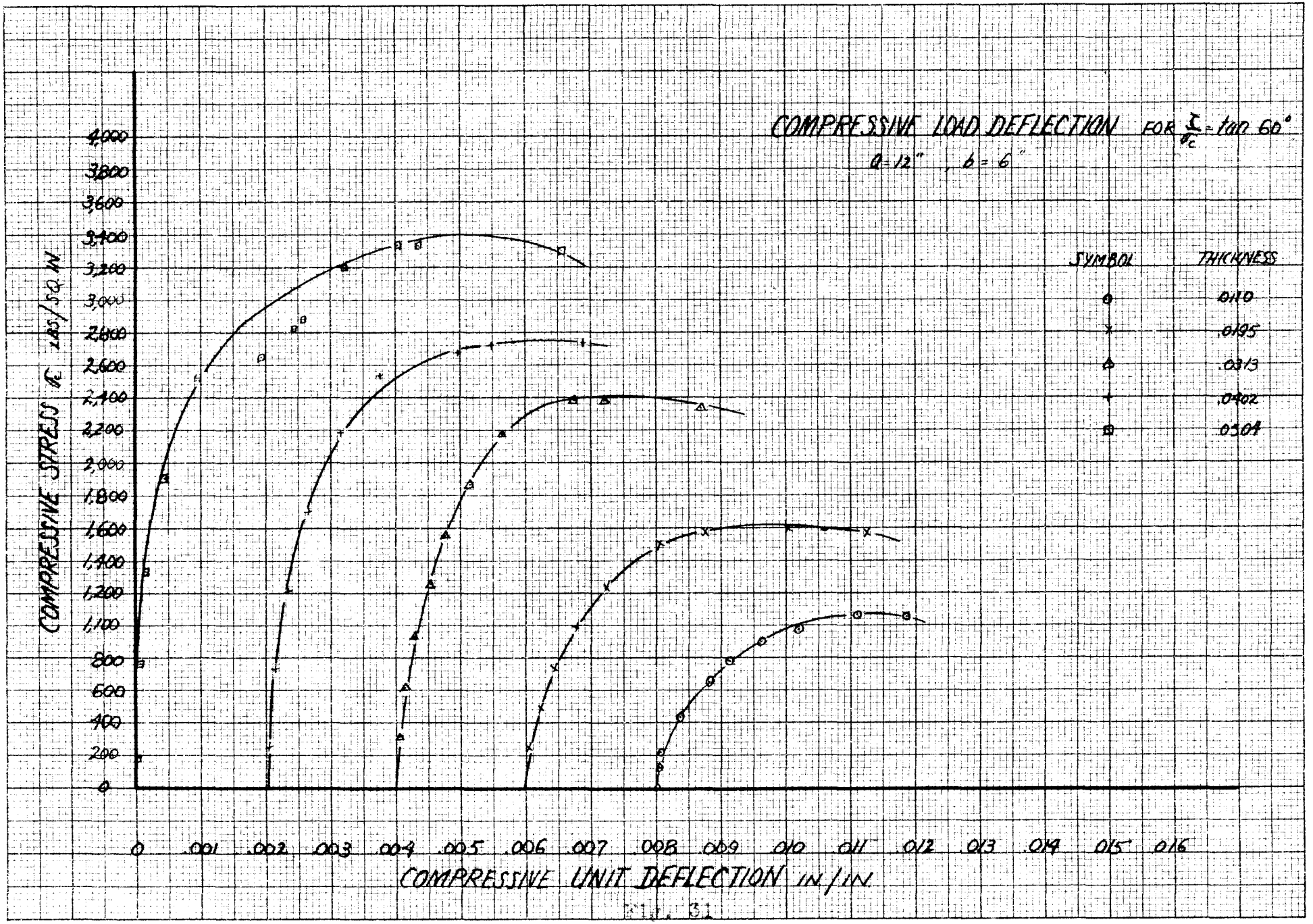
COMPRESSIVE LOAD DEFLECTION FOR $\frac{t}{a_c}$ = tan 60°
a = 12" , b = 6"
SYMBOL
THICKNESS
0110
.0195
.0313
.0402
.0504
COMPRESSIVE STRESS σ_c LBS/SQ IN
4,000
3,800
3,600
3,400
3,200
3,000
2,800
2,600
2,400
2,200
2,000
1,800
1,600
1,400
1,200
1,100
800
600
400
200
0
0 .001 .002 .003 .004 .005 .006 .007 .008 .009 .010 .011 .012 .013 .014 .015 .016
COMPRESSIVE UNIT DEFLECTION IN/IN

Fig. 31

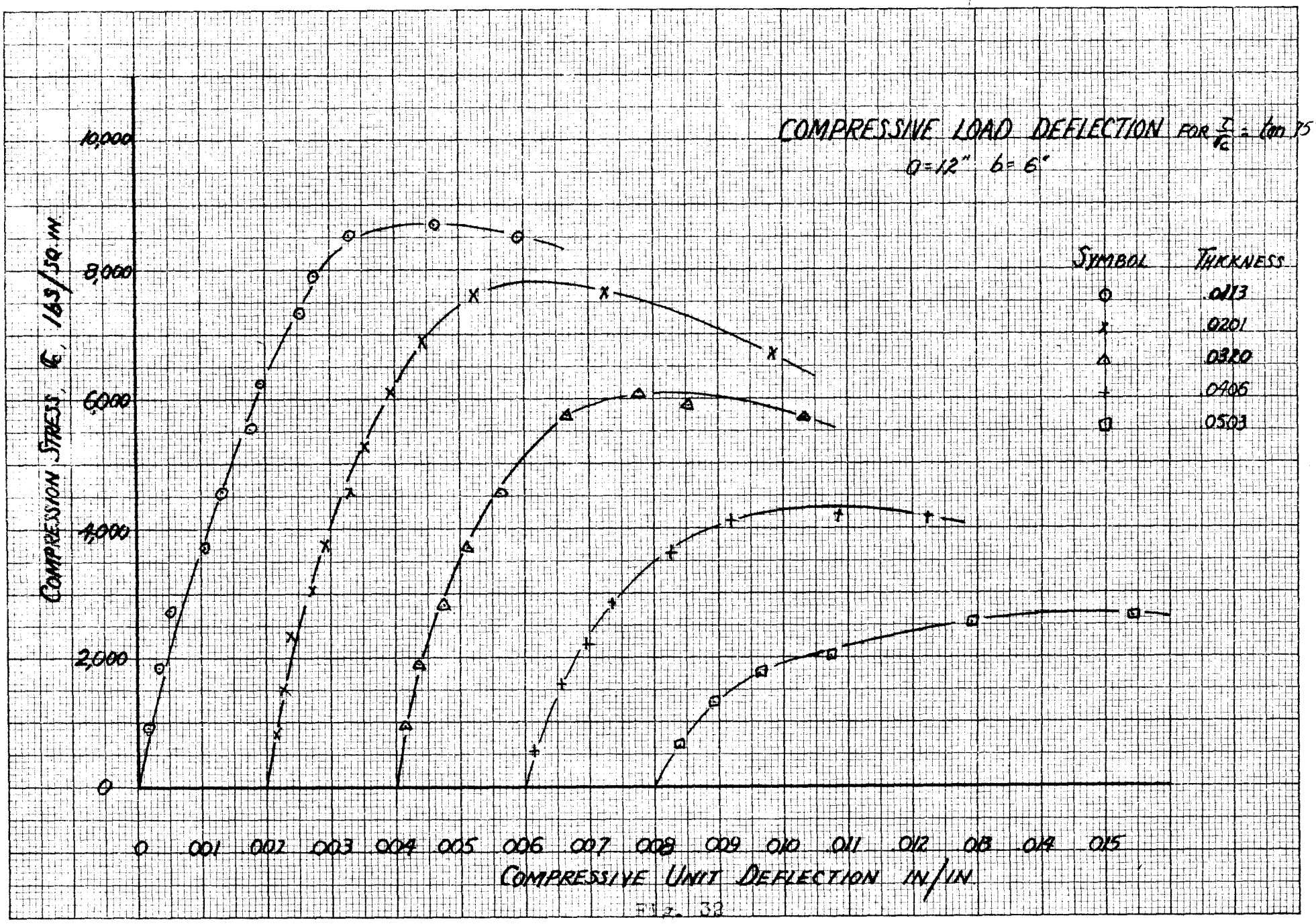
COMPRESSIVE LOAD DEFLECTION FOR $\frac{\tau}{\sigma_c} = \tan 75°$
θ = 12" b = 6"
SYMBOL
THICKNESS
.0113
.0201
.0320
.0406
.0503
COMPRESSION STRESS σ_c, LBS/SQ. IN.
10,000
8,000
6,000
4,000
2,000
0
0 .001 .002 .003 .004 .005 .006 .007 .008 .009 .010 .011 .012 .013 .014 .015
COMPRESSIVE UNIT DEFLECTION IN/IN

Fig. 38

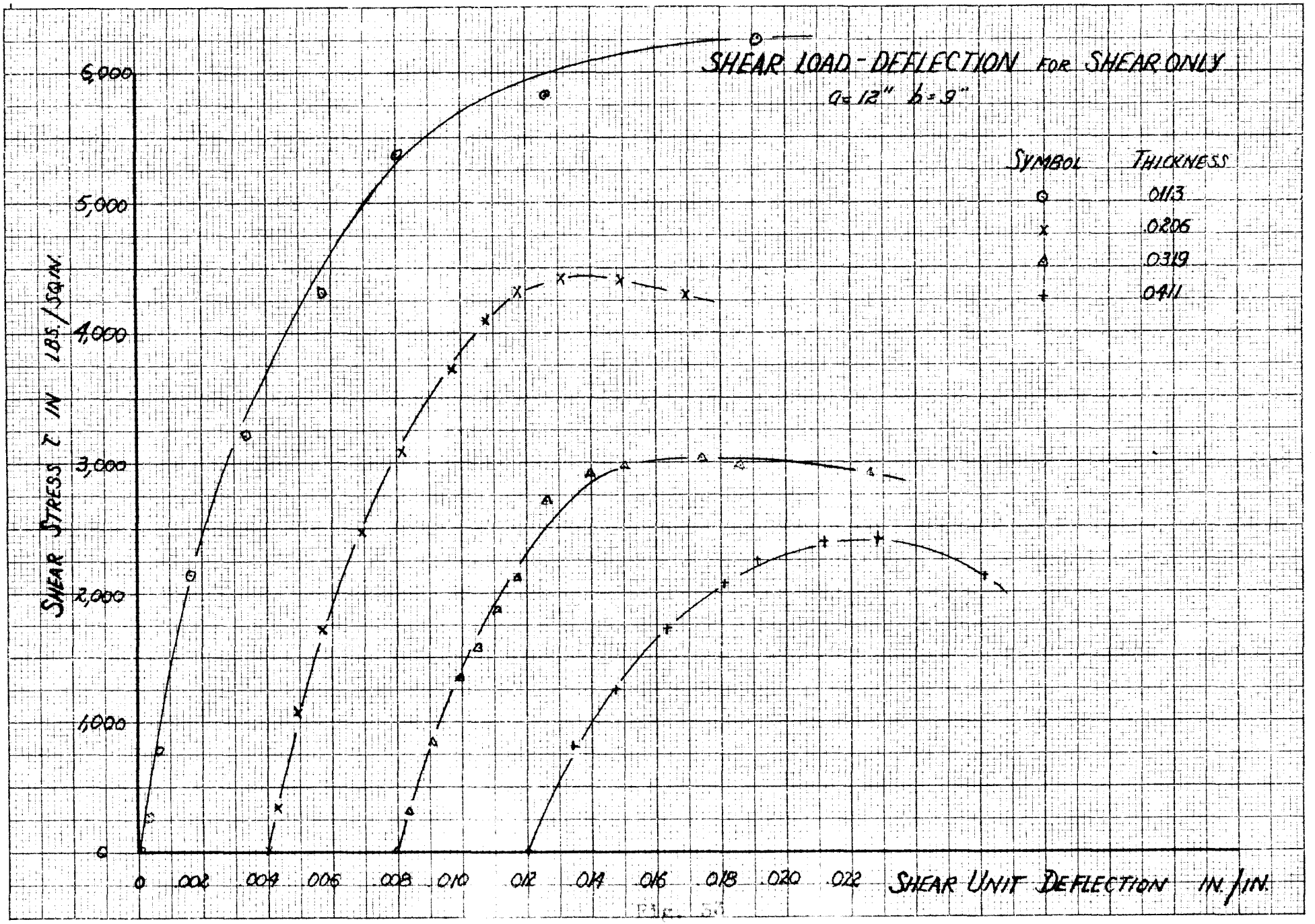
SHEAR LOAD - DEFLECTION FOR SHEAR ONLY
a = 12" h = 9"
SYMBOL
THICKNESS
0113
0206
0319
0411
SHEAR STRESS τ IN LBS./SQ.IN.
6,000
5,000
4,000
3,000
2,000
1,000
0
0
.002
.004
.006
.008
.010
.012
.014
.016
.018
.020
.022
SHEAR UNIT DEFLECTION IN./IN.

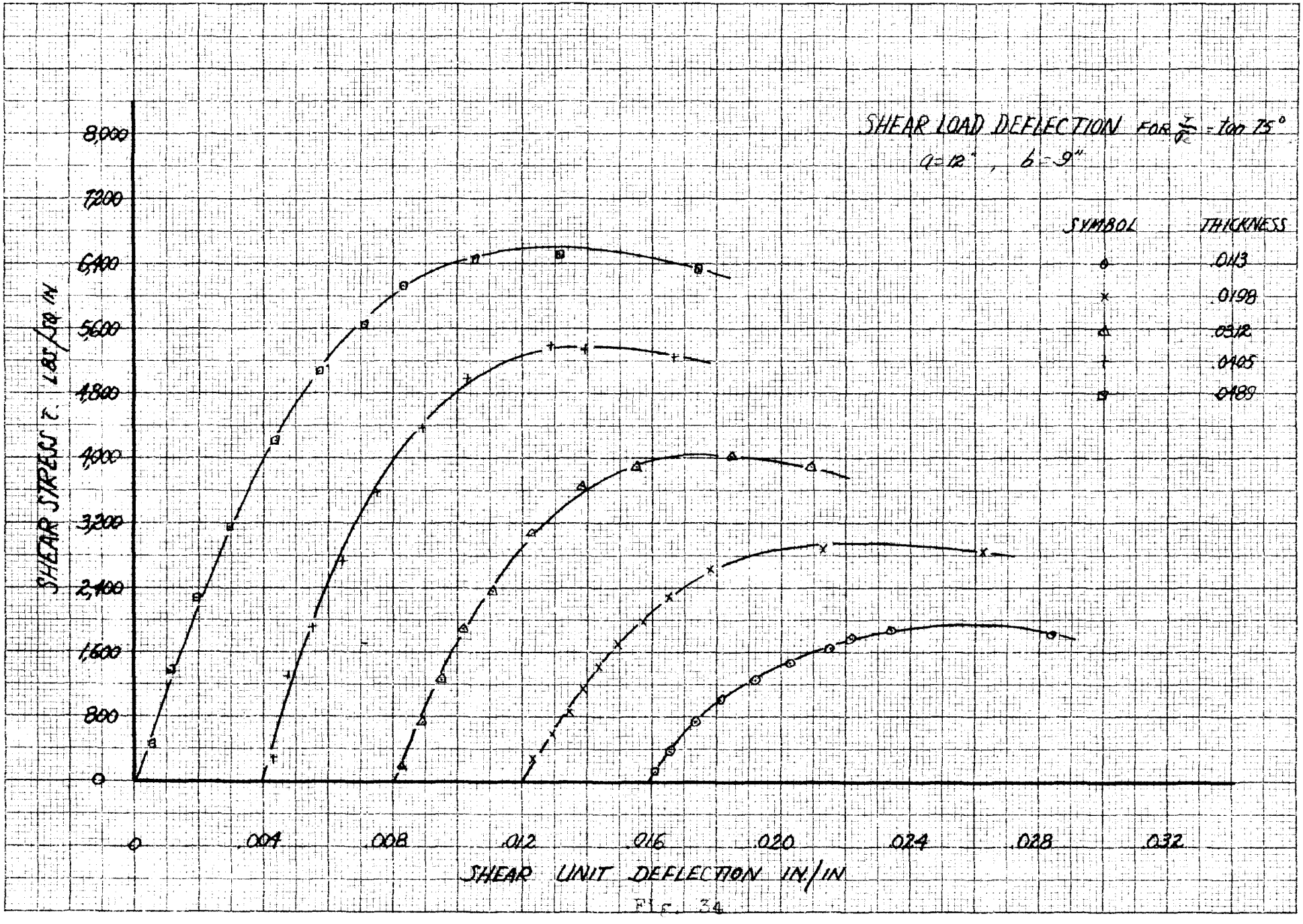
SHEAR LOAD DEFLECTION FOR $\frac{\tau}{\sigma_c}$ = tan 75°
a = 12", b = 9"
SYMBOL
THICKNESS
.043
.0198
.0312
.0105
.0189
SHEAR STRESS τ, LBS/SQ IN
8,000
7200
6,400
5600
4800
4000
3200
2,400
1,600
800
0
.004
.008
.012
.016
.020
.024
.028
.032
SHEAR UNIT DEFLECTION IN/IN

FIG. 34

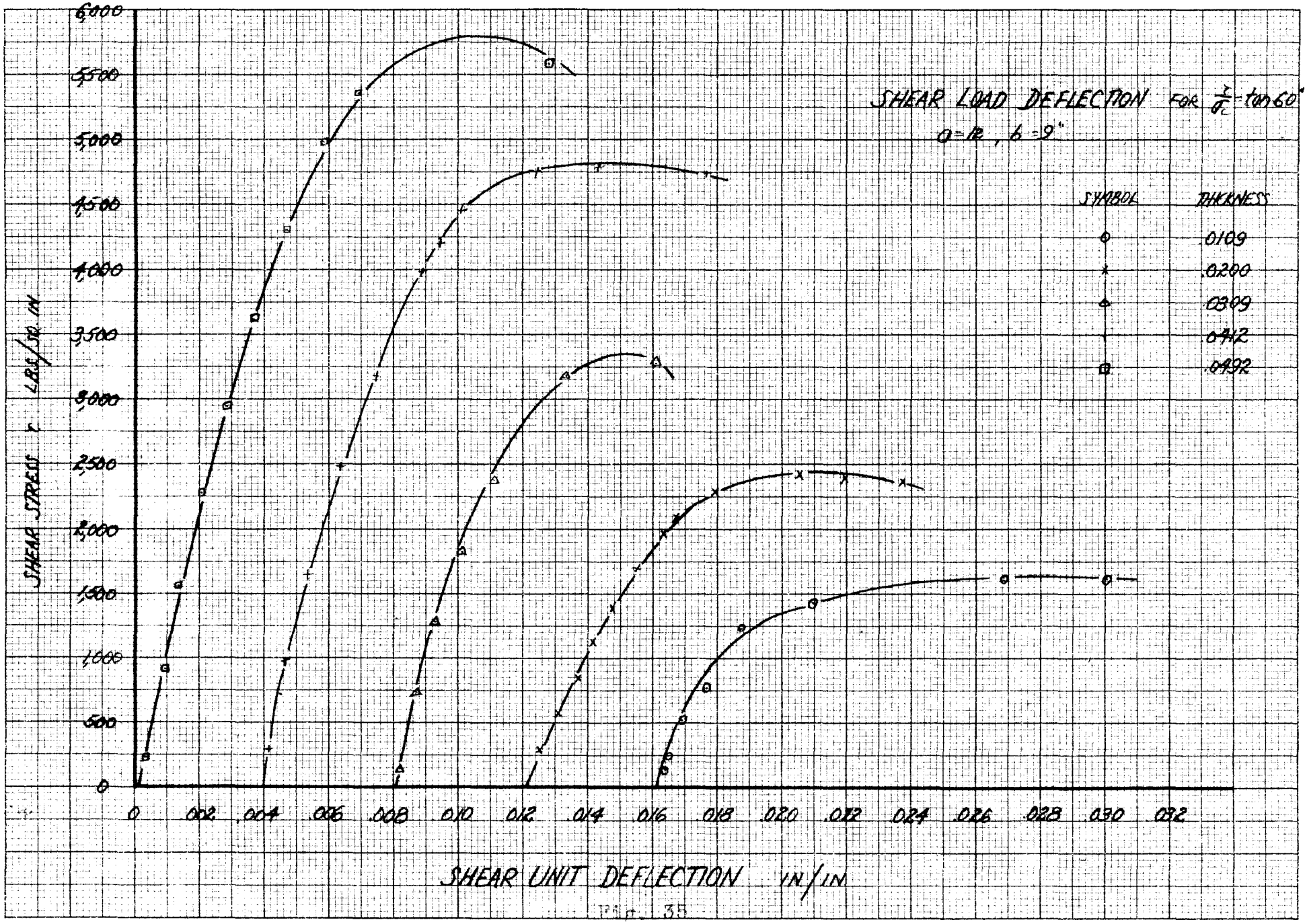
SHEAR LOAD DEFLECTION FOR $\frac{\tau}{\sigma_c} = \tan 60°$
a = 12, b = 9"
SYMBOL
THICKNESS
0 .0109
x .0200
Δ .0309
+ .0412
□ .0492
SHEAR STRESS τ LBS/SQ IN
6000
5500
5000
4500
4000
3500
3000
2500
2000
1500
1000
500
0
0
.002
.004
.006
.008
.010
.012
.014
.016
.018
.020
.022
.024
.026
.028
.030
.032
SHEAR UNIT DEFLECTION IN/IN

Plate 35

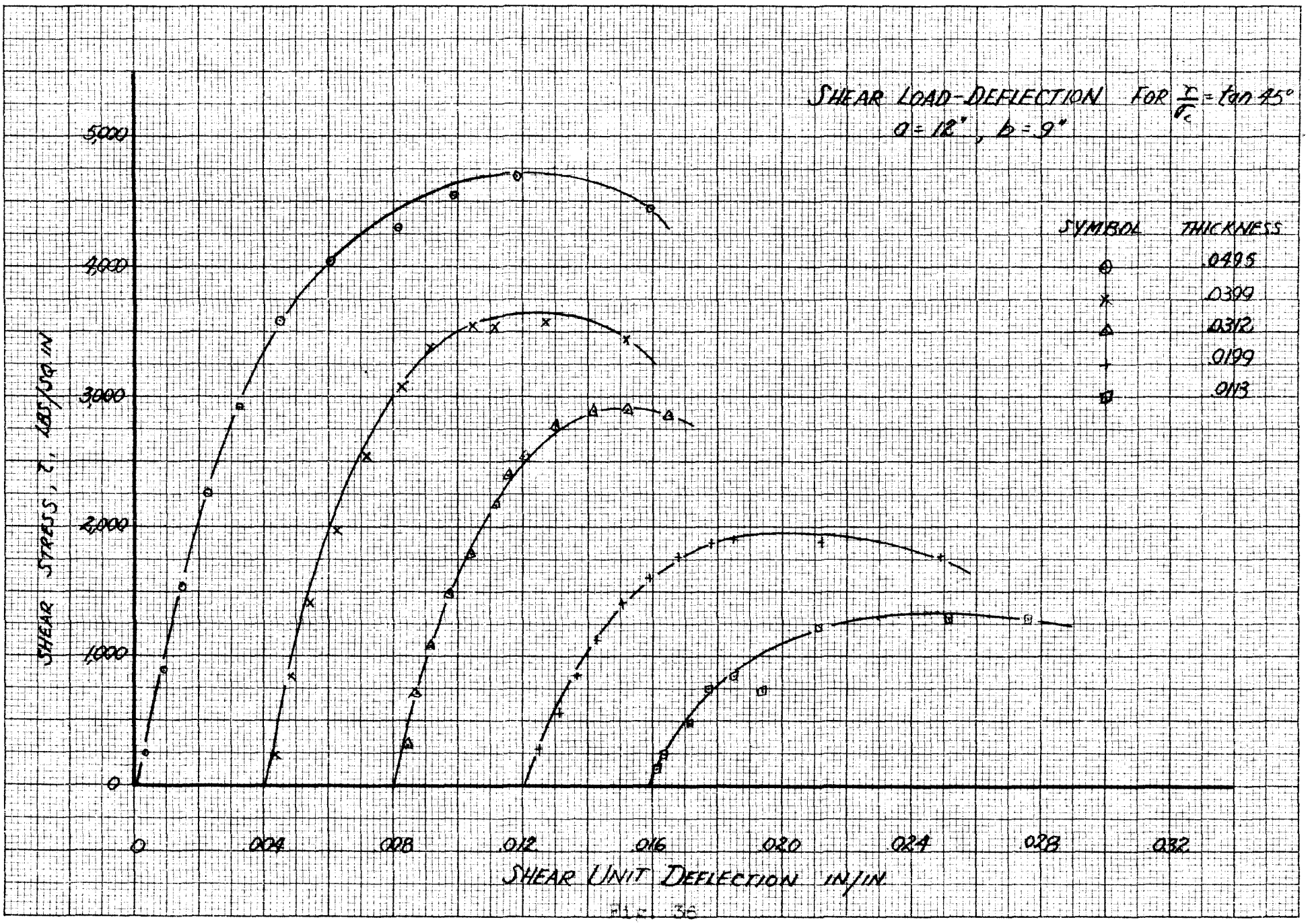
SHEAR LOAD-DEFLECTION FOR $\frac{x}{\theta_c} = \tan 45°$
a = 12", b = 9"
SYMBOL
THICKNESS
.0495
.0399
.0312
.0199
.0113
SHEAR STRESS, τ, LBS/SQ IN
0
1000
2000
3000
4000
5000
0
.004
.008
.012
.016
.020
.024
.028
.032
SHEAR UNIT DEFLECTION IN/IN

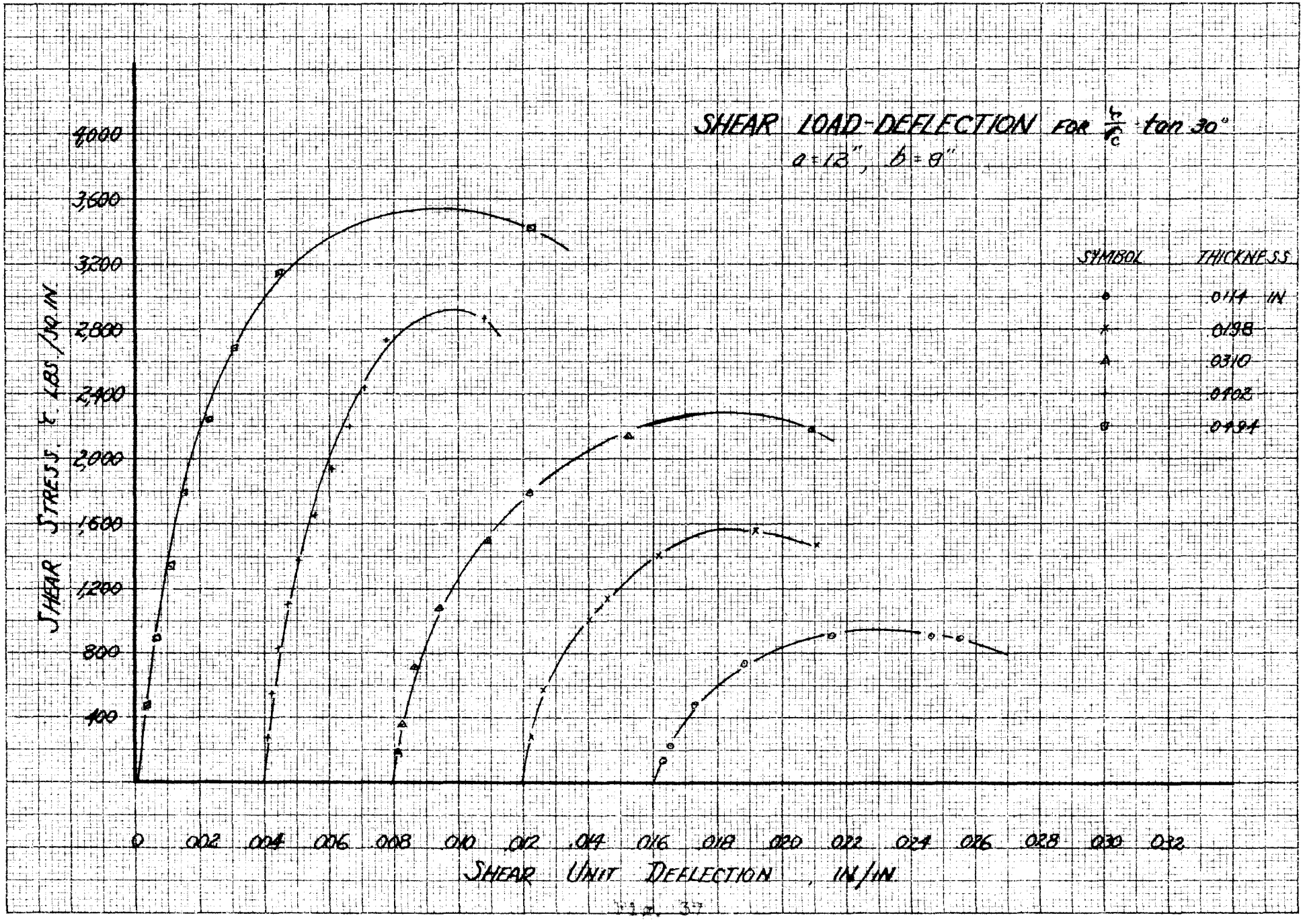
SHEAR LOAD-DEFLECTION FOR $\frac{h}{t_c}$ = tan 30°
a = 12", b = 8"
SYMBOL
THICKNESS
.0144 IN
.0138
.0310
.0102
.0191
SHEAR STRESS, τ, LBS./SQ. IN.
4000
3600
3200
2800
2400
2000
1600
1200
800
400
0
.002
.004
.006
.008
.010
.012
.014
.016
.018
.020
.022
.024
.026
.028
.030
.032
SHEAR UNIT DEFLECTION, IN./IN.

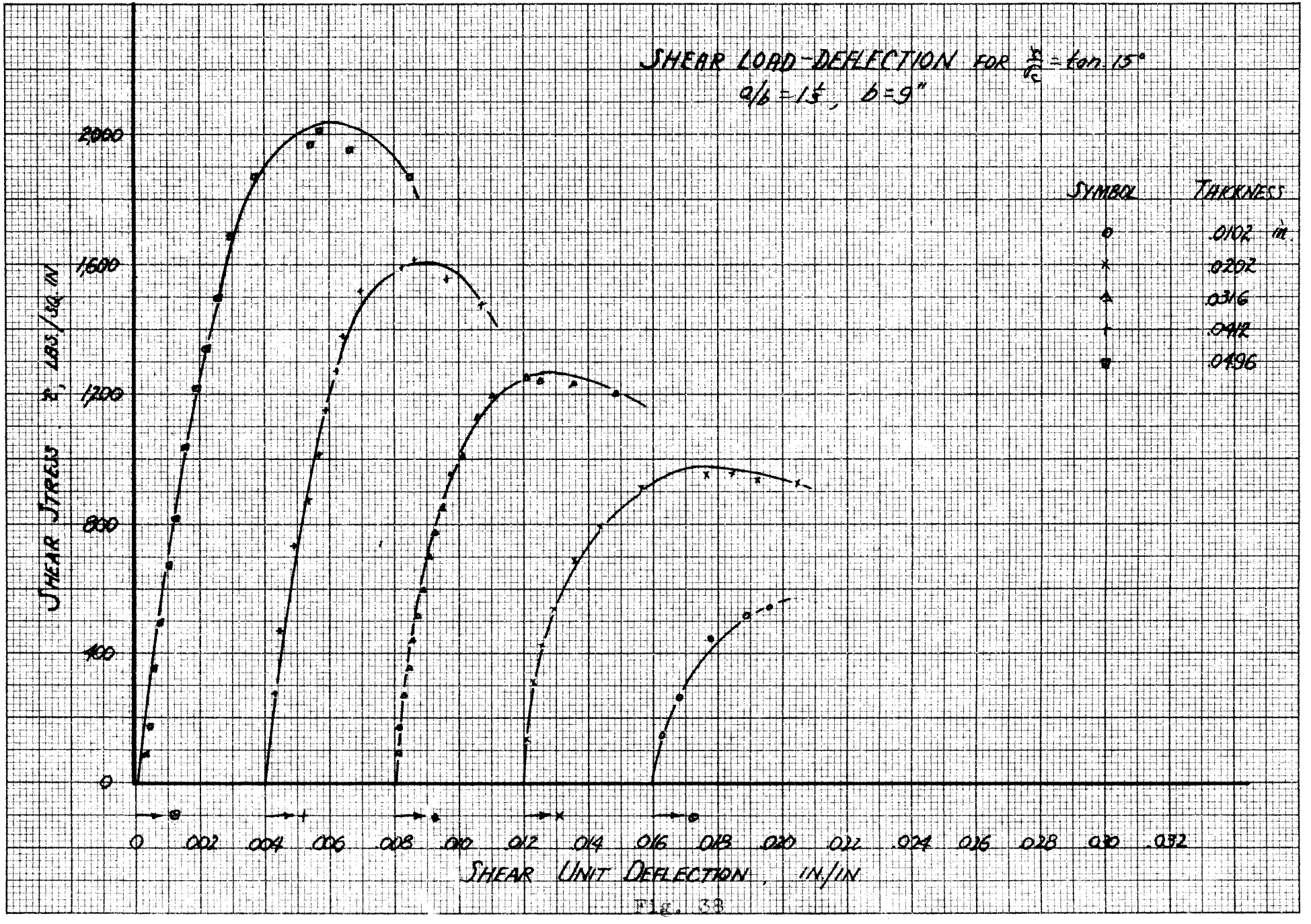
SHEAR LOAD-DEFLECTION FOR $\frac{N}{\sigma_c}$ = tan 15°
a/b = 1½, b = 9"
SYMBOL
THICKNESS
.0102 in.
.0202
.0316
.0412
.0496
SHEAR STRESS τ, LBS./SQ. IN.
2,000
1,600
1,200
800
400
0
0
.002
.004
.006
.008
.010
.012
.014
.016
.018
.020
.022
.024
.026
.028
.030
.032
SHEAR UNIT DEFLECTION, IN/IN.

Fig. 33

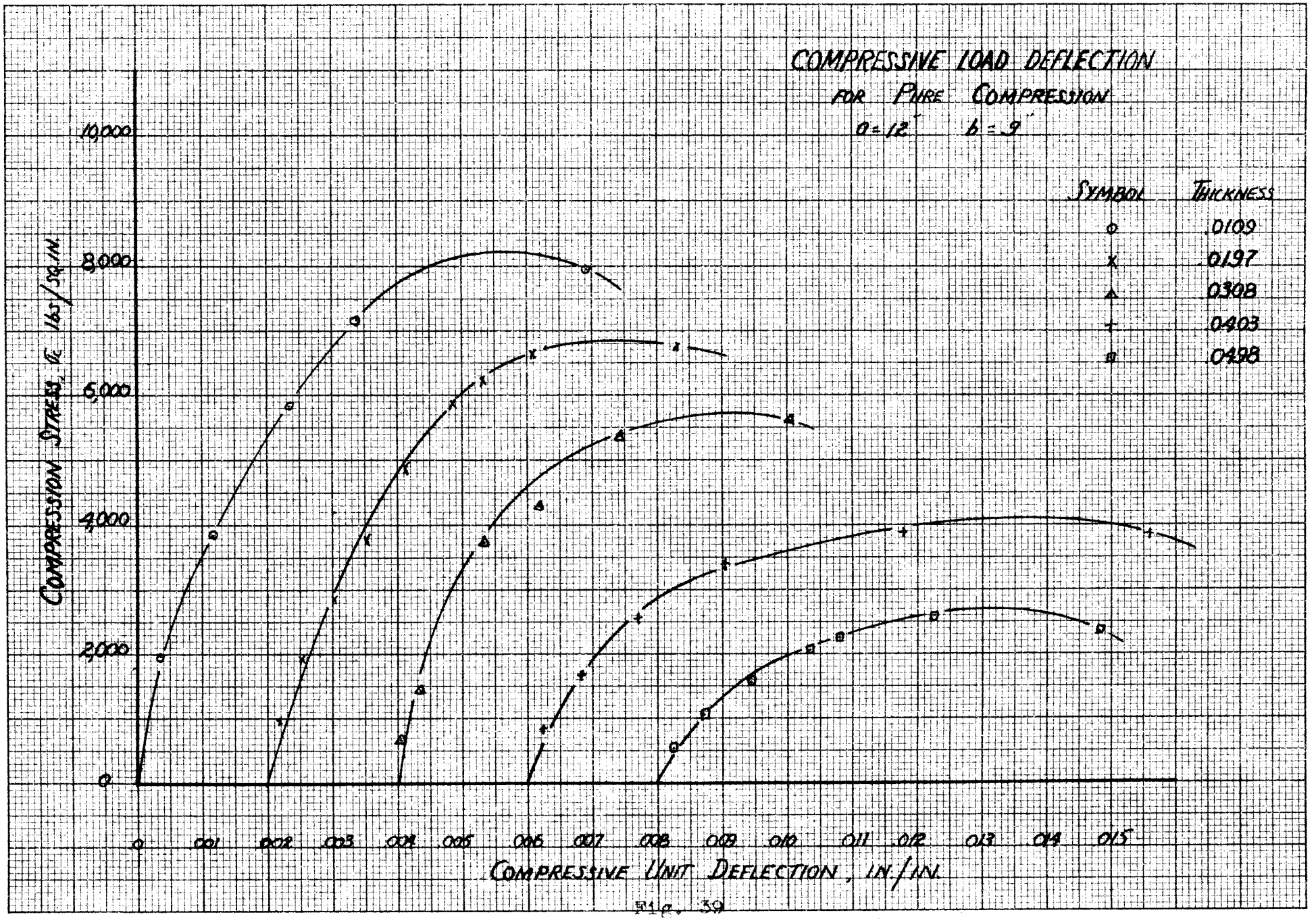
COMPRESSIVE LOAD DEFLECTION
FOR PURE COMPRESSION
a = 12" b = 9"
SYMBOL THICKNESS
o .0109
x .0197
Δ .0308
+ .0403
□ .0498
COMPRESSION STRESS, σc lbs/sq.in.
10,000
8,000
6,000
4,000
2,000
0
0 .001 .002 .003 .004 .005 .006 .007 .008 .009 .010 .011 .012 .013 .014 .015
COMPRESSIVE UNIT DEFLECTION, IN./IN.

Fig. 39

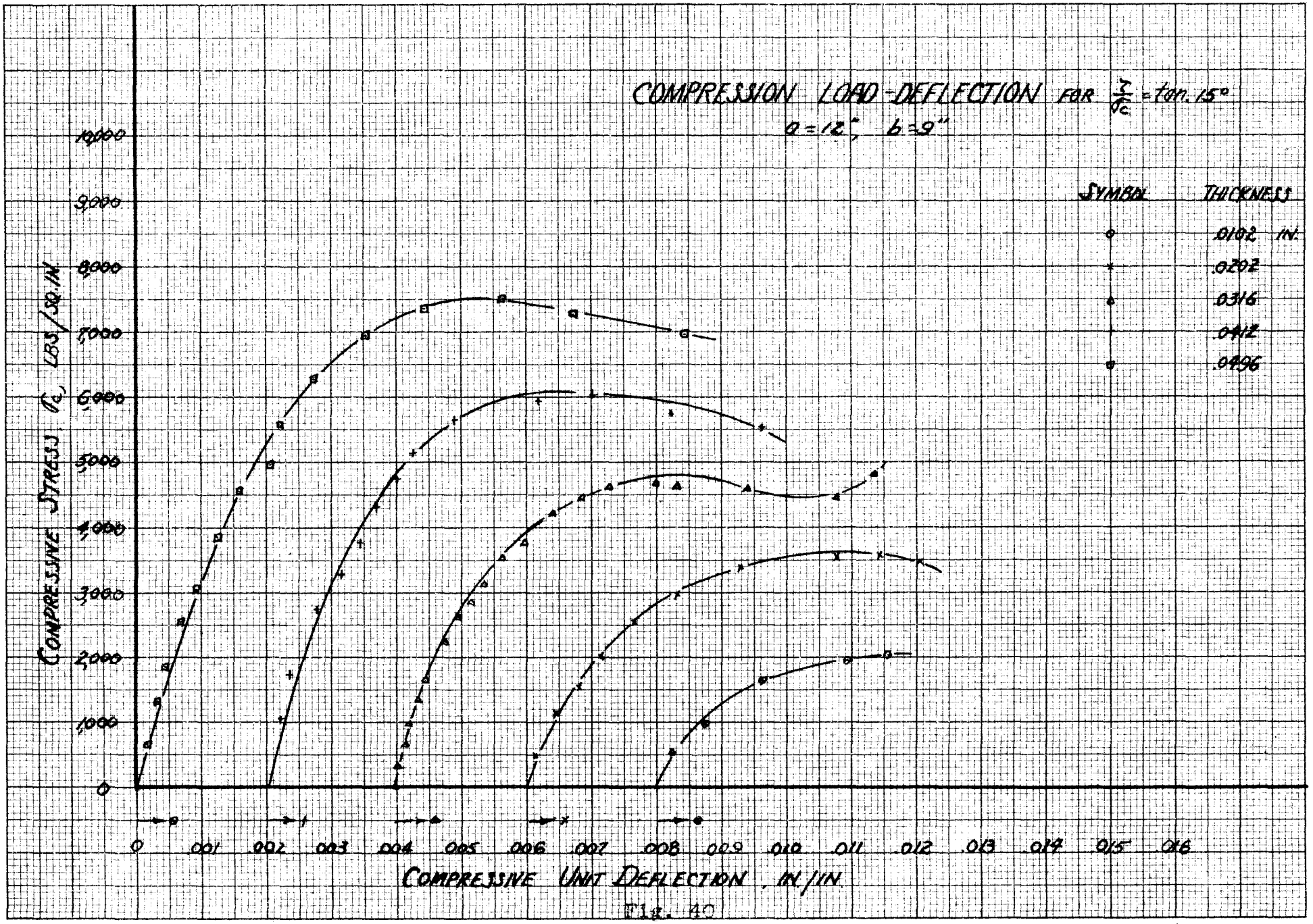
COMPRESSION LOAD-DEFLECTION FOR $\frac{y}{\rho c}$ = tan. 15°
a = 12", b = 9"
SYMBOL
THICKNESS
.0102 IN.
.0202
.0316
.0412
.0496
COMPRESSIVE STRESS (f_c), LBS/SQ.IN.
10000
9000
8000
7000
6000
5000
4000
3000
2000
1000
0
0
.001
.002
.003
.004
.005
.006
.007
.008
.009
.010
.011
.012
.013
.014
.015
.016
COMPRESSIVE UNIT DEFLECTION, IN/IN.

Fig. 40

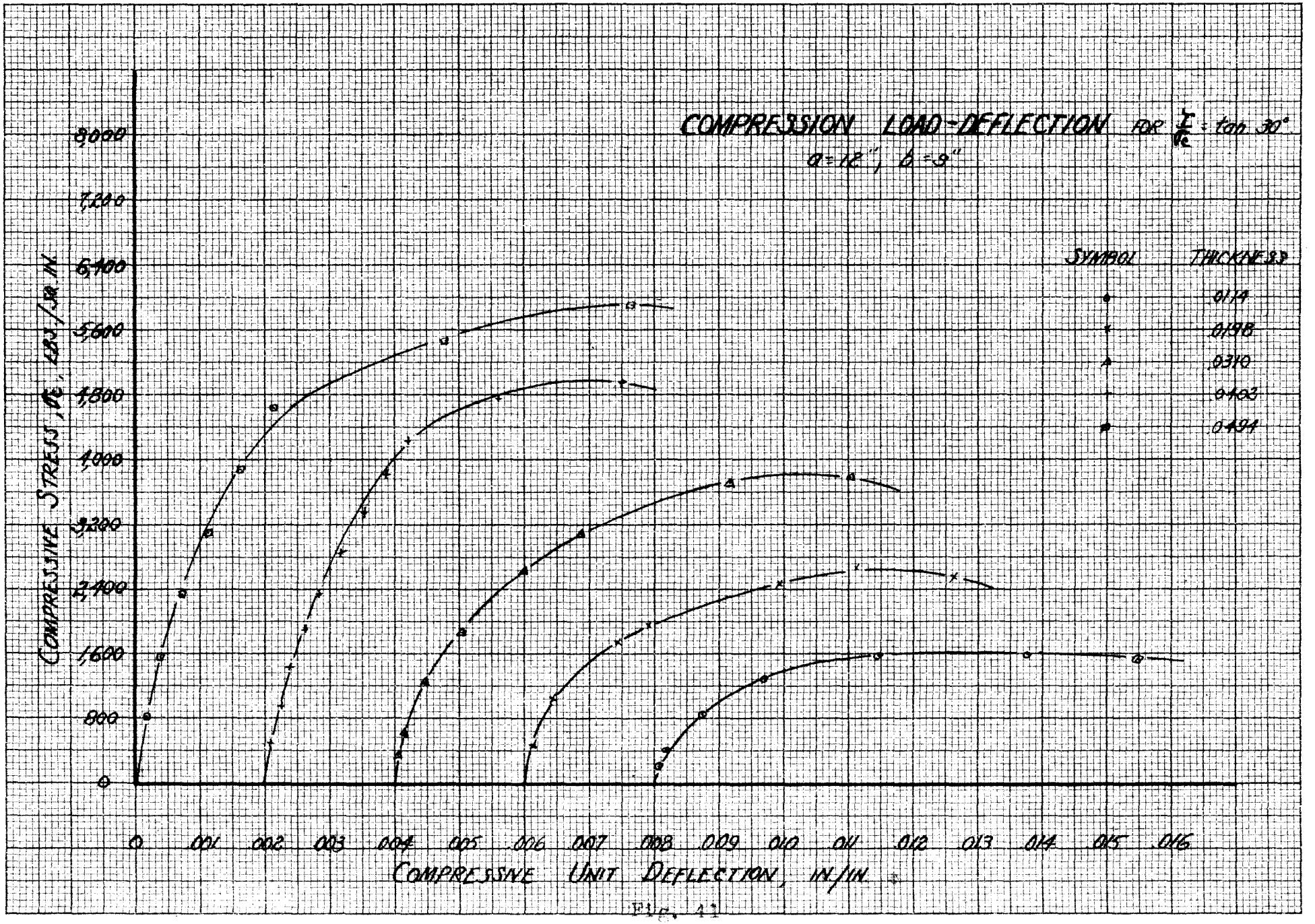
COMPRESSION LOAD-DEFLECTION FOR $\frac{T}{R_c} = \tan 30°$
a = 12", b = 9"
SYMBOL
THICKNESS
.0174
.0198
.0310
.0403
.0491
COMPRESSIVE STRESS, R_c, LBS/SQ IN.
8,000
7,200
6,400
5,600
4,800
4,000
3,200
2,400
1,600
800
0
.001
.002
.003
.004
.005
.006
.007
.008
.009
.010
.011
.012
.013
.014
.015
.016
COMPRESSIVE UNIT DEFLECTION, IN/IN.

Fig. 41

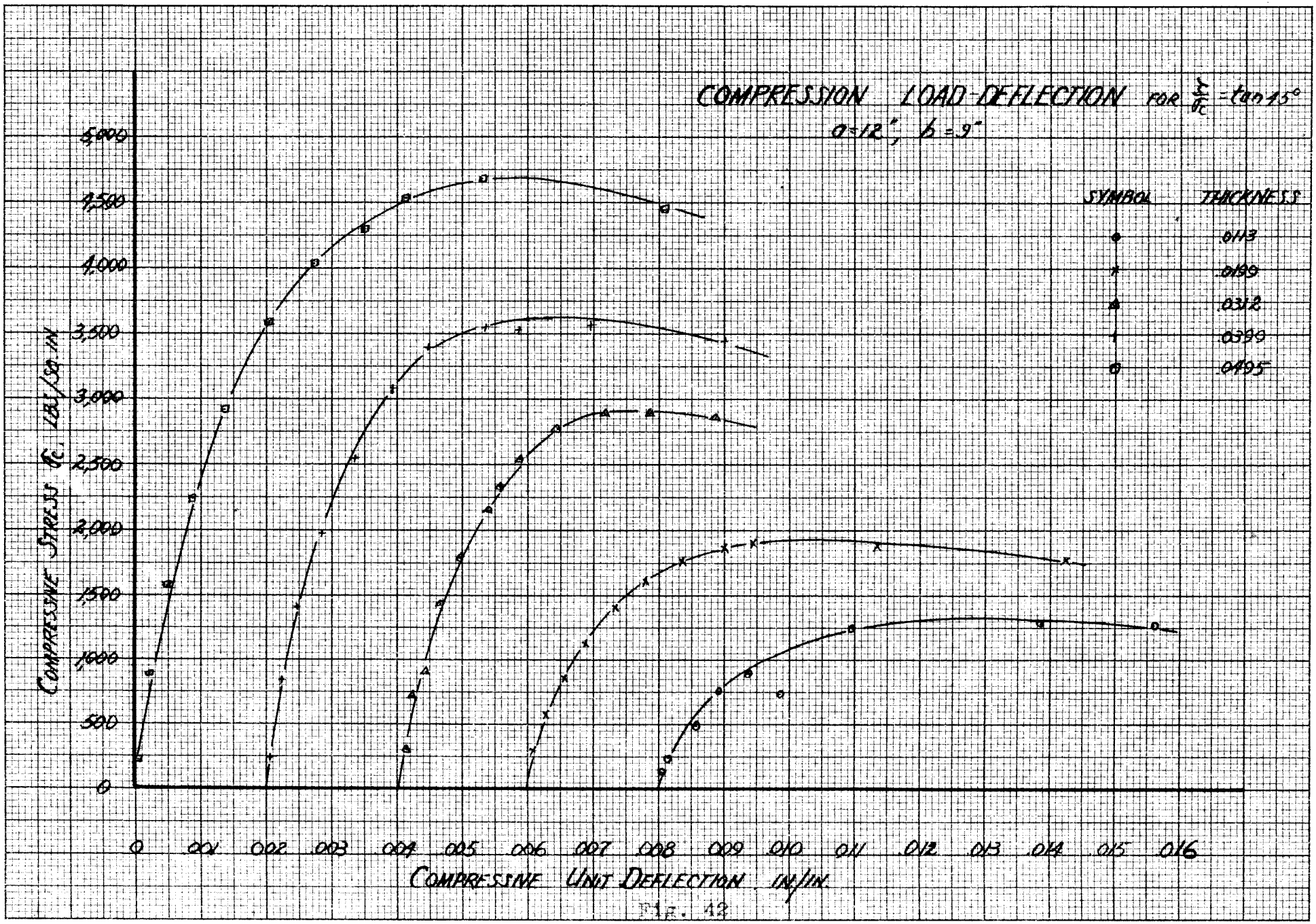
COMPRESSION LOAD-DEFLECTION for $\frac{t}{b_c} = \tan 15°$
a=12"; b=9"
SYMBOL
THICKNESS
.0113
.0199
.0312
.0399
.0495
Compressive Stress f_c, Lbs/Sq. in
5,000
4,500
4,000
3,500
3,000
2,500
2,000
1,500
1,000
500
0
0
.001
.002
.003
.004
.005
.006
.007
.008
.009
.010
.011
.012
.013
.014
.015
.016
Compressive Unit Deflection in/in.

Fig. 42

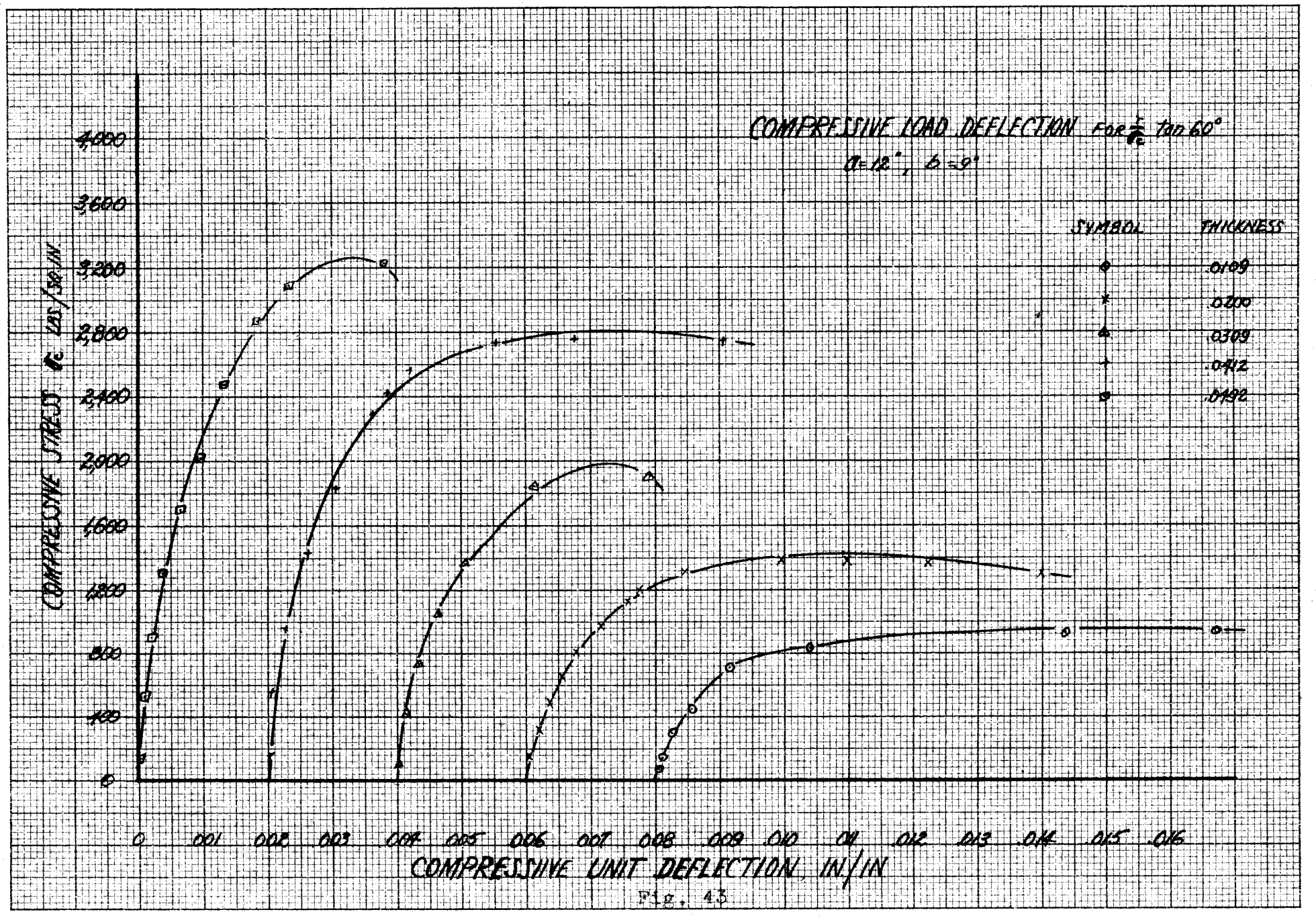
COMPRESSIVE LOAD DEFLECTION For $\frac{t}{E}$ tan 60°
a = 12", b = 9"
SYMBOL THICKNESS
.0109
.0200
.0309
.0412
.0492
COMPRESSIVE STRESS $\frac{P}{bt}$ LBS/SQ. IN.
4,400
3,600
3,200
2,800
2,400
2,000
1,600
1,200
800
400
0
0 .001 .002 .003 .004 .005 .006 .007 .008 .009 .010 .011 .012 .013 .014 .015 .016
COMPRESSIVE UNIT DEFLECTION, IN/IN

Fig. 43

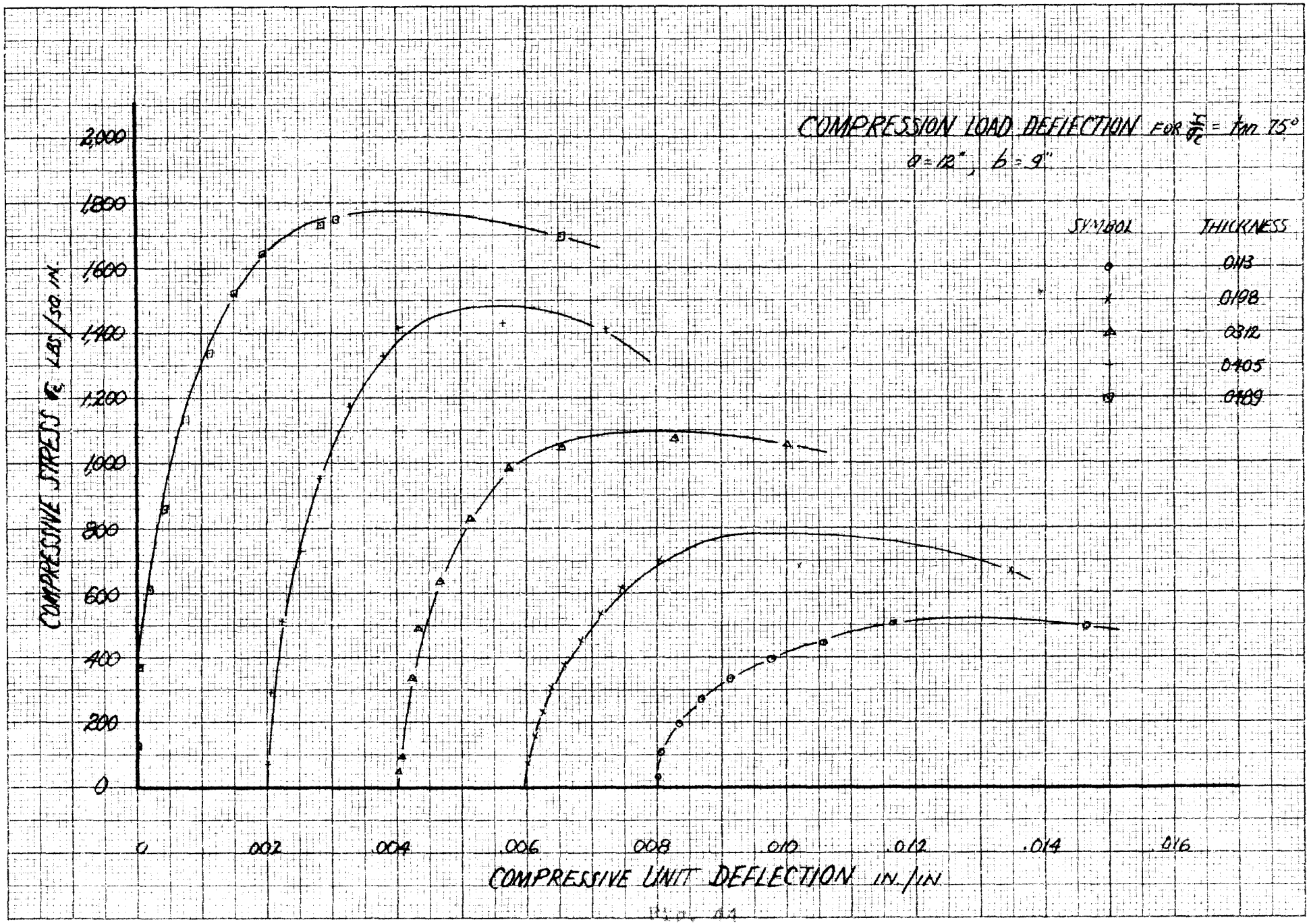
COMPRESSION LOAD DEFLECTION FOR $\frac{h}{a}$ = tan 75°
a = 12", b = 9"
SYMBOL
THICKNESS
.013
.0198
.0312
.0405
.0609
COMPRESSIVE STRESS σ_c LBS/SQ. IN.
2000
1800
1600
1400
1200
1000
800
600
400
200
0
0
.002
.004
.006
.008
.010
.012
.014
.016
COMPRESSIVE UNIT DEFLECTION IN./IN.

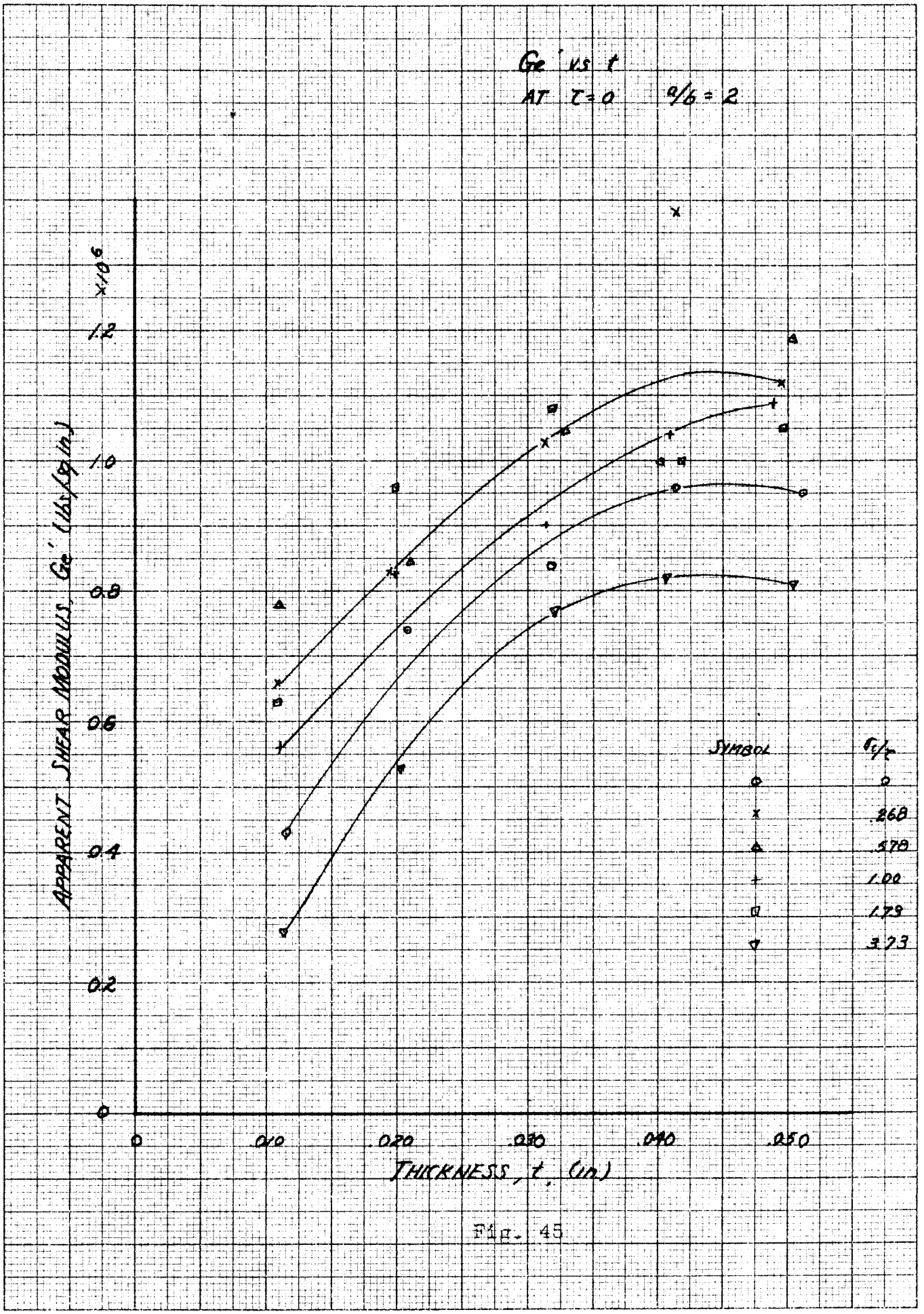
Ge' vs t
AT τ = 0 a/b = 2
APPARENT SHEAR MODULUS, Ge' (lbs/sq in.)
×10⁶
1.2
1.0
0.8
0.6
0.4
0.2
0
0
.010
.020
.030
.040
.050
THICKNESS, t, (in.)
SYMBOL
Gt/τ
0
.268
.570
1.00
1.79
3.73

Fig. 45

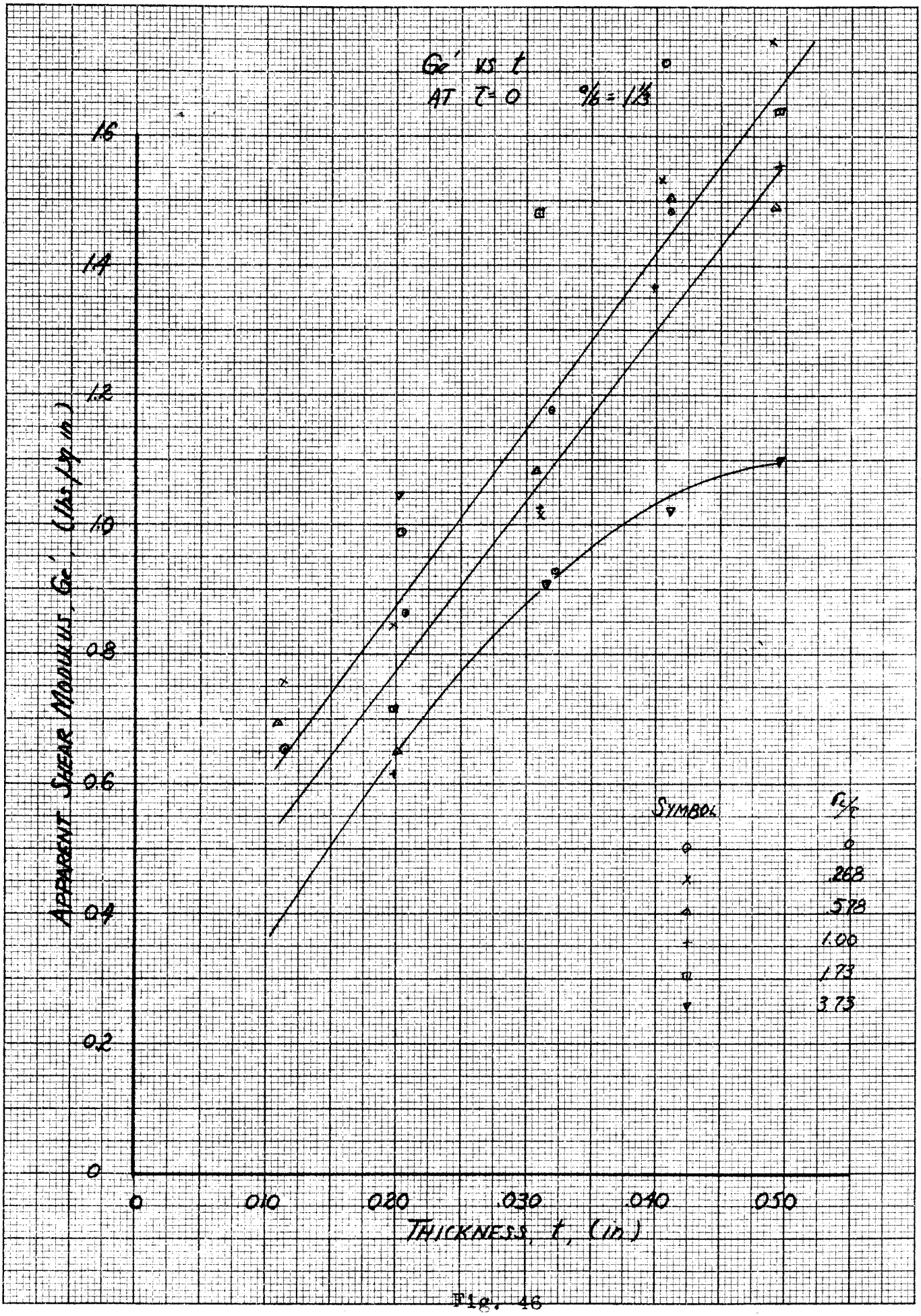
Ge' vs t
AT T = 0 % = 1 1/8
APPARENT SHEAR MODULUS, Ge', (lbs/sq in.)
1.6
1.4
1.2
1.0
0.8
0.6
0.4
0.2
0
0
.010
.020
.030
.040
.050
THICKNESS, t, (in.)
SYMBOL
Ge/c
0
.268
.578
1.00
1.73
3.73

Fig. 46

Pure Shear

a/b = 2, b = 6

t = .0109

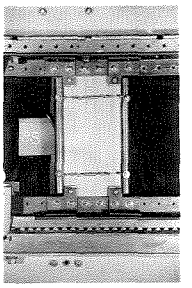

τ = 0

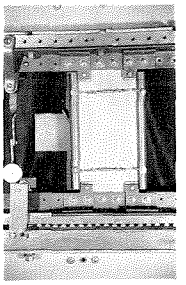

τ = 765

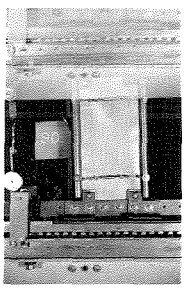

τ = 1240

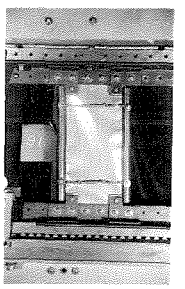

Failed

$\tau_{max.}$ = 1852

Fig. 47

Pure Shear

a/b = 2, b = 6

t = .0320

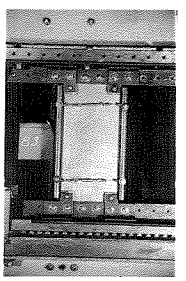

τ = 0

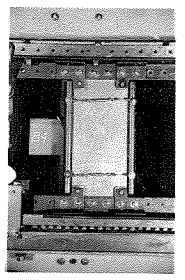

τ = 1950

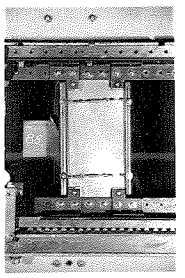

τ = 3340

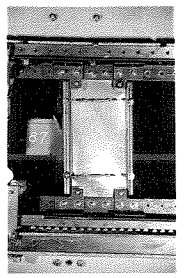

Failed

$\tau_{max.}$ = 4810

Fig. 48

Combined Shear & Compression

$$\frac{\tau}{\sigma_c} = 1.00$$

$a/b = 2,\ b = 6,\ t = .0108$

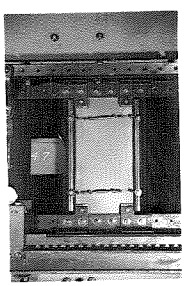

$\tau = 479$

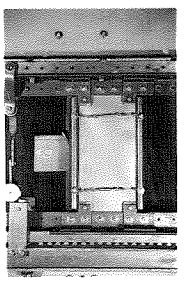

$\tau = 771$

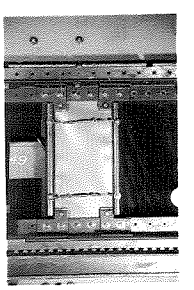

$\tau = 1098$

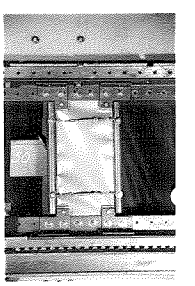

Failed

$\tau_{max.} = 1511$

Fig. 49

Combined Shear & Compression

$$\frac{\tau}{\sigma_c} = 1.00$$

$$a/b = 2,\ b = 6,\ t = .0310$$

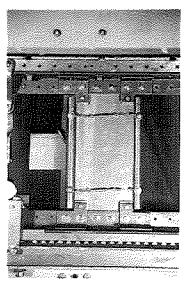

$\tau = 0$

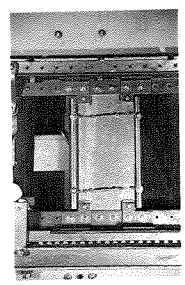

$\tau = 1380$

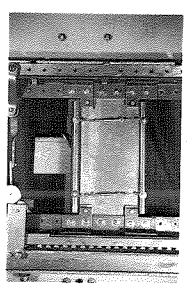

$\tau = 2080$

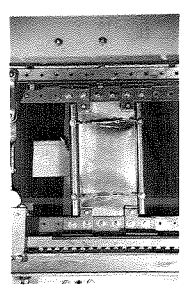

Failed

$\tau_{max.} = 3440$

Fig. 50

Pure Compression

a/b = 2, b = 6

t = .0119

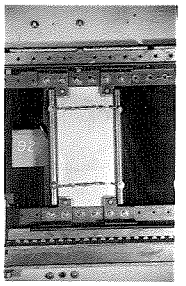

σ_c = 378

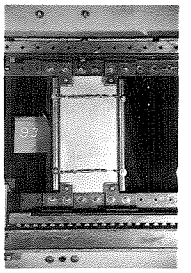

σ_c = 616

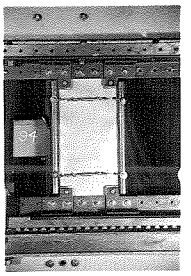

σ_c = 2342

Fig. 51

Pure Compression

a/b = 2, b = 6

t = .0319

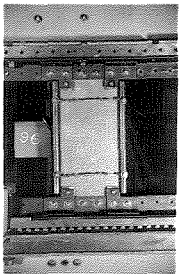

σ_c = 1458

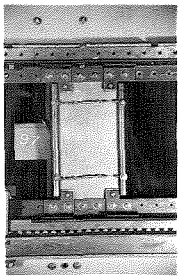

σ_c = 1992

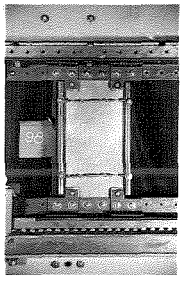

σ_c = 5065

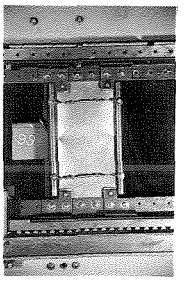

Failed

$\sigma_{c\ max.}$ = 7950

Fig. 52

Pure Shear

a/b = 1 1/3, b = 9

t = .0104

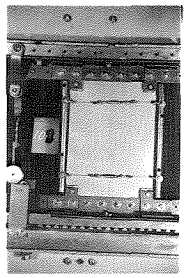

τ = 524

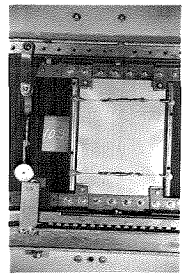

τ = 882

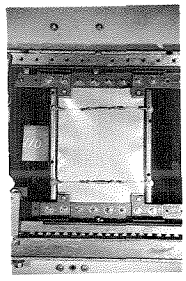

τ = 1540

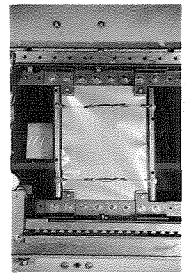

Failed

$\tau_{max.}$ = 2032

Fig. 53

Pure Shear

a/b = 1 1/3, b = 9

t = .0318

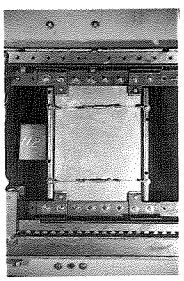

τ = 771

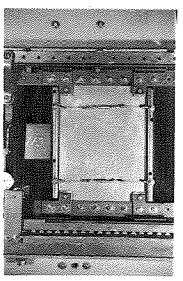

τ = 1170

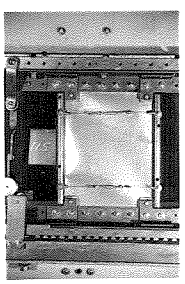

Failed

$\tau_{max.}$ = 2730

Fig. 54

Combined Shear & Compression

$\frac{\tau}{\sigma_c} = 1.00$

a/b = 1 1/3, b = 9, t = .0111

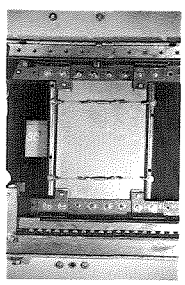

$\tau = 160$

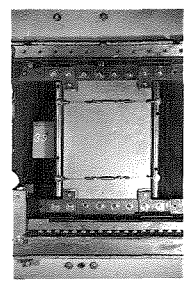

$\tau = 260$

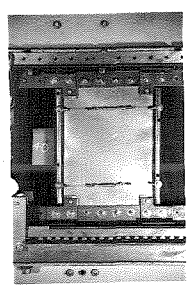

$\tau = 701$

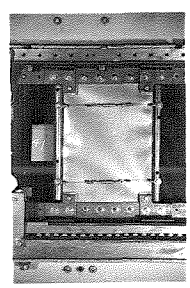

$\tau = 1142$

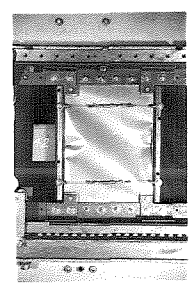

Failed

$\tau_{max.} = 1252$

Fig. 55

Combined Shear & Compression

$\frac{\tau}{\sigma_c} = 1.00$

a/b = 1 1/3, b = 9, t = .0316

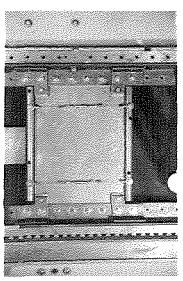

$\tau = 369$

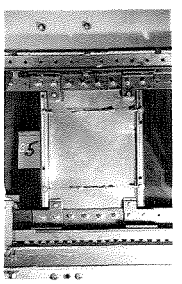

$\tau = 1290$

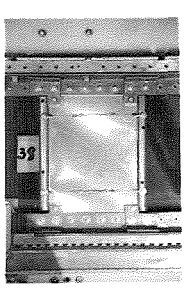

Failed

$\tau_{max.} = 2920$

Fig. 56

Pure Compression

a/b = 1 1/3, b = 9

t = .0104

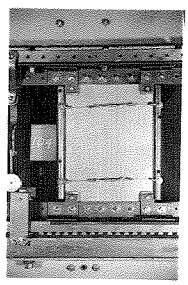

$\sigma_c = 662$

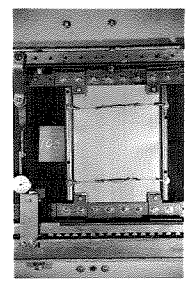

$\sigma_c = 1091$

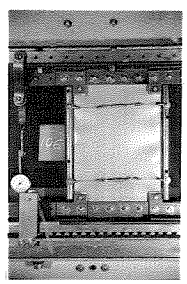

$\sigma_c = 2725$

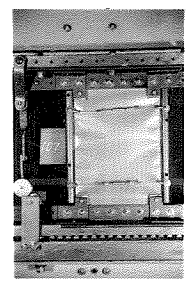

Failed

$\sigma_{c\,max} = 2725$

Fig. 57

Pure Compression

a/b = 1 1/3, b = 9

t = .0317

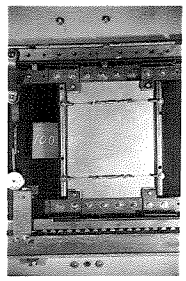

σ_c = 1590

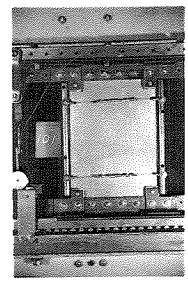

σ_c = 2675

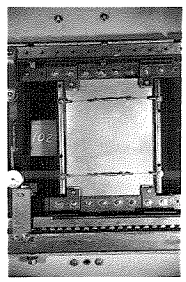

σ_c = 4060

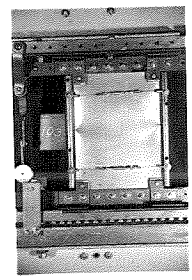

Failed

$\sigma_{c\,max.}$ = 5500

Fig. 58

IX. APPENDIX

Apparent Shear Modulus, G', for a Flat Panel with Slight Rotation of the Loaded End

1. 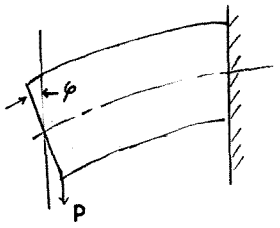

Panel loaded at the end with a load, P, while there is a slight rotation of the end through an angle φ .

2. Assumptions:

   a. Plate is held rigidly at the fixed end.

   b. Shear deflection shall be considered.

   c. Section are $\perp$ to the neutral axis.

   d. Couple applied at the loaded end will hold the section // to the fixed edge.

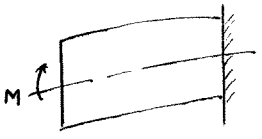

   e. Plate is not in the wave stage.

3. Method of Solution

   a. Obtain the expression for K in terms of G_e' and E.

$$K = \frac{\varphi \text{ actual}}{\varphi \text{ theoretical}} \quad ; \quad M = \frac{EI}{\ell}(K\varphi)$$

   b. Find the relationship between φ_k and τ.

   c. Determine $\varphi_{exp.}$ from $\varphi_{theo.}$ and K.

      $\varphi_{theo.}$ = ends are held parallel.

   d. Determine the values of K for various G_e'.

      (1) Also determine $\varphi_{exp.}$ for each value of K.

e. Plot the experimental results of $\varphi_{exp.}$ vs. τ.

(1) The value of K can be determined from the slope of the curve.

f. Comparison between calculated G_e' and actual G_e'.

g. Conclusions.

Solution

1. G_e' as a function of $M = \frac{EI}{\ell}(K\varphi)$ (1)

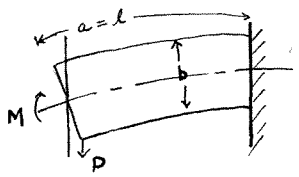

a. Apparent shear deflection, γ

$$\gamma = \frac{v}{\ell} = \frac{P\ell^2}{3EI} + \frac{2}{5}\frac{Pc^2}{IG} - \frac{M\ell}{2EI} \qquad (2)$$

where v = total deflection at end due to the bending and shear deflection.

b. Expression for M.

$$M = \frac{EI}{\ell}(K\varphi)$$

$$K = \frac{\varphi \text{ actual}}{\varphi \text{ theo.}}$$

φ actual = experimental value of φ

φ theo. = the ends are held parallel

c. Expression for φ theo.

(1) Slope of the neutral axis without the end moment, M.

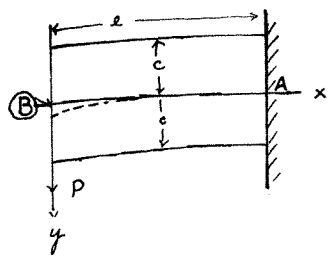

The expression for v at y = o, considering the fixed end is rigidly fixed and also the shear deflection.

$$(v)_{y=0} = \frac{Px^3}{6EI} - \frac{Pl^2x}{2EI} + \frac{Pl^3}{3EI} + \frac{2}{5}\frac{Pc^2}{IG}(l-x) \qquad (3)$$

Slope at any point

$$\frac{d(v)_{y=0}}{dx} = \frac{Px^2}{3EI} - \frac{Pl^2}{2EI} - \frac{2}{5}\frac{Pc^2}{IG} \qquad (4)$$

Slope at y = o, x = o, (B).

$$= -\frac{Pl^2}{2EI} - \frac{2}{5}\frac{Pc^2}{IG} \qquad (5)$$

but $\frac{dv}{dx} = \tan\varphi$

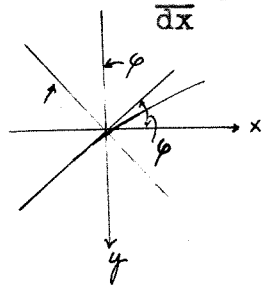

hence

$$\tan\varphi = +\frac{Pl^2}{2EI} + \frac{2}{5}\frac{Pc^2}{IG} \qquad (6)$$

from which

$$\varphi = \tan^{-1}\left(\frac{Pl^2}{2EI} + \frac{2}{5}\frac{Pc^2}{IG}\right) \qquad (7)$$

$$\therefore \quad \varphi \doteq \left(\frac{Pl^2}{2EI} + \frac{2}{5}\frac{Pc^2}{IG}\right) \qquad (7a)$$

From (7a) φ (actual) can be expressed in terms of φ (theo.) by applying correction factor, K.

$$\varphi_{(actual)} = K\left(\frac{Pl^2}{2EI} + \frac{2}{5}\frac{Pc^2}{IG}\right) \tag{8}$$

$$\text{and } M = \frac{EI}{l}\varphi = \frac{EI}{l}K\left(\frac{Pl^2}{2EI} + \frac{2}{5}\frac{Pc^2}{IG}\right) \tag{9}$$

d. Finally the expression for γ becomes

$$\gamma = \frac{Pl^2}{3EI} + \frac{2}{5}\frac{Pc^2}{IG} - \frac{l}{2EI}\left(K\frac{EI}{l}\left(\frac{Pl^2}{2EI} + \frac{2}{5}\frac{Pc^2}{IG}\right)\right)$$
$$= \frac{Pl^2}{12EI}(4-3K) + \frac{Pc^2}{5IG}(2-K) \tag{10}$$

for $c = \frac{b}{2} = \frac{l}{4}$, $\frac{a}{b} = 2$

$$G = \frac{E}{2.6}$$

Substitute these values into (10)

$$\gamma = \frac{Pl^2}{12EI}(4-3K) + \frac{Pl^2/16}{5I\frac{E}{2.6}}(2-K)$$
$$= \frac{Pl^2}{EI}\left[\left(\frac{4-3K}{12}\right) + \frac{2.6}{80}(2-K)\right]$$
$$= \frac{Pl^2}{EI}\left[.3333 - .25K + .065 - .0325K\right] \tag{11}$$
$$= \frac{Pl^2}{EI}\left[.3983 - .2825K\right]$$

but

$$P = \tau bt = \frac{\tau lt}{2}$$

and

$$I = \frac{bh^3}{12} = \frac{tl^3}{96}$$

$$G' = \frac{\tau}{\gamma} = \frac{\left(\frac{2P}{lt}\right)}{\frac{Pl^2}{EI}\left[.3983 - .2825K\right]} \tag{12}$$
$$= \frac{E}{(48)(.3983 - .2825K)}$$

Solve for K from eq. (12)

$$(48)(.3983 - .2825K)\,G'_e = E$$

hence

$$K = \frac{G'_e(48)(.3983) - E}{(48)(.2825)\,G'_e} \tag{13}$$

Assume $E = 10.3 \times 10^6$ lbs./sq. in.

for which

$$K = \frac{19.15\,G'_e - 10.3 \times 10^6}{13.59\,G'_e} \tag{13a}$$

2. Now express φ_K as a function of $\tau = \frac{P}{bt}$

a. $$\varphi_K \doteq K\left(\frac{pl^2}{2EI} + \frac{2}{5}\,\frac{Pc^2}{IG}\right) \tag{14}$$

but $c = \frac{l}{4}$, $I = \frac{tl^3}{96}$

$$G = \frac{E}{2.6}, \quad P = \frac{\tau l t}{2}$$

Substitute these values into eq. (14) so as to obtain a simple expression for φ_K

$$\varphi_K = K\left[\frac{\left(\frac{\tau l t}{2}\right)l^2}{2E\,\frac{tl^3}{96}} + \frac{2}{5}\,\frac{\left(\frac{\tau l t}{2}\right)\frac{l^2}{16}}{\frac{tl^3}{96}\,\frac{E}{2.6}}\right]$$

$$= K\left[\frac{24\tau}{E} + \frac{(6)(2.6)}{5}\,\frac{\tau}{E}\right]$$

$$= 27.12\,K\,\frac{\tau}{E} \tag{14a}$$

For $\varphi_{theo.}$ $K = 1$

$$\therefore \varphi_{theo.} = \frac{\tau}{E}(27.12)$$ (i.e., no rotation of the ends; they are held parallel).

b. $\varphi_{exp.}$ can be obtained from $\varphi_{theo.}$ and φ_K

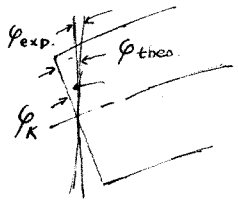

where:

$$\varphi_K = K\,\varphi_{theo.}$$

(1) From the figure it can be shown that

$$\begin{aligned}\varphi_{exp.} &= \varphi_{theo.} - \varphi_{K} \\ &= (1-K)\,\varphi_{theo.} \\ &= \frac{\tau}{E}(27.12)(1-K)\end{aligned} \qquad (15)$$

3. The values of K for various G'_e values

a. $$K = \frac{G'_e(19.15) - 10.3 \times 10^6}{13.59\,G'_e}$$

In deriving this expression for K, the value of G was taken to be $= \frac{E}{2(1+\nu)} = \frac{E}{2.6}$ $\nu = 0.3$

G'_e	K	$\varphi_{exp.} = \tau\, a_{\times 10^{-6}}$
.75	.402	1.58
1.00	.655	.908
1.25	.805	.514
1.50	.906	.248
1.80	.945	.145

$$\varphi_{exp.} = a\,\tau \qquad (16)$$

$$1 - K = \frac{a}{2.63 \times 10^{-6}}$$

a is the slope of the curve

$$\therefore K = 1 - \frac{a}{2.63 \times 10^{-6}}$$

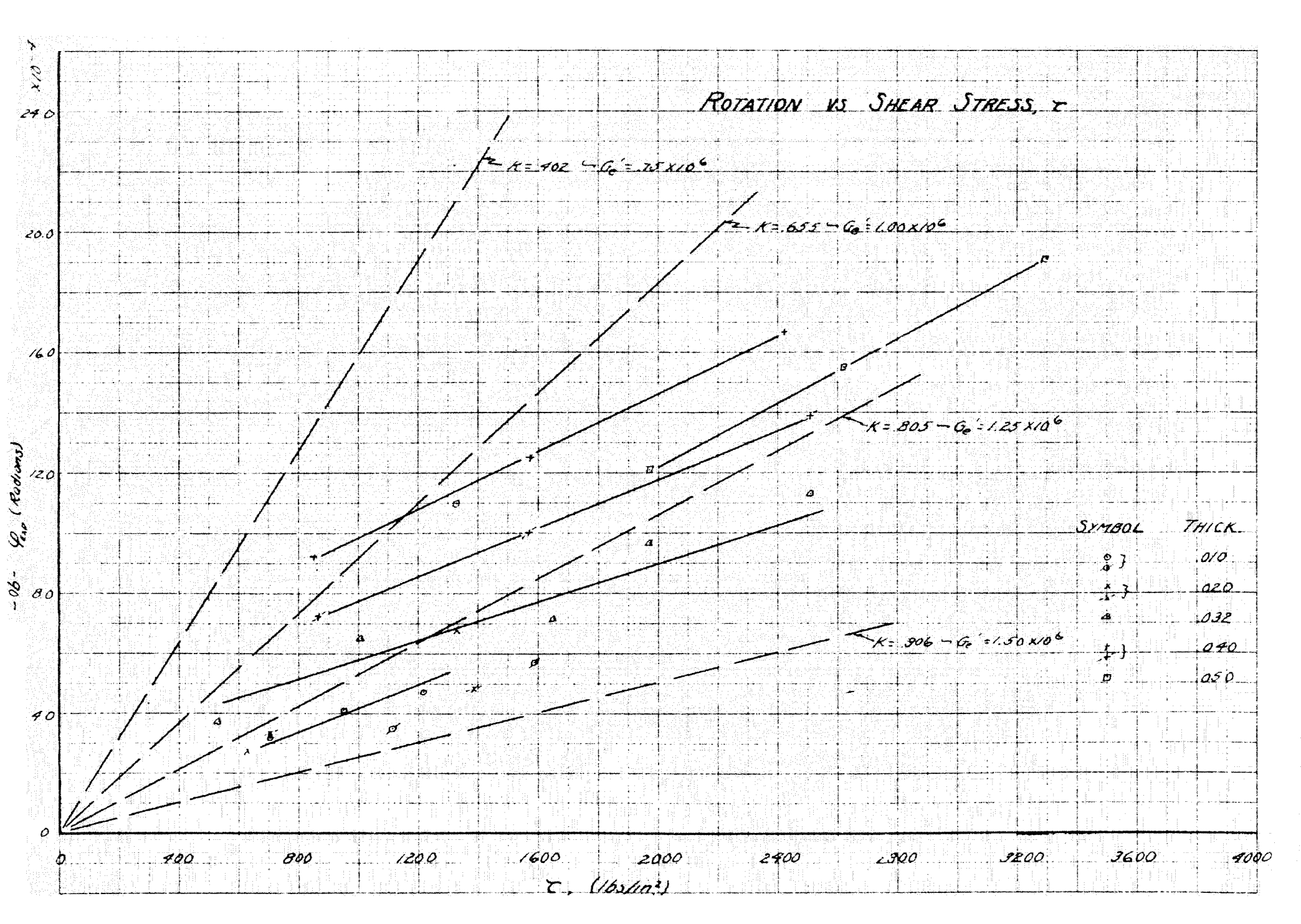
ROTATION VS SHEAR STRESS, τ
K = .402 — Ge = .75 x 10^6
K = .655 — Ge = 1.00 x 10^6
K = .805 — Ge = 1.25 x 10^6
K = .906 — Ge = 1.50 x 10^6
SYMBOL
THICK.
.010
.020
.032
.040
.050
-θ- φav (Radians)
x10^-4
24.0
20.0
16.0
12.0
8.0
4.0
0
0
400
800
1200
1600
2000
2400
2800
3200
3600
4000
τ, (lbs/in^2)

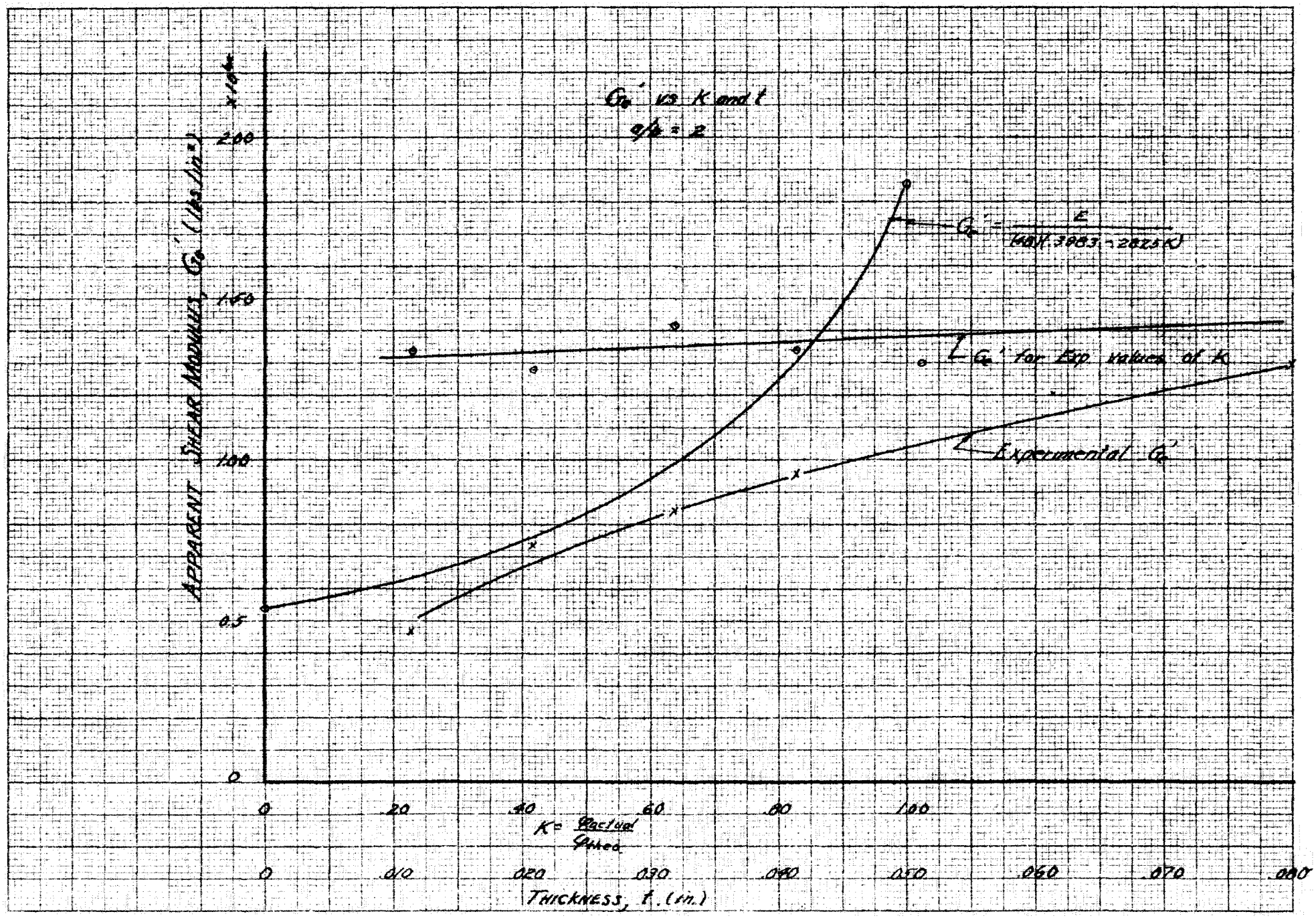
G_a' vs K and t
g/t = 2
APPARENT SHEAR MODULUS, G_a' (lbs/in²)
x 10⁶
2.00
1.50
1.00
0.5
0
$G_a' = \frac{E}{4(1+.3083+.2823K)}$
G_a' for Exp. values of K
Experimental G_a'
0
.20
.40
.60
.80
1.00
K = Gactual / Gused
0
.010
.020
.030
.040
.050
.060
.070
.080
THICKNESS, t. (in.)

for t = .040

$$a = \frac{(15.6 - 10.8) \times 10^4}{(2200 - 1200)} = 4.8 \times 10^{-7}$$

$$K = 1 - \frac{4.8 \times 10^{-7}}{2.63 \times 10^6} = .817$$

G_e' from the graph of G_e' vs. K.

$$= 1.28 \times 10^6$$

4. Calculation of φ_{exp} from Experimental Data

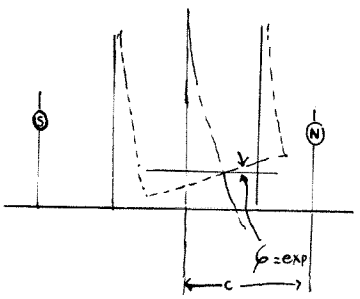

$$\tan \varphi_{exp.} = \frac{(\delta_N - (\delta_N + \delta_S)}{} \qquad (17)$$

$$\text{or } \varphi_{exp.} \doteq \frac{\delta_N - \left(\frac{\delta_N + \delta_S}{2}\right)}{c} \qquad (17a)$$

4. G_e' in terms of G and K.

a. $$\gamma = \frac{Pl^2}{3EI} + \frac{2}{5}\frac{Pc^2}{IG} - \frac{l}{2EI}\left[K\frac{EI}{l}\left(\frac{Pl^2}{2EI} + \frac{2}{5}\frac{Pc^2}{IG}\right)\right]$$

$$= \frac{Pl^2}{12EI}(4-3K) + \frac{Pc^2}{5IG}(2-K)$$

$$c = \frac{b}{2} = \frac{l}{4}, \quad \frac{a}{b} = 2$$

$$= \frac{Pl^2}{I}\left[\left(\frac{4-3K}{12E}\right) + \frac{(2-K)}{80G}\right]$$

$$\tau = \frac{2P}{lt}, \quad I = \frac{tl^3}{96}$$

$$G_e' = \frac{\tau}{\gamma} = \frac{\frac{2P}{lt}}{\frac{Pl^2}{\frac{tl^3}{96}}\left[\left(\frac{4-3K}{12E}\right) + \frac{(2-K)}{80G}\right]}$$

$$= \frac{1}{48}\frac{1}{\left[\left(\frac{4-3K}{12E}\right) + \left(\frac{2-K}{80G}\right)\right]}$$

$$G_e' = \frac{1}{48}\left[\frac{960\,EG}{320G - 240\,KG + 24E - 12KE}\right]$$

$$G_e' = \frac{5EG}{20G(4-3K) + 3E(2-K)} \qquad (18)$$

b. Or

$$G = \frac{-3EG'_e(2-K)}{20G'_e(4-3K)-5E} \tag{19}$$

6. Comparison between the calculated values of G'_e and the experimental results.

a. G'_e was calculated by the following method:

(1) The value of K was determined from the curve of $\varphi_{exp.}$ vs. τ for each thickness.

(2) G'_e was determined from the equation

$$G'_e = \frac{E}{(48)(.3383 - .2825K)}$$ by using the experimental values of K.

b. The calculated and experimental G'_e are plotted on page 92.

(1) The calculated values of G'_e are higher than the experimental results.

(2) $$G'_e = \frac{5EG}{20G(4-3K)+3E(2-K)}$$

$$= \frac{5E}{20(4-3K)+3\frac{E}{G}(2-K)}$$

$$= \frac{a}{b\ \frac{c}{G}} \tag{20}$$

The calculated values of G'_e are larger than the experimental values because of the following reasons:

(a) In obtaining the value of G'_e, the value of G was assumed to be $\frac{E}{2(1+.3)}$ but if G is

actually less than the assumed value, the calculated G_e' will be lower, if this correct G is used.

(b) G_e' will be lower if the value of K is taken to be smaller than the experimental result.

7. Conclusion:

a. Further careful study should be made to determine why the calculated G_e' is larger than the experimental G_e'; whether it is due to the variation of G or K, or due to the buckling phenomena.

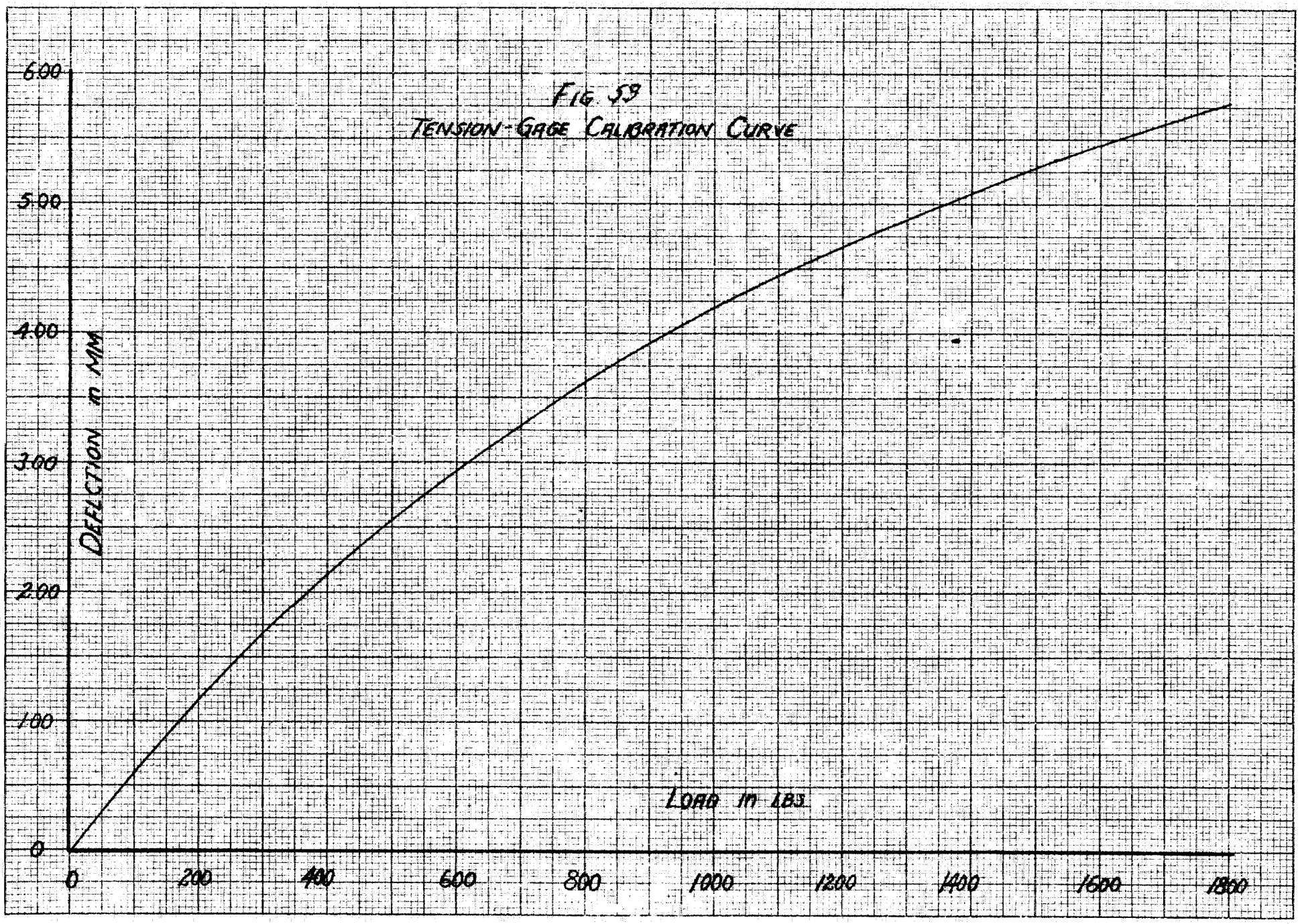
FIG 59
TENSION-GAGE CALIBRATION CURVE
DEFLECTION IN MM
LOAD IN LBS
6.00
5.00
4.00
3.00
2.00
1.00
0
0
200
400
600
800
1000
1200
1400
1600
1800

DATA SHEET

Specimen No.	Thick. in.	Length in.	R/t	L/R	Load, P lbs.	σ_{ACT}	σ_{THEO}	$\frac{\sigma_{ACT}}{\sigma_{THEO}}$	E 10^6	$\frac{\sigma_{ACT}}{E}$ 10^{-4}
PC- 1	.0059	5.00	1081	.784		6136	17100	.359	30.6	2.00
PC- 6	.0059	5.00	1081	.784		6919	17100	.405	"	2.26
A-44	.0061	3.02	1045	.474	1233	5300	17700	.299	"	1.73
A-45	.0061	3.04	1045	.477	1290	5280	17700	.298	"	1.73
PC-13	.0059	2.05	1081	.322		7754	17100	.453	"	2.53
PC-14	.0059	2.05	1081	.322		7347	17100	.429	"	2.40
A- 8	.0058	1.53	1100	.240	1836	7980	16800	.475	"	2.61
A- 7	.0058	.91	1100	.143	2490	10550	16800	.628	"	3.45
PC-20	.0059	.58	1081	.091		14680	17100	.858	"	4.79
A-63	.0062	.25	1010	.039	5490	21800	19050	1.130	"	7.13
A-65	.0061	.24	1045	.038	5470	22400	17700	1.260	"	7.32
PC- 4	.0085	9.00	750	1.410		6976	24200	.289	29.0	2.41
PC-15	.0085	9.00	750	1.410		9026	24200	.375	"	3.11
PC-16	.0085	9.00	750	1.410		9780	24200	.405	"	3.37
A-61	.0085	7.03	750	1.100	2378	7000	23300	.300	"	2.41
A- 2	.0085	5.08	750	.800	2730	8020	23300	.344	"	2.77
PC-11	.0091	5.00	700	.785		7610	25900	.293	"	2.63
A- 1	.0085	2.93	750	.460	2470	7260	23300	.311	"	2.50
A-13	.0090	2.02	709	.317	4460	12400	24700	.496	"	4.28
A-17	.0091	1.60	700	.251	5346	14650	24900	.588	"	5.05
A-14	.0082	1.02	780	.159	5230	15900	23400	.680	"	4.50
A-16	.0091	.51	700	.080	7995	21950	24900	.880	"	7.56
A-13	.0089	.52	720	.081	8750	24500	24400	1.000	"	8.45
A-64	.0085	.24	750	.038	12525	36800	23300	1.580	"	12.70
B- 1	.0051	9.03	1350	1.410	890	4360	15352	.286	31.5	1.38
B- 2	.0051	9.03	1250	1.410	1075	6250	15250	.410	"	1.98
B- 3	.0051	9.00	1250	1.410	622	3250	15250	.213	"	1.03
A-23	.0056	9.00	1140	1.410	740	3300	16250	.203	"	1.04
A-24	.0057	9.01	1120	1.410	800	3500	16500	.212	"	1.11
A-58	.0055	7.00	1160	1.100	684	3110	16400	.190	"	.97
A-60	.0055	6.99	1160	1.100	708	3220	16400	.196	"	.99
A- 6	.0055	5.08	1160	.800	738	3580	16400	.218	"	1.13
A-37	.0051	3.88	1250	.609	798	3910	15200	.257	"	1.24
A-10	.0053	2.89	1203	.453	910	4290	15800	.272	"	1.38
A- 5	.0055	2.00	1160	.314	1143	5210	16400	.318	"	1.65
A-46	.0051	1.54	1250	.242	1375	6730	15200	.443	"	2.13
A- 4	.0053	1.02	1203	.083	1840	3670	15800	.549	"	2.75
A- 3	.0053	.54	1203	.085	2080	9850	15800	.623	"	3.12
A- 9	.0053	.53	1203	.083	2748	12970	15800	.821	"	4.11
A-54	.0052	.27	1225	.043	2918	14100	15500	.910	"	4.47

DATA SHEET

Specimen No.	Thick. in.	Length in.	R/t	L/R	Load, P lbs.	$\sigma_{Act.}$	σ_{theo}	$\frac{\sigma_{Act}}{\sigma_{theo.}}$	E 10^6	σ_{Act}/E 10^{-4}
PC- 2	.0041	5.00	1555	.784		2305	12600	.193	32.4	.711
PC- 3	.0041	5.00	1555	.784		3750	12600	.298	"	1.160
A-70	.0040	5.03	1595	.790	410	2560	12300	.208	"	.790
A-71	.0041	5.03	1555	.790	385	2330	12600	.185	"	.720
A-35	.0041	3.03	1555	.475	450	2740	12600	.218	"	.845
A-36	.0041	3.03	1555	.477	450	2740	12600	.218	"	.845
A-35	.0041	2.00	1555	.314	614	3740	12600	.298	"	1.155
A-36	.0041	2.03	1555	.318	580	3525	12600	.280	"	1.080
A-38	.0039	1.95	1635	.306	602	3860	12000	.322	"	1.190
A-39	.0040	1.95	1592	.306	611	3820	12280	.311	"	1.180
PC-17	.0041	1.55	1555	.243		4882	12600	.387	"	1.510
PC-19	.0041	.94	1555	.147		7140	12600	.566	"	2.200
PC-18	.0041	.58	1555	.091		10476	12600	.830	"	3.230
A-52	.0040	.24	1592	.038	1976	12350	12280	1.000	"	3.820
A-53	.0040	.25	1592	.039	1988	12400	12280	1.010	"	3.830
PC- 5	.0031	9.00	2056	1.410		2081	9380	.222	32.0	.650
A-66	.0032	9.00	2000	1.410	249	2090	9660	.194	"	.653
A-68	.0033	9.00	1950	1.410	223	1700	9960	.171	"	.531
A-69	.0033	9.00	1950	1.410	234	1775	9960	.178	"	.555
A-55	.0035	7.04	1820	1.100	233	1665	10600	.157	"	.520
A-56	.0035	7.03	1820	1.100	235	1680	10600	.158	"	.525
A-21	.0035	5.08	1820	.796	243	1730	10600	.163	"	.541
A-42	.0031	3.02	2050	.475	253	2360	9380	.252	"	.737
A-43	.0031	3.03	2050	.475	257	2400	9380	.255	"	.750
A-32	.0033	1.54	1930	.242	400	3030	9280	.324	"	.946
A-33	.0031	1.54	2050	.242	426	3440	9380	.367	"	1.075
A-28	.0031	.90	2055	.141	578	4660	9380	.497	"	1.455
A-27	.0035	.97	1820	.152	585	4180	10600	.394	"	1.309
A-47	.0031	.95	2050	.149	643	5190	9380	.554	"	1.620
A-13	.0034	1.00	1875	.157	602	4430	10300	.430	"	1.390
A-11	.0034	.53	1875	.083	903	6630	10300	.644	"	2.070
A-12	.0032	.55	1995	.086	911	7120	9680	.735	"	2.320
A-50	.0031	.23	2050	.036	1315	10580	9380	1.128	"	3.300
A-51	.0031	.23	2050	.036	1160	9320	9380	.995	"	2.910
PC- 7	.0021	9.00	3035	1.410		1083	6650	.163	32.5	.333
PC- 8	.0021	9.00	3035	1.410		801	6650	.120	"	.248
A-57	.0025	7.00	2550	1.100	74	735	7930	.092	"	.221
A-58	.0025	6.96	2550	1.090	80	800	7930	.101	"	.329
A-34	.0021	5.03	3030	.790	87	1035	6666	.155	"	.347
A-62	.0025	5.03	2550	.790	84	840	7930	.106	"	.250
A-40	.0021	3.03	3030	.475	104	1238	6666	.186	"	.388
A-41	.0021	3.02	3030	.474	108	1285	6666	.193	"	.398
PC-12	.0021	2.05	3035	.322		1540	6650	.231	"	.456
A-30	.0024	1.54	2670	.242	172	1800	7600	.237	"	.537
A-31	.0022	1.55	2890	.237	168	1910	6970	.274	"	.582
PC- 9	.0021	1.05	3035	.165		2881	6650	.433	"	.880
PC-10	.0021	.532	3035	.083		4501	6650	.679	"	1.345
A-39	.0021	.38	3035	.060	418	4980	6670	.747	"	1.485
A-48	.0021	.24	3035	.038	525	6250	6670	.938	"	1.865
A-49	.0021	.24	3035	.038	586	6990	6670	1.050	"	2.085